REPORT DOCUMENTATION PAGE

DTIC FILE COPY

1a. REPORT SECURITY CLASSIFICATION: Unclassified

1b. RESTRICTIVE MARKINGS

2a. SECURITY CLASSIFICATION AUTHORITY

3. DISTRIBUTION/AVAILABILITY OF REPORT: Approved for public release, distribution unlimited

AD-A224 126

5. MONITORING ORGANIZATION REPORT NUMBER(S): AFOSR-TR- 90 0747

DTIC ELECTE JUL 20 1990 S E

6a. NAME OF PERFORMING ORGANIZATION: Boston University, Col. of Eng. Boston, MA 02215

6b. OFFICE SYMBOL (If applicable)

7a. NAME OF MONITORING ORGANIZATION: AFOSR

6c. ADDRESS (City, State, and ZIP Code): 110 Cummington Street, Boston, MA 02215

7b. ADDRESS (City, State, and ZIP Code): Building 410, Bolling AFB, D.C. 20332-6448

8a. NAME OF FUNDING/SPONSORING ORGANIZATION: Dept of the Air Force

8b. OFFICE SYMBOL (If applicable): NA

9. PROCUREMENT INSTRUMENT IDENTIFICATION NUMBER: Contract No. F49620-86-C-0040

8c. ADDRESS (City, State, and ZIP Code): Air Force Office of Scientific Research, Bolling Air Force Base, DC 20332-6448

10. SOURCE OF FUNDING NUMBERS

PROGRAM ELEMENT NO.	PROJECT NO.	TASK NO.	WORK UNIT ACCESSION NO.
61102F	2302	B1	

11. TITLE (Include Security Classification): Analysis of Dynamic Transient Response and Postflutter Behavior of Super-Maneuvering Airplane (U)

12. PERSONAL AUTHOR(S): Luigi Morino Slobodan R. Sipcic

13a. TYPE OF REPORT	13b. TIME COVERED	14. DATE OF REPORT (Year, Month, Day)	15. PAGE COUNT
Final	FROM 87/4/15 TO 88/8/14	88/08/15	14

16. SUPPLEMENTARY NOTATION

17. COSATI CODES			18. SUBJECT TERMS (Continue on reverse if necessary and identify by block number)
FIELD	GROUP	SUB-GROUP	Dynamic transien response Postflutter behavior Critical behavior

19. ABSTRACT (Continue on reverse if necessary and identify by block number)

In the first part of this research a general geometrically-exact Lagrangian mechanics formulation for the aeroelastic analysis of a maneuvering aircraft has been presented, see Morino and Baillieul (1988) for the details. The motion of the aircraft is expressed in terms of the location of the origin of a body frame of reference, the rigid-body rotation of the body frame of reference, and a deformation. The orthogonal rotation matrix describing the orientation of the body frame with respect to a chosen inertial frame of reference is used, as Lagrangian coordinate for the rotational degrees of freedom. The Lagrangian equations of motion for the corresponding degrees of freedom have been obtained. In the second part of this research a formulation has been specialized to the case of a fluttering buckled plate on an aircraft undergoing a pitching maneuver, see Sipcic and Morino (1989) for details. Assuming that the maneuvering of the aircraft is prescribed, the Lagrange equations of motion for the elastic degree of freedom has been derived. This equation is then used to study the response of the panel of an aircraft engaged in a pull-up maneuver. The large-amplitude responses are investigated by using the digital computer. Long-time histories, three-dimensional view of orbits, phase planes, and (continued)

20. DISTRIBUTION/AVAILABILITY OF ABSTRACT: ☐ UNCLASSIFIED/UNLIMITED ☐ SAME AS RPT. ☑ DTIC USERS

21. ABSTRACT SECURITY CLASSIFICATION: Unclassified

22a. NAME OF RESPONSIBLE INDIVIDUAL: Spencer T. Wu

22b. TELEPHONE (Include Area Code): (202) 767-6962

22c. OFFICE SYMBOL: NM

19. (continued)
power spectra of the response are presented. The numerical simulation for periodic and chaotic response are conducted in order to analyze the influence of the maneuvering to the dynamic behavior of the panel. As the maneuvering (load factor) increases, system exhibits complicated dynamic behavio including period-multiplying and demultiplying bifurcations and chaos.

FINAL TECHNICAL REPORT
ON AFOSR CONTRACT No. F49620-86-C-0040

Covering the period April 15, 1987 to August 14, 1988

Submitted by Luigi Morino and Slobodan Sipcic
Boston University, Boston MA 02215

Summary

In the first part of this research a general geometrically-exact Lagrangian mechanics formulation for the aeroelastic analysis of a maneuvering aircraft has been presented, see Morino and Baillieul (1988) for the details. The motion of the aircraft is expressed in terms of the location of the origin of a body frame of reference, the rigid-body rotation of the body frame of reference, and a deformation. The orthogonal rotation matrix describing the orientation of the body frame with respect to a chosen inertial frame of reference is used, as Lagrangian coordinate for the rotational degrees of freedom. The Lagrangian equations of motion for the corresponding degrees of freedom have been obtained.

In the second part of this research a formulation has been specialized to the case of a fluttering buckled plate on an aircraft undergoing a pitching maneuver, see Sipcic and Morino (1989) for details. Assuming that the maneuvering of the aircraft is prescribed, the Lagrange equations of motion for the elastic degree of freedom has been derived. This equation is then used to study the response of the panel of an aircraft engaged in a pull–up maneuver. The large–amplitude responses are investigated by using the digital computer. Long–time histories, three–dimensional view of orbits, phase planes, and power spectra of the response are presented. The numerical simulation for periodic and chaotic response are conducted in order to analyze the influence of the maneuvering to the dynamic behaviour of the panel. As the maneuvering (load factor) increases, system exhibits complicated dynamic behavior including period–multiplying and demultiplying bifurcations and chaos.

Keywords: aircraft;
Dynamic Response;
Lagrangian functions;
bifurcation (mathematics);
maneuverability. (CP)

1 The Equation of Motion

Let us summarize the formulation and the results of the first part of this research presented in Morino and Baillieul (1988); details of the formulation are in the original report. As mentioned before the motion of the aircraft is expressed in terms of the motion of the origin of a body frame of reference, the rigid–body rotation of the body frame of reference, and a deformation, which in turn is expressed (in the body frame of reference) in terms of specified functions $\boldsymbol{\phi}_r(\xi^\alpha)$, as

$$\mathbf{u}(\xi^\alpha, t) = \sum_r u_r(t)\boldsymbol{\phi}_r(\xi^\alpha) \tag{1}$$

Introducing an unconventional approach (*i.e.*, using the rotation matrix as a Lagrangian coordinate), and the following the conventional procedure for Lagrangian mechanics (*i.e.*, calculating the kinetic energy, the potential energy, and the work done by the external forces, and substituting these in the Lagrangian equations of motion) one obtains: for the translational degrees of freedom,

$$\begin{aligned} &m\mathrm{D}_t\dot{\mathbf{x}}_0 + \mathrm{D}_t^2\mathbf{s} = m(\dot{\mathbf{v}}_0 + \boldsymbol{\Omega}\mathbf{v}_0) + \dot{\boldsymbol{\Omega}}\mathbf{s}_0 + \boldsymbol{\Omega}^2\mathbf{s}_0 \\ &+ \sum_r \left(\mathbf{I}\ddot{u}_r + 2\boldsymbol{\Omega}\dot{u}_r + \dot{\boldsymbol{\Omega}}u_r + \boldsymbol{\Omega}^2 u_r\right)\mathbf{s}_r = \mathbf{f}_0 = m\mathbf{R}^{\mathrm{T}}\,\mathbf{g} + \mathbf{e}_0 \end{aligned} \tag{2}$$

for the rotational degrees of freedom,

$$\mathrm{D}_t\mathbf{h}_0 + \mathbf{s} \times \mathrm{D}_t\mathbf{v}_0 = \mathbf{m}_A + \sum \mathbf{m}_r u_r + \mathbf{s} \times \mathbf{g}_B \tag{3}$$

and finally for the elastic degrees of freedom,

$$\begin{aligned} &\mathbf{s}_r^{\mathrm{T}}\left(\frac{d\mathbf{v}_0}{dt} + \boldsymbol{\Omega}\mathbf{v}_0\right) + \mathbf{b}_r^{\mathrm{T}}\,\dot{\boldsymbol{\omega}} + \sum_s m_{rs}\ddot{u}_s - \dot{\boldsymbol{\omega}}^{\mathrm{T}} \sum_s \mathbf{b}_{rs}u_s - 2\boldsymbol{\omega}^{\mathrm{T}} \sum_s \mathbf{b}_{rs}\dot{u}_s \\ &-\boldsymbol{\omega}^{\mathrm{T}}\,\mathbf{J}_r\boldsymbol{\omega} - \sum_s \boldsymbol{\omega}^{\mathrm{T}}\,\mathbf{J}_{rs}\boldsymbol{\omega}\,u_s + \frac{\partial \mathcal{E}}{\partial u_r} = f_r \end{aligned} \tag{4}$$

For the definition of the coefficients in terms of the $\boldsymbol{\phi}_n$, as well as the details of the derivation the reader is referred to the original report.

The formulation includes all the geometric non-linearities, but has been focussed primarily on the dynamic ones, which arise from the coupling between the rigid-body rotation of the frame of reference and the other degrees of freedom. The structural ones arise from the non-linear terms in the expression of the strain tensor.

Finally, the simplification resulting from the use of the natural modes of vibration for the functions ϕ_r has been indicated. The relationship between the finite-element and vibration-mode formulation has been examined. It was shown that finding the approximate modes of vibration from a finite-element formulation and using the corresponding Lagrange equation of motion is fully equivalent to transforming the system of finite-element equations in such a way that the linear portion of the system is diagonal. If the natural modes of vibration is less than the number of unknowns in the original finite-element equations, this corresponds to reducing the number of unknowns (and the corresponding equations) in the transformed system.

2 Dynamic of Fluttering Plate in Maneuvering Aircraft

In order to study the effect of maneuvering on the elastic response of the fluttering plate in the maneuvering airplane we assume the rigid–body motion of the frame of reference to be prescribed. Hence Eqs. 2, 3 are not used, and in Eq. 4 ω is prescribed and therefore the inertial terms are linear in u_r (with time dependent coefficients). A constant velocity pull–up maneuver has been assumed. Following the classical panel–flutter approximation and the conventional procedure of Lagrangian mechanics, the equations of motion are given by

$$\ddot{\mathbf{u}} + \delta\dot{\mathbf{u}} + \mathbf{G}\mathbf{u} + \dot{\omega}\mathbf{d} + \omega\mathbf{v} = \mathbf{p} + \mathbf{f}(u) + \gamma\omega^2\mathbf{u} \tag{5}$$

For the definition of the coefficients, as well as the details of the derivation the reader is referred to the original report.

Equations 5 are a set of ordinary, nonlinear differential equations in time. The cubic type of non–linearities are of a geometric origin and are associated with the occurrence of tensile stresses in the middle surface. The coupling between the rigid–body rotation of the frame of reference and the elastic degrees of freedom is represented by the fourth term. Note that by assuming $\omega = 0$ Eqs. 5 properly reduce to a classical panel flutter equations.

3 Numerical Experimentation

The extensive numerical simulation for periodic and chaotic response are conducted in order to analyze a behaviour of the fluttering panel of the maneuvering airplane, for details see original report by Sipcic and Morino (1989). Several important conclusions derive from the preceding work, see Fig. 1 and sequence

of Figs. 2(a) thru (r) as the example. The new limit cycle has been observed in the non-maneuvering case. It was shown that chaos could occur in a maneuvering case for system parameters in the actual flight range. The presence of a load factor can transform the response from the fixed point into a simple periodic or even chaotic state. It can also suppress the periodic character of the motion, transforming the response into a fixed point (compare responses Fig. 2(a) and (r)). Regions of the chaotic motion with an island of non–sinusoidal periodic motion has been observed, see Figs. 2(l) thru 2(q). Relatively sudden jumps between these two regimes were found. For some values of the load factor, a cascade of period–multiplying bifurcations begins, culminating in chaos Figs. 2(d) thru 2(h), followed by a series of period–demultiplying bifurcations as the system returns to a starting limit cycle response Figs. 2(h) thru 2(k). The region of intermittent and transient chaos has been observed as well.

4 Concluding Remarks

A general geometrically-exact Lagrangian mechanics formulation for the aeroelastic analysis of a maneuvering aircraft has been presented. The motion of the aircraft is expressed in terms of the location of the origin of a body frame of reference, the rigid-body rotation of the body frame of reference, and a deformation, given as a linear combination of prescribed functions, ϕ_r. The Lagrangian equations of motion for the corresponding degrees of freedom have been obtained. The advantages of identifying ϕ_r with the natural modes of vibration (instead of finite-element test functions) have been discussed.

In the second part of this research a general geometrically–exact Lagrangian mechanics formulation for the aeroelastic analysis of a maneuvering aircraft has been specialized to the case of a fluttering plate undergoing a pitching maneuver. The formulation includes geometric non–linearities associated with the occurrence of tensile stresses in the middle surface, as well as coupling between the rigid–body rotation of the frame of reference and the other degrees of freedom. The general response of the system were simulated on the digital computer by using a fourth order Runge–Kutta algorithm with adaptive step size control. Long–time histories, three–dimensional view of orbits, phase planes, and power spectra have been used to characterize the response.

The results indicate that the study of this deterministic system is important from the practical and theoretical viewpoints. First, the fact that maneuvering can change the character of the panel response is of practical interest to the

aeroelasticians as it affects, for instance, fatigue analysis. Secondly, the techniques employed in this study can be extended to the problem of flow induced vibration, with all non–linearities geometrical and dynamical included, of the flexible aircraft or rotating structures. From the theoretical point of view since this physical system is a rich source of static and dynamic instabilities and associated limit cycle motions it could be used for instance as a test case for assessing techniques for the study of nonlinear dynamics and chaos.

Subjects for the consideration in future research include the use of other stability concepts such as Liapunov exponents, and Poincare maps. Application of a complementary methods of differentiable dynamics, in particular, of center manifold and bifurcation theory, to analyze the problem from a qualitative viewpoint would be helpful. Knowledge of the generic structures of attracting sets in N–space, might make the interpretation of numerical solutions of evolution equations considerably clear.

References

Morino, L., and Baillieul, J., (1988), "A Geometrically-Exact Non-Linear Lagrangian Formulation for the Dynamic Analysis of Flexible Maneuvering Aircraft", Technical Report 88-1, Boston University.

Sipcic, R. S., and Morino, L., (1989), "Chaotic Response of Fluttering Panel, the Influence of Maneuvering", Technical Report 89-1, Boston University.

ACKNOWLEDGEMENTS

Research sponsored by the Air Force Office of Scientific Research (AFSC), under Contract No. F49620-86-C-0040. The United States Government is authorized to reproduce and distribute reprints for governmental purposes notwithstanding any copyright notation herein. The authors wish to thank Dr. Anthony K. Amos of the Air Force Office of Scientific Research, Mr. Carey S. Buttrill of NASA Langley Research Center, and Professor Gvido Sandri of Boston University for the valuable discussions on this work.

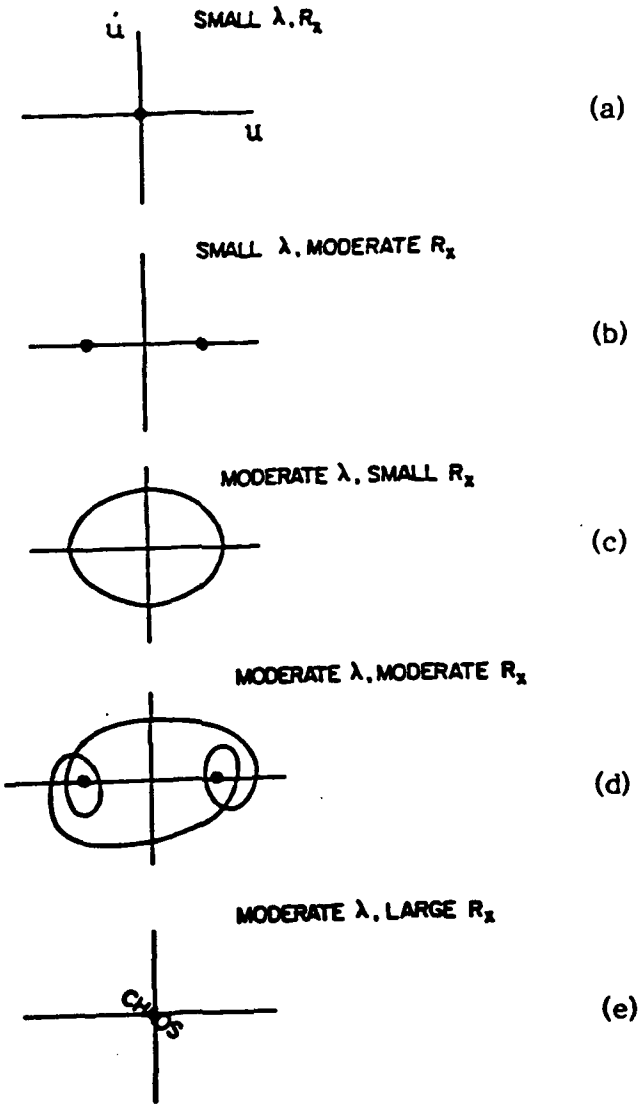

Figure 1 Sketch of representative phase plane orbits

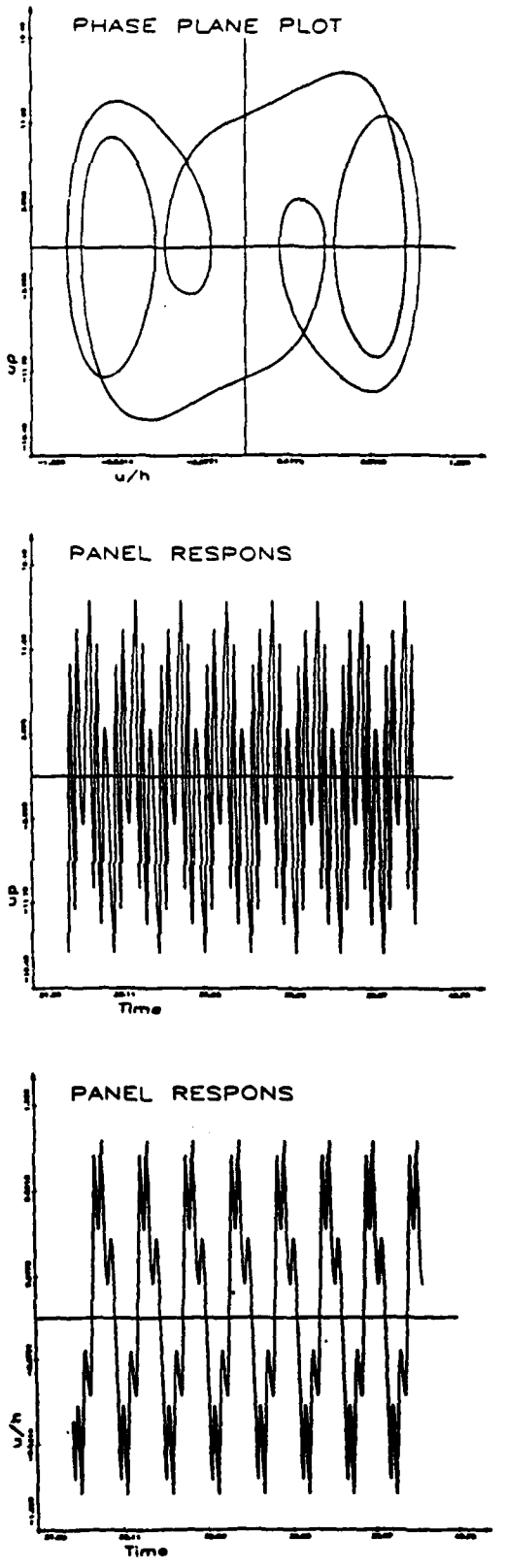

Figure 1a New more complicated limit cycle response for $\lambda = 119.5$, and $R_a = -4.0\pi^2$

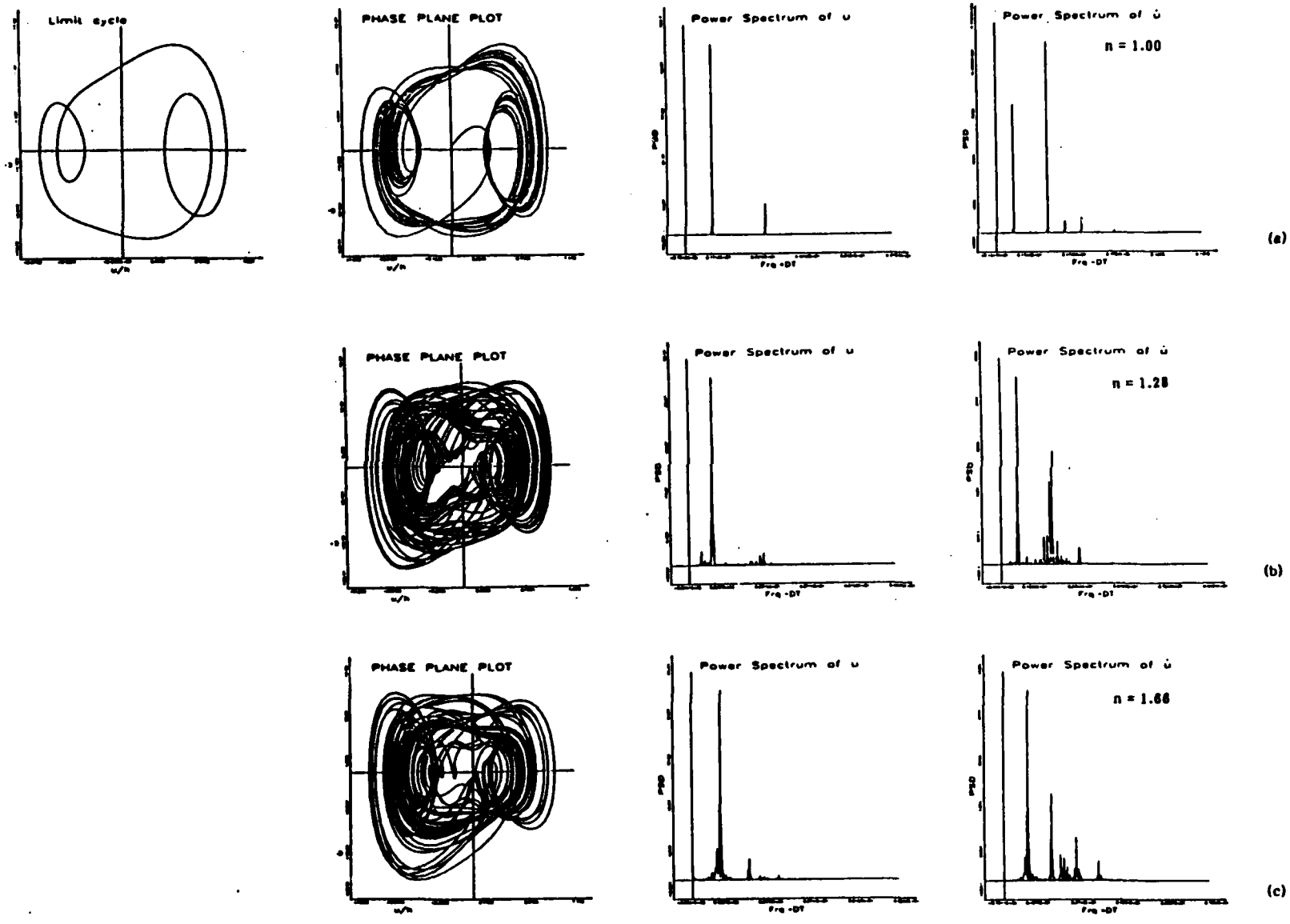

Figure 2 Phase-plane portraits and accompanying frequency spectra of system response. The maneuvering varies from $n = 1.0$, to $n = 3.0$

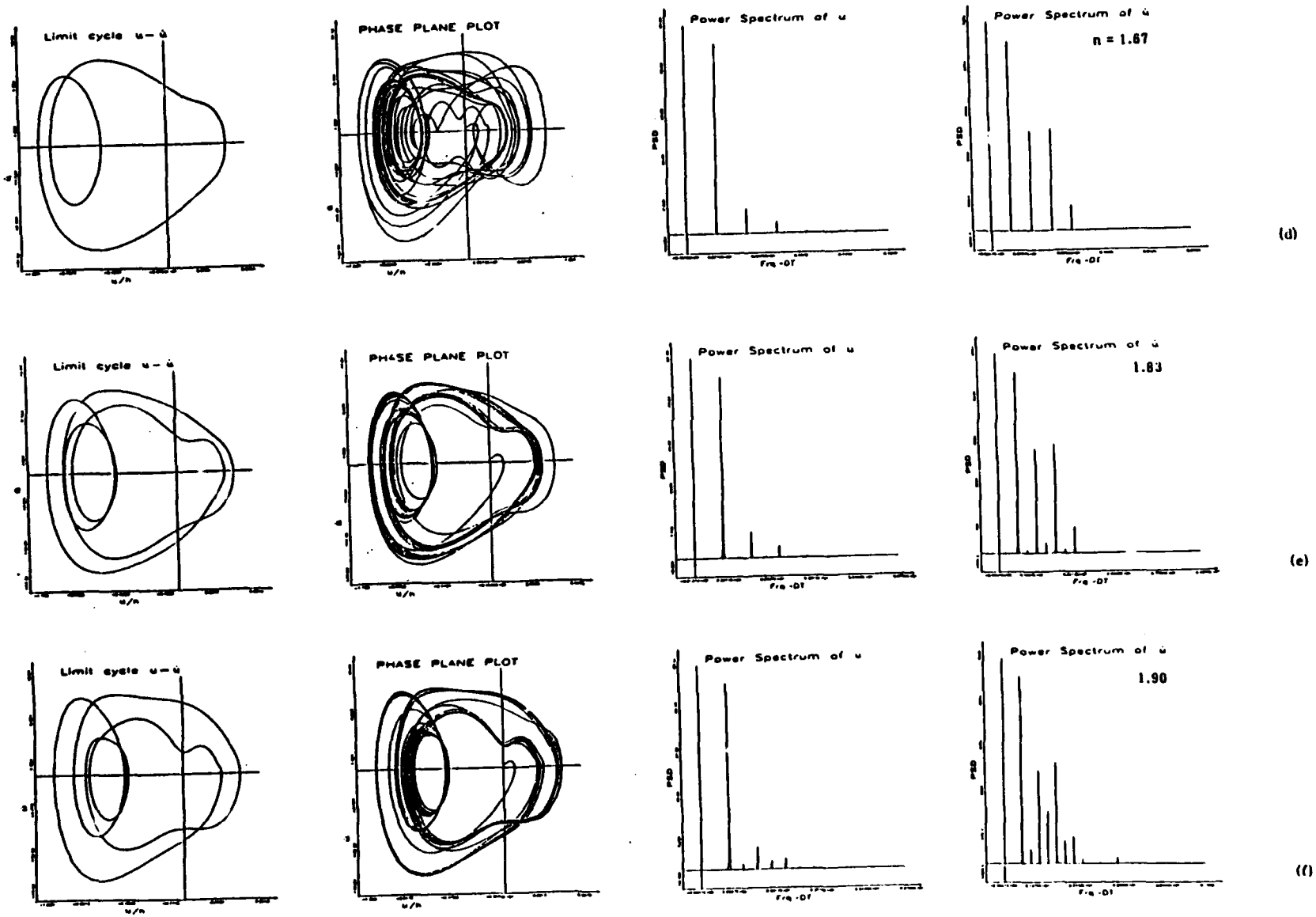

Figure 2 Continued

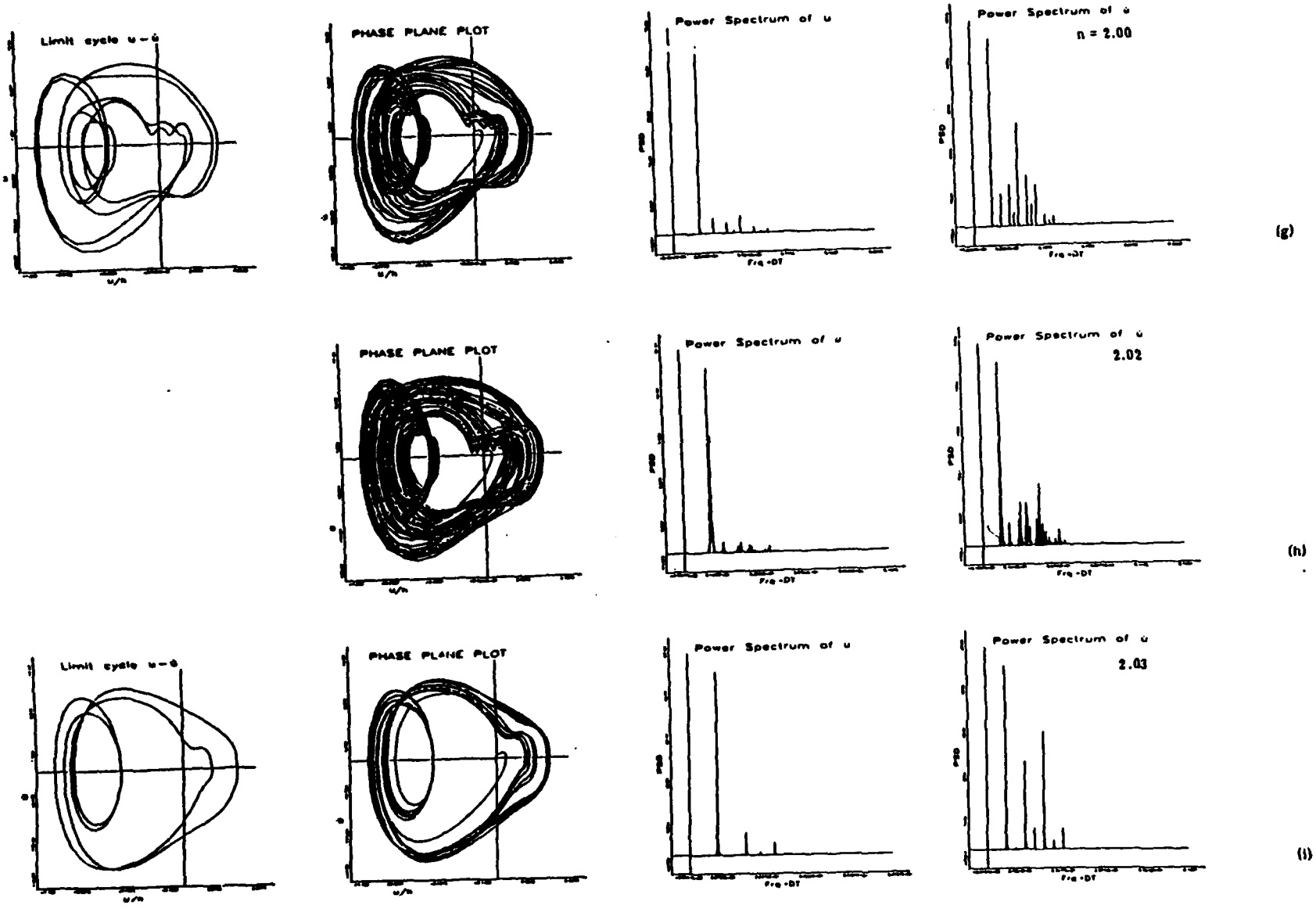

Figure 2 Continued

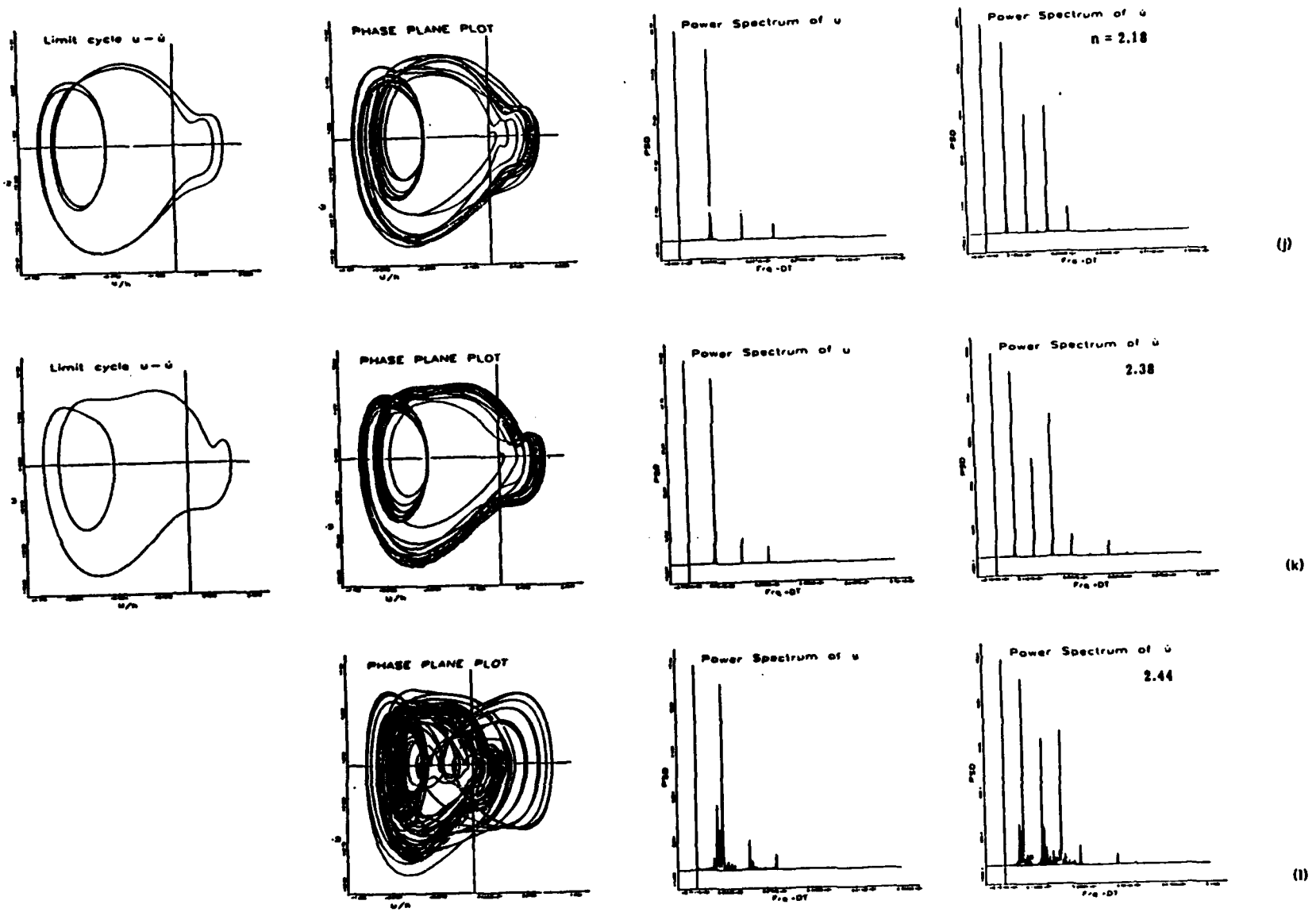

Figure 2 Continued

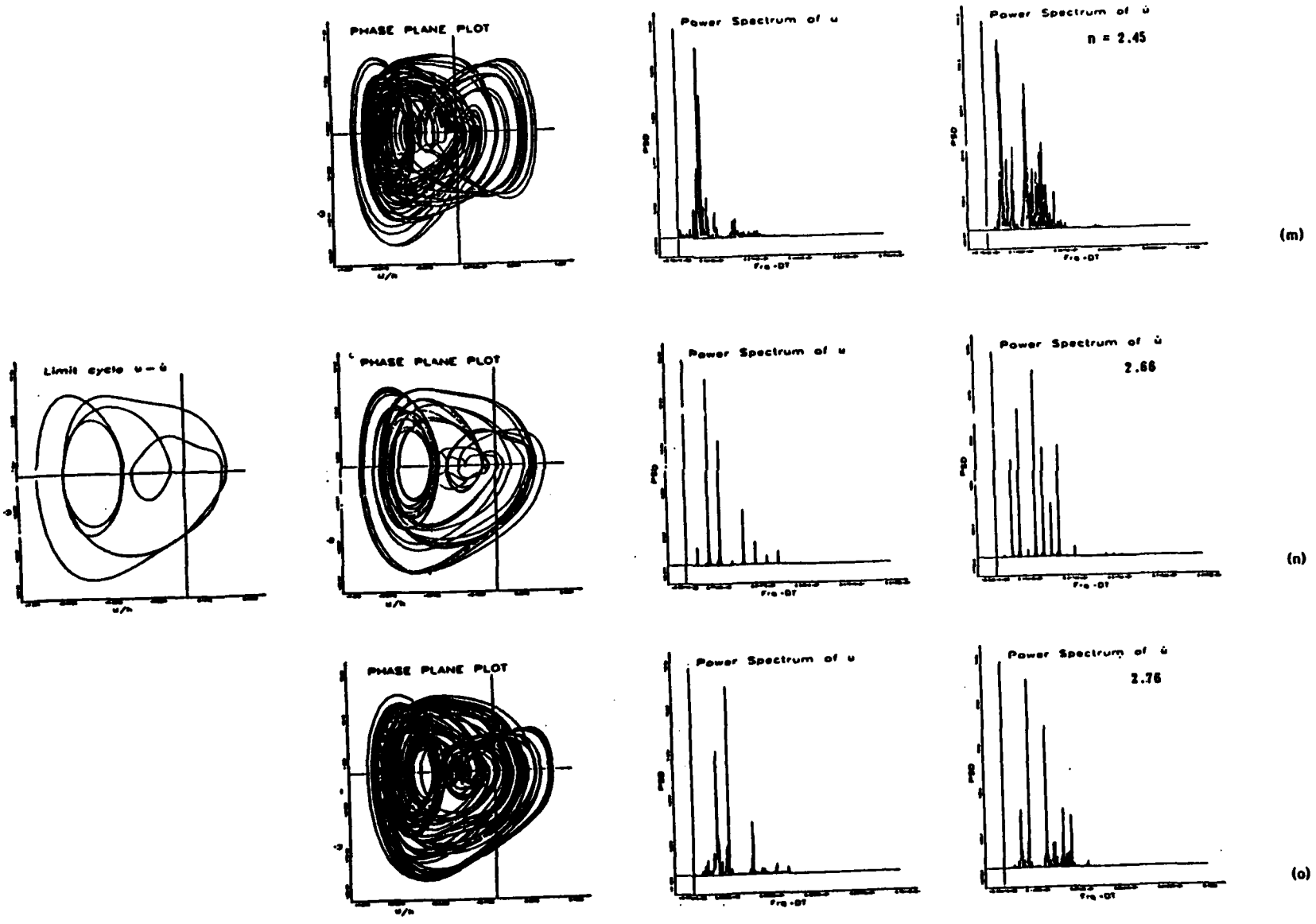

Figure 2 Continued

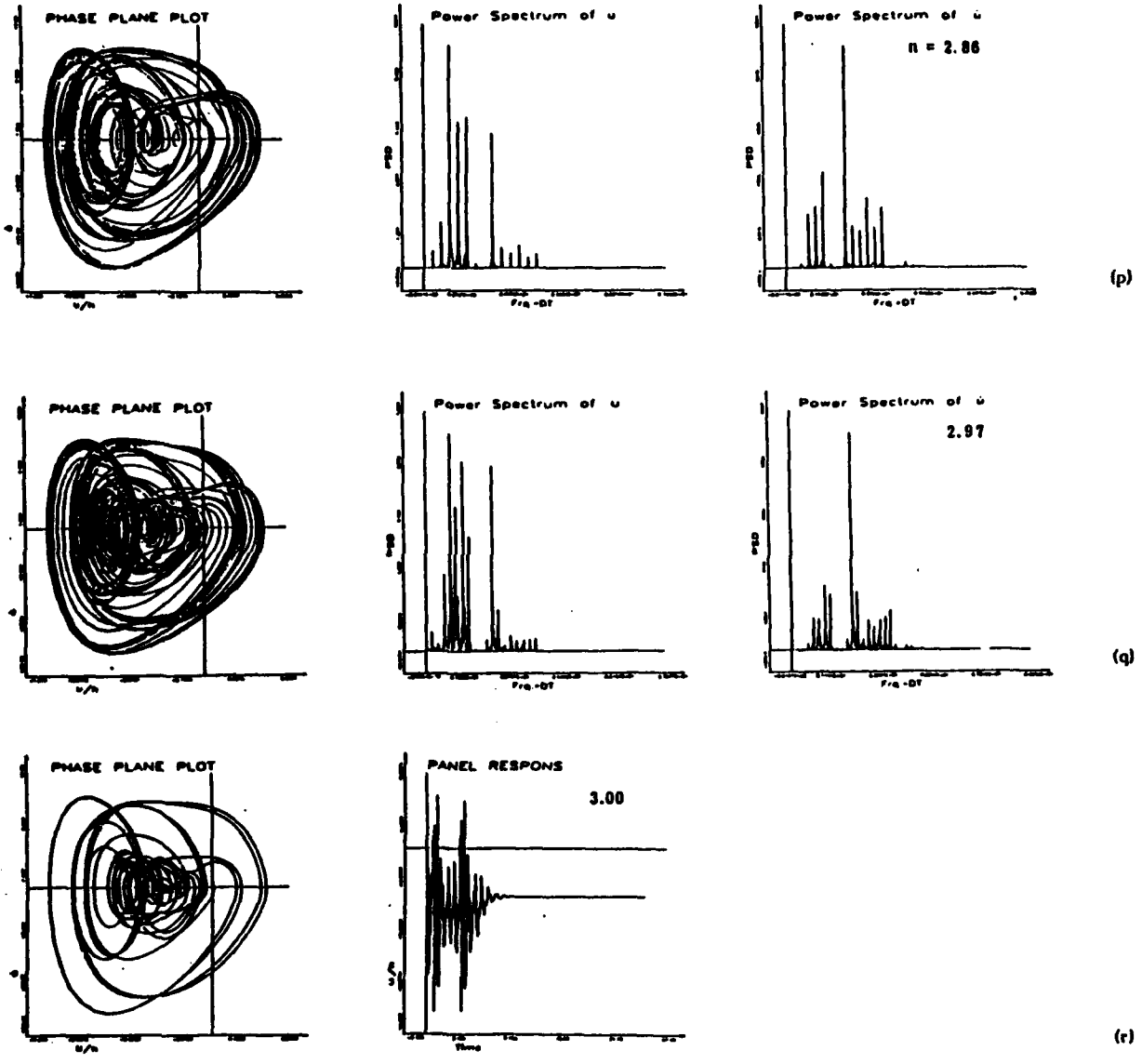

Figure 2 Continued

CCAD-TR-89-01

CENTER for COMPUTATIONAL and APPLIED DYNAMICS
BOSTON UNIVERSITY
BOSTON MASS. 02215

CHAOTIC RESPONSE OF FLUTTERING PANEL THE INFLUENCE OF MANEUVERING

Slobodan R. Sipcic
and
Luigi Morino

September 1989

TABLE of CONTENTS

LIST of FIGURES

SUMMARY

The influence of maneuvering on the response of a fluttering buckled plate on an aircraft has been studied. Assuming that the maneuvering of the aircraft is prescribed, the Lagrange equations of motion for the elastic degree of freedom have been derived. The formulation includes geometric non-linearities associated with the occurrence of tensile stresses, as well as coupling between the rigid-body rotation of the frame of reference and the other degrees of freedom. This equation is then used to study the response of the panel of an aircraft engaged in a pull-up maneuver. General concepts from the modern theory of dynamical systems, with emphasis on chaotic behavior, are presented. The large-amplitude responses are investigated by using the digital computer. Long-time histories, three-dimensional view of orbits, phase planes, and power spectra of the response are presented. We have chosen the system parameters such that there are two equilibrium positions for the non-maneuvering case. The numerical simulation for periodic and chaotic response are conducted in order to analyze the influence of the maneuvering on the dynamic behavior of the panel. As the maneuvering (load factor) increases, the system exhibits complicated dynamic behavior including period-multiplying and demultiplying bifurcations and chaos.

SECTION 1
INTRODUCTORY REMARKS

1.1 Overview

This report deals with the response of a flexible structure, including the dynamical and structural non–linearities. The main motivation for this work is the aeroelastic analysis of maneuvering airplanes; therefore aircraft will be emphasized throughout this report.

The large amount of material here suggested a division of the study into two main areas, theoretical and numerical. The theoretical approach is given in Section 2 and 3. Since this research is continuation of the work by Morino and Baillieul on the geometrically–exact formulation of maneuvering–aircraft dynamics their results are briefly discussed in Section 2. Assuming that the maneuvering of the aircraft is prescribed, and following the conventional procedure of Lagrangian mechanics, the Lagrange equations of motion for the elastic degree of freedom are derived. These are the governing equations for the physical system considered here. The main ideas behind the modern theory of nonlinear systems are presented in Section 3. The reader unfamiliar with the subject hopefully will get sufficient information in order for him to be able to follow the interpretation of phenomena appearing during the numerical experimentation. The numerical results are presented in Section 4. The governing equations are integrated numerically by using a fourth–order Runge–Kutta algorithm. Some unusual non–maneuvering responses are presented in Subsection 4.1. The effect of varying the load factor was studied in great detail; only representative results are presented in this report. In order to understand the dynamic problem, the character of the solution has been examined in Subsection 4.2 in physical terms. In Subsection 4.3 the results of the simulation of the influence of maneuvering to a periodic response are presented. A chaotic responses are examined in Subsection 4.4. Finally, the time dependent maneuvering is considered in Subsection 4.5. In examining and discussing the results, attention is drawn to the routes to chaos. The system exhibits very complicated dynamic behavior including period multiplying and demultiplying, bifurcations, and chaos. An important result of this work is the conclusion that maneuvering can change the character of the response from periodic, or even fixed point, to chaotic, and *vice versa*.

Although many numerical experiments were performed varying all of the parameters, only the results necessary to make discussion complete and clear are presented. Long time histories, three–dimensional view of orbits, phase planes, and power spectra of the response (defined in Section 3) were the dynamic tools used in studying of the system considered here.

1.2 Objectives of Report

In this report the equations for the analysis of the dynamics of a fluttering buckled plate on an aircraft undergoing a pitching maneuver have been derived. The equations include geometric non–linearities associated with the occurrence of tensile stresses, as well as the coupling between the rigid–body rotation of the frame of reference and the the elastic degrees of freedom. These equations are then used to study the response of the panel of an aircraft engaged in a pull–up maneuver.

This research has its own theoretical merits in understanding the influence of the maneuvering on the panel response and occurrence of chaos in a system. The complexity of the physical system considered here justifies the use of the simulation approach. Long–time histories, three–dimensional view of orbits, phase planes, and power spectra of the response are studied. Finally, as a long term goal, we believe that the techniques employed in this study can be extended to the problem of flow–induced vibration of the flexible aircraft, with all the non–linearities included (geometric, dynamic, and aerodynamic).

1.3 Review of State of the Art

During the last two decades, formulations for the analysis of flight dynamics and structural dynamics of a flexible aircraft, as well as related formulations in the field of dynamics of large space structures, have been developed. An overview of the recent developments and trends in the field of flexible aircraft dynamics are given in Morino and Baillieul (1987).

Since a buckled fluttering plate is a prototypical system, a brief review of the recent developments is in order. One of the approaches to the treatment of the flow induced oscillations relies on the selection of relatively simple models which provides a reasonable reproduction of the behavior observed on the real physical system. The complete partial differential equation is replaced by an ordinary differential equation on a state space of low order. For example in Dowell and Pezeshki (1986, 1987), Zavodney and Nayfeh (1988), or Zavodney et. all (1989) Duffing's equation has been used as a model for the sinusoidally excited buckled plate. In the another approach the non–linear partial differential equation is recast, by Galerkin or Rayleigh–Ritz methods, as a set of ordinary differential equations which are then solved for specific initial conditions by numerical integration techniques. This approach is perhaps best illustrated in the work of Dowell and Ilgamov (1988). A dissipative partial differential equation modeling a buckled beam was considered by Holmes and Marsden (1981). They presented one of the very few analytical results available on chaos in a continuous system.

Note that none of the above work has addressed the problem presented here: the response of a flexible plate of a maneuvering aircraft including the effect of the rigid–body rotation of the frame of reference on the deformation.

SECTION 2
THE EQUATION OF MOTION

The dynamics of a structure has been formulated using Lagrangian mechanics in terms of a "body frame of reference". This frame of reference is clearly defined in the case of a rigid body. In the case of a flexible structure, the motion of the structure can be expressed in terms of the motion of the origin of a body frame with respect to a chosen inertial frame, the rigid–body rotation of the body frame around its origin, and a deformation with respect to a reference configuration rigidly connected to the body frame. The orientation of the body frame with respect to the inertial frame of reference is defined through the orthogonal rotation matrix.

We will use the following notations. An arrow above a lower case letter designates a vector in a three dimensional physical space. Superscripted latin letters designate the Cartesian components of vectors and tensors. A boldface lower–case letter designates a column matrix. A boldface capital letter designates a matrix; in particular, I designates the identity matrix.

2.1 Lagrange Equations of Motion for a Flexible Aircraft

Let us summarize the formulation and the results presented in Morino and Baillieul (1988); details of the formulation are in the original report. As mentioned before the motion of the aircraft is expressed in terms of the motion of the origin of a body frame of reference, the rigid–body rotation of the body frame of reference, and a deformation. Indicating with $\mathbf{x}$ the coordinates in the inertial frame, with $\mathbf{x}_0$ the coordinates of the origin P_0 of the body frame, with $\mathbf{s}$ the body–axis coordinates of a point P in the body frame at time $t = 0$ (reference condition) and with $\mathbf{u}$ the body–axis components of the displacement of the structure with respect to reference condition, we have,

$$\mathbf{x}(\xi^a, t) = \mathbf{x}_0(t) + \mathbf{R}(t)\left[\mathbf{s}(\xi^a) + \mathbf{u}(\xi^a, t)\right] \tag{2.1}$$

where ξ^a is a system of material coordinates, (*i.e.*, a system of coordinates, in general curvilinear, that is convected with the material point). Typically, these coincide numerically with the components x_i of $\mathbf{s}$. Note that the matrix $\mathbf{R}$ represents a rigid–body rotation. Next let us assume that a deformation is given as a linear combination of prescribed functions, ϕ_r, with unknown coefficients, *i.e.*,

$$\mathbf{u}(\xi^a, t) = \sum_r u_r(t)\boldsymbol{\phi}_r(\xi^a) \tag{2.2}$$

In the rest of this subsection the resulting Lagrangian equations of motion are presented for all the degrees of freedom, *i.e.*, translational $\mathbf{x}_0$, rotational $\mathbf{R}$, and elastic u_r; details of the derivation are in the original report.

The following notation will be used,

$$m = \iiint_V \rho \, dV \tag{2.3}$$

$$\mathbf{s}_0 = \iiint_V \rho \, \mathbf{z} \, dV \tag{2.4}$$

$$\mathbf{s}_r = \iiint_V \rho \, \boldsymbol{\phi}_r \, dV \tag{2.5}$$

$$m_{rs} = \iiint_V \rho \, \boldsymbol{\phi}_r^{\mathrm{T}} \boldsymbol{\phi}_s \, dV = m_{sr} \tag{2.6}$$

$$\mathbf{b}_r = \iiint_V \rho \, \mathbf{z} \times \boldsymbol{\phi}_r \, dV \tag{2.7}$$

$$\mathbf{b}_{rs} = \iiint_V \rho \, \boldsymbol{\phi}_r \times \boldsymbol{\phi}_s \, dV = -\mathbf{b}_{sr} \tag{2.8}$$

$$\mathbf{J}_0 = \iiint_V \rho \, (\mathbf{z}^{\mathrm{T}} \mathbf{z} \mathbf{I} - \mathbf{z}\mathbf{z}^{\mathrm{T}}) \, dV = \mathbf{J}_0^{\mathrm{T}} \tag{2.9}$$

$$\mathbf{J}_r = \iiint_V \rho \left[\boldsymbol{\phi}_r^{\mathrm{T}} \mathbf{z} \mathbf{I} - \frac{1}{2} (\boldsymbol{\phi}_r \mathbf{z}^{\mathrm{T}} + \mathbf{z} \boldsymbol{\phi}_r^{\mathrm{T}}) \right] dV = \mathbf{J}_r^{\mathrm{T}} \tag{2.10}$$

$$\mathbf{J}_{rs} = \iiint_V \rho \left[\boldsymbol{\phi}_r^{\mathrm{T}} \boldsymbol{\phi}_s \mathbf{I} - \frac{1}{2} (\boldsymbol{\phi}_r \boldsymbol{\phi}_s^{\mathrm{T}} + \boldsymbol{\phi}_s \boldsymbol{\phi}_r^{\mathrm{T}}) \right] dV = \mathbf{J}_{rs}^{\mathrm{T}} = \mathbf{J}_{sr} \tag{2.11}$$

First, consider the translational degrees of freedom. Noting that, by definition of center of mass, $\mathbf{s} = m(\mathbf{x}_G - \mathbf{x}_0)$, the Lagrangian equations of motion for the translational degrees of freedom are given, in body axes, by

$$\begin{aligned} & m \mathrm{D}_t \dot{\mathbf{x}}_0 + \mathrm{D}_t^2 \mathbf{s} = m(\dot{\mathbf{v}}_0 + \boldsymbol{\Omega} \mathbf{v}_0) + \dot{\boldsymbol{\Omega}} \mathbf{s}_0 + \boldsymbol{\Omega}^2 \mathbf{s}_0 \\ & + \sum_r \left(\mathbf{I} \ddot{u}_r + 2 \boldsymbol{\Omega} \dot{u}_r + \dot{\boldsymbol{\Omega}} u_r + \boldsymbol{\Omega}^2 u_r \right) \mathbf{s}_r = \mathbf{f}_0 = m \mathbf{R}^{\mathrm{T}} \mathbf{g} + \mathbf{e}_0 \end{aligned} \tag{2.12}$$

where $\boldsymbol{\Omega} = \mathcal{A}(\boldsymbol{\omega})$ and $\mathcal{A}$ denotes the operator that maps an arbitrary vector into a skew-symmetric matrix. Furthermore, $\mathbf{v}_0 = \mathbf{R}^{\mathrm{T}} \dot{\mathbf{x}}_0$, D_t denotes the operator $D_t(\cdot) = \mathbf{I} \partial(\cdot)/\partial t + \boldsymbol{\Omega}(\cdot)$, and $\mathbf{e}_0$

$$\mathbf{e}_0 = \oiint_S \mathbf{t} \, dS \tag{2.13}$$

is the aerodynamic resultant.

Next, consider the rotational degrees of freedom. With an orthogonal–matrix variable, $\mathbf{R}$, and following the procedure of Baillieul and Levi (1987), the Lagrange equation of motion for the rotation around the point P_0 can be written as,

$$\mathrm{D}_t \mathbf{h}_0 + \mathbf{s} \times \mathrm{D}_t \mathbf{v}_0 = \mathbf{m}_A + \sum \mathbf{m}_r u_r + \mathbf{s} \times \mathbf{g}_B \tag{2.14}$$

This coincides with the equation of conservation of the angular momentum obtained from Newtonian Mechanics. Note that, $\mathbf{h}_0 = \mathbf{J}\boldsymbol{\omega} + \mathbf{b}$ is the angular momentum around the point P_0 of the motion about P_0, and

$$\mathbf{m}_A = \oiint_S \mathbf{z} \times \mathbf{t} \, dS \tag{2.15}$$

is the aerodynamic moment (about the origin P_0 of the body frame of reference) acting on the undeformed configuration, whereas

$$\mathbf{m}_r = \iint_S \boldsymbol{\phi}_r \times \mathbf{t}\, dS \tag{2.16}$$

is the change in moment due to the change in $\mathbf{x}$ caused by a unit increase of the Lagrangian coordinate u_r (for a prescribed distribution of $\mathbf{t}$).

Finally, consider the Lagrangian equations of motion for the elastic degrees of freedom. Following the conventional procedure of Lagrangian mechanics one obtains the equations of motion for the Lagrangian coordinate u_r, in body axes, as:

$$\mathbf{s}_r^T \left(\frac{d\mathbf{v}_0}{dt} + \boldsymbol{\Omega}\mathbf{v}_0\right) + \mathbf{b}_r^T \dot{\boldsymbol{\omega}} + \sum_s m_{rs}\ddot{u}_s - \dot{\boldsymbol{\omega}}^T \sum_s \mathbf{b}_{rs} u_s - 2\boldsymbol{\omega}^T \sum_s \mathbf{b}_{rs}\dot{u}_s$$
$$-\boldsymbol{\omega}^T \mathbf{J}_r \boldsymbol{\omega} - \sum_s \boldsymbol{\omega}^T \mathbf{J}_{rs}\boldsymbol{\omega}\, u_s + \frac{\partial \mathcal{E}}{\partial u_r} = f_r \tag{2.17}$$

where $\mathcal{E}$ is the elastic energy, and $\boldsymbol{\omega}$ are the components of the angular velocity in the body frame of reference.

2.2 Dynamics of a Fluttering Plate in a Maneuvering Aircraft

In this subsection the Lagrange equations of motion obtained above are specialized to the case of a fluttering buckled plate on an aircraft undergoing a pitching maneuver. Since we want to study the effect of maneuvering on the elastic response, we assume the rigid–body motion of the frame of reference to be prescribed. Hence Eqs. 2.12, 2.14 are not used, and in Eq. 2.17 $\boldsymbol{\omega}$ is prescribed and therefore the inertial terms are linear (with time dependent coefficients). Consider a right–handed body frame of reference with base vectors $\vec{j}_1, \vec{j}_2, \vec{j}_3$. We will assume constant velocity pull–up maneuver, *i.e.*, $\mathbf{v}_0 = -v_0\vec{j}_1$, with $\boldsymbol{\omega} = -\omega\vec{j}_2$, and $v_0 = constant$. Furthermore, the modes $\boldsymbol{\phi}_r$ are all in the direction $\vec{j}_3$, and therefore the following simplifications are possible: $m_{rs} = M_r\delta_{rs}$ (where δ_{rs} designates the Kronecker delta and $M_r = m_{rr}$ indicates the generalized mass, see Eq. 2.6), $\mathbf{b}_{rs} = 0$ (see Eq.2.8), and $\mathbf{J}_{rs} = M_r\delta_{rs}(\mathbf{I} - \mathbf{I}_3)$ (where $\mathbf{I}_3 = [\delta_{i3}]$, see Eq. 2.11). In addition, $\mathbf{s}_r = s_r\vec{j}_3$, and $\mathbf{b}_r = b_r\vec{j}_2$. Thus, the Lagrangian equations for the elastic degrees of freedom 2.17 simplify considerably and are given by

$$s_r\omega v_0 + b_r\dot{\omega} + \sum_s m_{rs}\ddot{u}_s - \sum_s \omega^2 m_{rs}\, u_s + \frac{\partial \mathcal{E}}{\partial u_r} = f_r \tag{2.18}$$

with $r = 1, ..., N$.

Consider once more a thin plate having length a and thickness h and undergoing cylindrical bending in response to one side airflow, see Fig. 1. In such a case the axial extension, v, can be written to first order approximation as

$$v(z) = -\frac{1}{2}\int_0^z \left(\frac{\partial u}{\partial z}\right)^2 dz, \tag{2.19}$$

Thus the elastic energy is

$$\mathcal{E} = \frac{D}{2}\int_0^a \left(\frac{\partial^2 u}{\partial z^2}\right)^2 dz + \frac{K}{2}\left[\int_0^a \left(\frac{\partial u}{\partial z}\right)^2 dz\right]^2, \tag{2.20}$$

where D is a plate bending stiffness, and K a spring constant per unit spanwise length of panel. Substituting Eq. 2.2 into the elastic energy, Eq. 2.20, and differentiating with respect to u_r one obtains

$$\frac{\partial \mathcal{E}}{\partial u_r} = D\sum_s e_{rs}u_s + K\sum_m\sum_s k_{rms}u_m^2 u_s, \tag{2.21}$$

where

$$\begin{aligned} k_{rms} &= \int_0^a (\phi_m')^2 dx \int_0^a \phi_r'\phi_s' dx, \\ e_{rs} &= \int_0^a \phi_s''''\phi_r dx = \int_0^a \phi_s''\phi_r'' dx. \end{aligned} \tag{2.22}$$

In the last equation, an integration by parts has been used with $\phi_r = \phi_s = 0$ at $z = 0$.

We will assume that the plate is exposed to a in–plane tensile load, N_x, to a static pressure difference across the plate, ΔP, and that the exciting dynamic pressure difference is given by the quasi–steady aerodynamic theory, *i.e.*,

$$p - p_\infty = \frac{2q}{\beta}\left[\frac{\partial u}{\partial z} + \frac{M^2-2}{M^2-1}\frac{1}{v_0}\frac{\partial u}{\partial t}\right] \tag{2.23}$$

where $q = \rho v_0^2/2$ is the dynamic pressure, M is the Mach number, and $\beta = \sqrt{M^2-1}$, Bisplinghoff and Ashley (1962).

Following the conventional procedure of Lagrangian mechanics, *i.e.*, calculating the virtual work done by the external forces, combining these expressions with Eqs. 2.2, 2.18, and 2.21 one obtains

$$\begin{aligned} &s_r w v_o + b_r \dot{w} + \sum_s m_{rs}\ddot{u}_s - \sum_s w^2 m_{rs}u_s + D\sum_s e_{rs}u_s + K\sum_m\sum_s k_{rms}u_m^2 u_s \\ &+N_x\sum_s n_{rs}u_s + \frac{2q}{\beta}\left[\sum_s (u_s p_{rs} + \dot{u}_r \hat{p}_{rs})\right] = \Delta P\, p_r, \end{aligned} \tag{2.24}$$

where

$$\begin{aligned} s_r &= \rho_m \tau \int_0^a \phi_r dx, \\ b_r &= -\rho_m \tau \int_0^a x\phi_r dx, \\ m_{rs} &= \rho_m \tau \int_0^a \phi_r\phi_s dx, \\ k_{rms} &= \int_0^a (\phi_m')^2 dx \int_0^a \phi_r'\phi_s' dx, \end{aligned}$$

$$
\begin{aligned}
p_{rs} &= \int_0^a \phi_s' \phi_r' dx, \\
p_r &= \int_0^a \phi_r dx, \\
\hat{p}_{rs} &= \frac{\beta^2 - 1}{\beta^2 v_0} \int_0^a \phi_r \phi_s dx, \\
n_{rs} &= -\int_0^a \phi_s'' \phi_r dx = \int_0^a \phi_s' \phi_r' dx.
\end{aligned} \tag{2.25}
$$

In the last equation an integration by parts has been used with $\phi_r = \phi_s = 0$ at $z = 0$.

In order to put Eq. 2.24 in a dimensionless form, we introduce the following dimensionless parameters and coordinates:

$$
\begin{aligned}
& a_r = \frac{u_r}{h}, \quad \tau = t\left(\frac{D}{\rho_m h a^4}\right)^{\frac{1}{2}}, \\
& \Omega = \frac{\omega a}{v_o}, \quad \lambda = \frac{2qa^3}{\beta D}, \\
& R_x = \frac{N_x a^2}{D}, \quad P = \frac{\Delta P\, a^4}{D h}, \\
& \mu = \frac{\rho a}{\rho_m h}, \quad \alpha = \frac{Ka}{(Ka + Eh)}.
\end{aligned} \tag{2.26}
$$

Substituting $\phi_r = \sin(r\pi z/a)$ into Eq. 2.25, and the result in Eq. 2.24, the equation of motion in dimensionless matrix form reads

$$
\ddot{\mathbf{a}} + \delta \dot{\mathbf{a}} + \mathbf{G}\mathbf{a} + \dot{\Omega}\mathbf{d} + \Omega \mathbf{v} = \mathbf{p} + \mathbf{f}(a) + \gamma \Omega^2 \mathbf{a} \tag{2.27}
$$

where $\mathbf{G} = [g_{rm}]$, $\mathbf{d} = \{d_r\}$, $\mathbf{v} = \{v_r\}$, $\mathbf{p} = \{p_r\}$, $\mathbf{f} = \{f_r\}$, and

$$
\begin{aligned}
& f_r = 3(r\pi)^4 \alpha (1 - \nu^2) a_r \sum_m m^2 a_m^2, \\
& g_{rm} = 2\lambda \frac{rm}{r^2 - m^2}\left[1 - (-1)^{r+m}\right] + \left[(r\pi)^2 R_x + (r\pi)^4\right]\delta_{rm}, \\
& \delta = \left(\frac{\lambda \mu}{M}\right)^{\frac{1}{2}}, \\
& d_r = 2\frac{(-1)^r}{\pi r}\left(\frac{\beta\lambda}{\mu}\right)^{\frac{1}{2}} \frac{a}{h}, \\
& v_r = 2\frac{\beta\lambda}{\mu}\,\frac{a}{h}\,\frac{\left[1 - (-1)^r\right]}{\pi r}, \\
& \gamma = -\frac{\beta\lambda}{\mu}, \\
& p_r = 2P\frac{\left[1 - (-1)^r\right]}{\pi r},
\end{aligned} \tag{2.28}
$$

with $m,\ r = 1, \ldots, N$ for the elastic degrees of freedom. Eqs. 2.27 are a set of ordinary, nonlinear differential equations in time. The cubic type of non–linearities are of a

geometric origin associated with the occurrence of tensile stresses in the middle surface. The coupling between the rigid–body rotation of the frame of reference and the elastic degrees of freedom is represented by the fourth term. Note that by assuming $\Omega = 0$ Eqs. 2.27 properly reduce to a classical panel flutter equations, see Bolotin 1963, or Dowell 1966, for example. This set of equations have been solved by a direct numerical integration.

SECTION 3
ANALYSIS OF NONLINEAR SYSTEMS

In this section we introduce the main ideas behind the modern theory of nonlinear systems or, more precisely, the qualitative theory of differentiable dynamical systems. Our goal is to provide sufficient information to the reader who is not familiar with a subject in order for him to be able to follow the interpretation of phenomena appearing during the numerical experimentation. Readers desiring more detailed discussion in nonlinear dynamical systems should consult books such as Berge, Pomeau, and Vidal (1984), Holden (1986), Moon (1987). Readers looking for the more rigorous formulations should consult books such Guckenheimer and Holmes (1983), Anosov and Arnold (1988), or Arnold (1989).

It should be emphasized that, during the last decade there has been an increased interest in the mathematics of chaotic dynamics. The literature is quite extensive and a review is not attempted here. However, the book on chaos by Hao Bai-Lin (1984) should be mentioned: it includes an introduction as well as reprints of several important publications on chaos (fortyone papers), and over five hundred references.

3.1 Classical Nonlinear Dynamics Theory

In this subsection, a brief review of nonlinear vibration theory is presented. The idea is simply to define and review the basic concepts of classical nonlinear vibration, so that we may later be able to contrast these with the concepts of the modern theory of nonlinear systems.

3.1.1 Vector Fields, Differential Equations

Consider a real, finite dimensional, linear space $V = R^n$. A vector field, defined in a domain U of the space V, is a map which associates to each point $\mathbf{x} \in U$ a vector $\mathbf{v}$, based at $\mathbf{x}$, in the space V. The equation

$$\dot{\mathbf{x}} = \mathbf{v}(\mathbf{x}, t), \quad \mathbf{x} \in U \subset V, \tag{3.1}$$

is called the differential equation corresponding to the vector field $\mathbf{v}$. In Eq. 3.2 the following notation has been used $(\dot{}) = d(\ )/dt$, and the variable t is called "time". If the right hand side is time independent

$$\dot{\mathbf{x}} = \mathbf{v}(\mathbf{x}), \tag{3.2}$$

the differential equation is called autonomous[1].

[1] Note that the terms "autonomous" and "time" in the above definitions came out of physics; for instance, the evolution law of a physically autonomous system (*i.e.*, a system which does not interact with other systems), does not usually depend on time

The domain U is called the phase space of this equation, and $\mathbf{x}(t)$ is the state vector. A system of differential equations such as 3.1 or 3.2 is called a flow in the domain U.

Often we are given an initial condition $\mathbf{x}(0) = \mathbf{x}_0 \in U$ and we seek a solution $\mathbf{x}(\mathbf{x}_0, t)$ or simply $\mathbf{x}(t)$ which satisfies 3.1 or 3.2. An integral curve of a differential equation is the graph of a solution; a phase curve or trajectory or orbit is the projection of an integral curve on the phase space along the t–axis.

One wishes to analyze the evolution of arbitrary physical systems described by the differential equations 3.1, or 3.2. The objective of the analysis is to characterize in broad outline the critical aspects of system behavior, not the details. These critical aspects are discussed below.

3.1.2 Dissipative Systems

Let $\mathbf{v}$ be a vector field. If div $\mathbf{v} \equiv 0$, then the phase flow of Eq.3.2 preserves volume. If div $\mathbf{v} < 0$ everywhere in the phase space, then the phase space flow decreases volume as time increases (*i.e.*, the volume corresponding to a set of points at $t = 0$ decreases it time). In this case the equation is said to be dissipative.

Note that contraction of the volume can be obtained by reduction of all lengths, or by a decrease of some of the lengths, accompanied by the less rapid increase of other lengths. This remark is important for showing that divergence of phase trajectories in some direction remains possible, even in a dissipative system. Knowledge of the way in which the decreasing of the volume takes place, and of the speed at which it occurs are essential for a complete dynamical description.

3.1.3 Singular Points

The concept of an singular point, which was used extensively in linear dynamic systems, carries over directly to nonlinear dynamic systems.

A singular point of a vector field $\mathbf{v}$ is a point at which the vector field vanishes. A singular point of a differential equations 3.1, or 3.2 is a singular point of the corresponding vector field $\mathbf{v}$.

The singular points of a differential equation are sometimes called equilibrium points.

Since equilibrium points are solutions to nonlinear equations, finding such solutions is somewhat more of an accomplishment than for the linear case. Furthermore, the equilibrium points distribution may be more complex than for a linear case; the system may have none, one, or more equilibrium points and they may be in any pattern in phase space.

Ultimately, however, as in the linear case, interest centers not just on the existence of equilibria, but also on their stability properties.

The problem of stability depends on whether the system is dissipative or conservative. We will deal with the dissipative systems only.

3.1.4 Stability

Let $\mathbf{x}_0$ be a singular point of a vector field $\mathbf{v}$. A stationary solution of an autonomous differential equation 3.2 (*i.e.*, a solution whose image is an equilibrium point) is said to be Lyapunov stable if all solutions of the equation, with initial conditions in a sufficiently small neighborhood of the equilibrium point, are defined for all $t \geq 0$ and converge uniformly (with respect to time) to the stationary solution as the initial conditions tend to the equilibrium point, Fig. 2.a.

A stationary solution is said to be asymptotically stable if it is Lyapunov stable and if, in addition, all solutions with initial conditions sufficiently close to the equilibrium point under consideration tend to this equilibrium point as $t \to \infty$.

A stationary solution is marginally stable if it is stable but not asymptotically stable.

A solution is unstable if it is not stable.

Lyapunov stability of any solution of any differential equation (autonomous or not) is defined in similar manner. That is, the solutions for all $t \geq 0$ are required to converge uniformly to the solution in question as their initial values at $t = 0$ tend to the initial value of the solution in question.

According to the basic definitions, stability of a stationary solution is a local property of the vector field (defining the differential equation) at the corresponding equilibrium point. Therefore, to conduct an analysis of stability it is often theoretically legitimate, and mathematically convenient to replace full nonlinear description 3.2 with the linear approximation at the singular point.

3.1.5 Linearization and Stability

Let $\mathbf{x}_0$ be a singular point of a differentiable vector field $\mathbf{v}$, and let $\mathbf{A}$ be the Jacobian matrix of the vector field $\mathbf{v}$

$$\mathbf{A} = [a_{ij}], \qquad a_{ij} = \frac{\partial v_i}{\partial x_j}(\mathbf{x}_0). \tag{3.3}$$

The equation

$$\dot{\mathbf{x}} = \mathbf{A}\mathbf{x}, \tag{3.4}$$

is called the linearization of Eq. 3.2 at the singular point $\mathbf{x}_0$. A singular point of a vector field is said to be non–degenerate if the Jacobian matrix is nonsingular at this point. The field $\mathbf{A}\mathbf{x}$ is called the linear part of the field $\mathbf{v}$ at $\mathbf{x}_0$.

If all the eigenvalues of the linear part of a vector field $\mathbf{v}$ at a singular point have negative real part, then the singular point $\mathbf{x}_0$ is asymptotically stable for the nonlinear system. If at least one eigenvalue has a positive real part, the singular point is not Lyapunov stable. If any one of the eigenvalues has zero real part, then stability cannot be determined by linearization.

We say that a singular point is hyperbolic if the linear part of the vector field v has no eigenvalue with real part zero. A hyperbolic singular point is either unstable or asymptotically stable.

If all eigenvalues of the linear part of a vector field v at a hyperbolic singular point have negative real parts, the singular point is called a sink; if they are all positive the singular point is a source. If both signs occur, the singular point is a saddle point.

3.1.6 Cycles

It is well known that in a physical system whose law of evolution does not change in time, periodic regimes may be established. A mathematical description of these phenomenon is given by the theory of cycles developed by H. Poincarè.

A closed phase curve of some flow in U, arising from a nonlinear vector field v, is called a cycle. Choose a point A on the curve and draw a local cross section $\Sigma \subset U$, of dimension $n-1$, where n denotes the dimension of the phase space, Fig. 2.b. The hypersurface, Σ must be chosen so that the flow is everywhere transverse to it, *i.e.*, $\mathbf{v}(\mathbf{x}) \cdot \mathbf{n}(\mathbf{x}) \neq 0$ for all $\mathbf{x} \in \Sigma$, where $\mathbf{n}(\mathbf{x})$ is the unit normal to Σ at $\mathbf{x}$. Phase curves which start at points of Σ sufficiently close to the original point of the cycle return to Σ. Thus we obtain a set of points around A corresponding to the starting points. This relationship defines a map of Σ into itself which is called first return map or Poincarè map.

The mathematical study of such maps is similar to that for differential equations. One can find equilibrium points of the map and one can classify these equilibrium points by the study of linearized maps about the equilibrium points.

It is apparent that the point A on the cycle is an equilibrium point of the Poincarè map, and that the stability of an equilibrium point for the Poincarè map reflects the stability of closed phase curve for the flow. Furthermore, Poincarè maps have the same kind of topological properties as the flow from which they arise. For example if the flow, Eq. 3.2, is dissipative, so that volumes in the phase space are contracted, then the map contracts areas in the plane Σ.

A closed phase curve is called a limit cycle if the fixed point of the corresponding first return map is isolated.

Multipliers of a cycle are defined to be the eigenvalues of the linear part of the first return map at the fixed point corresponding to the cycle.

A cycle is said to be Lyapunov (orbitally) if, for an arbitrarily small neighborhood C of the cycle, all trajectories which start in a sufficiently small neighborhood of the cycle do not emerge from C.

A cycle is said to be Lyapunov asymptotically stable if it is Lyapunov stable, and if all the phase curves with initial condition sufficiently close to the cycle approach the cycle asymptotically as $t \to \infty$.

If the modulus of every multiplier of a cycle is less then one, then the cycle is Lyapunov asymptotically stable.

3.2 Chaos in Dissipative Systems

In this subsection we will define the different types of time–evolution of a dissipative systems, including those which at first seem totally disordered, chaotic.

3.2.1 Asymptotic Behavior of a Dissipative System, Attractors

Consider an autonomous dissipative system in the phase space U. By definition of dissipative system, the phase space flow decreases volume as time increases. Continued decreasing of volume in phase space means that as $t \to \infty$ the phase curves of an evolutionary process get closer and closer to a compact set $M \subset U$, the attractor. Motions starting in some volume of phase space, the basin of attraction for the attractor, can follow complicated transients but, as $t \to \infty$, they finally approach the attractor. The attractor M is invariant under the flow; any motion on the attractor is confined to the attractor. There is not transient motion on the attractor; all transients in a dissipative system are in the basin of attraction of an attractor on the approach to an attractor, and are not on attractors.

Asymptotically stable singular points and Lyapunov asymptotically stable cycles are particular cases of attractors.

3.2.2 Strange Attractors

A strange attractor is an attracting set that is not a singular point nor a periodic cycle, and for which almost all solutions display sensitive dependence on initial conditions. Thus a trajectory asymptotic to a strange attractor M rapidly approaches the subset $M \subset U$ but thereafter wanders erratically about the "surface" of M.

3.2.3 Characterising the Attractors

There are several ways to identify and to characterize the nature of a dynamical regime. We will explain here the power spectrum method used latter during numerical experimentation.

Let $\mathbf{v}$ be a nonlinear vector field in the domain U. Let $x(t)$ be a component of the state vector $\mathbf{x}$. Note that numerical simulation generally provides a discrete sequence of real numbers $\{x_j\}$, $j \in Z$ regularly spaced at time intervals Δt. In practice this sequence of numbers is necessarily finite; suppose that we have N consecutive sampled values. We define the Fourier transform of a discrete time series $\{x_j\}$ to be the operation creating a corresponding discrete series $\{X(\omega_k)\}$ such that

$$X(\omega_k) = \sum_{j=1}^{N} x_j e^{-i\omega_k j}, \tag{3.5}$$

over discrete set of frequencies

$$\omega_k = \frac{2\pi k}{N}, \quad k = -N/2, ..., N/2. \tag{3.6}$$

The power spectrum of x_j for $j = 1, ..., N$ is defined as

$$P_N(\omega_k) = K|X(\omega_k)|^2, \tag{3.7}$$

where K is a scale factor, see Priestley (1981) for details,[2].

Having defined the discrete Fourier transform and power spectrum of the discrete series, we return to the explanation of a relationship between the nature of the series and the form of its power spectrum.

In essence, the spectrum of a periodic series of period T is made up of a peak at the frequency $1/T$. A quasiperiodic sequence has r fundamental frequencies ω_j, $j = 1, ..., r$; its Fourier spectrum contains components at all frequencies of the form

$$|\omega_1 m_1 + \omega_2 m_2 + ... + \omega_r m_r|, \tag{3.8}$$

where m_j are arbitrary integers. When the series is neither periodic nor quasiperiodic, it is called aperiodic, the Fourier spectrum is then continuous.

3.2.4 Pseudo–Definition of Chaos

Given that no precise scientific definition exists for the noun "chaos" or for the adjective "chaotic", we will consider these words to be synonymous with certain properties. Following Berge, Pomeau, and Vidal (1984), we will say that the dynamical regime is chaotic if its power spectrum contains a continuous part–a broad band–regardless of the possible presence of the peaks.

The real difficulty is that a power spectrum that looks continuous cannot be automatically attributed to an chaotic regime because this is also the appearance of the spectrum of a quasiperiodic regime with a very high number of frequencies.

The definition is pragmatic; it lacks rigor and contains unavoidable ambiguities.

3.3 Bifurcation Theory–Ways in Which Chaos Appears

So far we have been dealing with an individual systems, and now let us consider systems whose behavior, expressed in terms of state vector $\mathbf{x} \in U$ is in some way controlled by external variables. The latter are collected in a control parameter μ; one can often take $\mu \in R^m$. The family of differential equations

$$\dot{\mathbf{x}} = \mathbf{v}_\mu, \quad \mathbf{x} \in U \subset R^n, \quad \mu \in R^m, \tag{3.9}$$

[2]Note that the fast Fourier transform algorithm has been used to compute the discrete Fourier transform during the numerical simulation.

generates a flow or vector field on U.

The state space in this case can be pictured as filled with flow lines defined by Eq. 3.9 which approaches the attractors in U as $t \to \infty$; there may also be saddle type solutions in U. The structure of the collection of attracting sets $\mathcal{A}$ in U is clearly important; one may wish to know what qualitative solution types can exists and in particular to classify the ways in which $\mathcal{A}$ might change with μ (as $\mathbf{v}_\mu$ changes). Qualitative changes in $\mathbf{v}_\mu$ are referred to as bifurcations.

3.3.1 Structural Stability

It may be helpful, before discussing bifurcations, to give a working definition of structural stability and codimension.

A vector field is structurally stable if its qualitative structure is not destroyed by a small perturbation in $\mathbf{v}_\mu$.

It is clear that a vector field possessing a non-hyperbolic fixed point cannot be structurally stable, since a small perturbation can remove it (if the linearized matrix is noninvertible, having a zero eigenvalue), or turn it into a hyperbolic sink, a saddle, or a source (if the matrix has purely imaginary eigenvalues). Similar observations apply to periodic orbits and we conclude: if the flow is structurally stable all fixed points and closed orbits must be hyperbolic. This is a necessary but not sufficient condition to guarantee structural stability, since some global effects also come into play. For example, in the case of a structurally stable system on the plane, besides the above conditions there must also be no orbits connecting saddle points.

The codimension of a bifurcation will be the smallest dimension of a parameter space which contains the bifurcation in a persistent way.

Let us illustrate this concept in a three–dimensional parameter space ($m = 3$). The locus of points in parameter space where some condition is satisfied, say change of stability of a solution, is generally a surface Σ. Almost any line D (dimension one) crosses this surface; by moving along D, we eventually intersect Σ and observe the corresponding bifurcation. Thus we say that the bifurcation is of codimension one. If we have two conditions, these will both be verified only along the line of intersection L of the two surfaces Σ_1 and Σ_2 associated with the two conditions. An arbitrary line has no chance of intersecting L; we must move along a surface (dimension two) to cross a line of bifurcations. This is an example of the codimension two bifurcation.

What we have just said for $m = 3$ can be generalized to any other value of m simply by replacing the words: space, surface, etc., by hyperspace, hypersurface, etc. In a sense the codimension of a degenerate fixed point (limit cycle, etc.) describes its degree of structural stability; hyperbolic fixed points are of codimension 0. The higher the codimension the more varied and complex are the ways in which the singularity can unfold in response to perturbations. To generically capture a codimension k singularity one needs a k–parameter vector field.

3.3.2 Bifurcation

A Bifurcation occurs when a vector field passes through a regime of structural instability and suffers a qualitative change. The parameter values at which this change occur are called bifurcation values.

There are two main approaches open to us, local and global analysis. Local analysis is generally performed by studying the vector field near the bifurcating equilibrium point or closed orbit, and bifurcating solutions are also found in a neighborhood of that limit set. If the dynamical properties involve global aspects of flows, they cannot be deduced from local information, and a global analysis is necessary. Note that even a study of local two–parameter bifurcations requires an understanding of global bifurcations, since they occur naturally in two–parameter families. Also note that the global combinations of local events may be extremely complex.

We will examine only local bifurcations of individual equilibria and periodic orbits referring the reader interested in bifurcations of codimension two and codimension three to more specialized articles and books.

Codimension One Bifurcations of Equilibria
Consider a flow

$$\dot{\mathbf{x}} = \mathbf{v}_\mu(\mathbf{x}), \tag{3.10}$$

on the smooth vector field $\mathbf{v}_\mu$, with $\mathbf{x} \in R^n, \mu \in R$. Assume that at $\mu = \mu_0, \mathbf{x} = \mathbf{x}_0$, Eq. 3.10 has an equilibrium point at which there is a zero eigenvalue (for the linear part of the vector field). It can be shown (The Center Manifold Theorem[3]) that the dynamic on the centre manifold is locally equivalent to one in which x is one dimensional. The possible bifurcations are represented by the following three differential equations which depend on a single parameter μ (see Table 1.).

Table 1. The local models on the centre manifolds

The local model	Name of bifurcation
$\dot{x} = \mu \pm x^2$	Saddle–node (or turning point)
$\dot{x} = \mu x \pm x^2$	Transcritical
$\dot{x} = \mu x \pm x^3$	Pitchfork

Taking the minus sign in the case of saddle–node bifurcation one immediately sees that for $\mu < 0$ there are no fixed points and that for $\mu > 0$ there are two, a saddle at $(-\sqrt{\mu}, 0)$and a sink at $(+\sqrt{\mu}, 0)$. Similar analysis is possible for other cases, and the evolution of the attractors may be pictured as in Figs. 3.a, 3.b, and 3.c.

Consider now a system given by Eq. 3.10 with a parameter value μ_0 and equilibrium $\mathbf{x}_0$ at which the linear part of vector field $\mathbf{v}_\mu$ has a simple pair of pure imaginary

[3] We have not defined or discussed the center manifold theorem because it is not relevant for the discussions later in this report other than to understand the typical bifurcations encountered. Interested readers should consult Guckenheimer and Holmes (1983), for introductions to the subject.

eigenvalues and no other eigenvalues with zero real parts. Here the local model on the centre manifold is given by

$$\begin{aligned} \dot{x}_1 &= x_2 \pm x_1[\mu - (x_1^2 + x_2^2)], \\ \dot{x}_2 &= -x_1 \pm x_2[\mu - (x_1^2 + x_2^2)]. \end{aligned} \tag{3.11}$$

Taking the plus sign one can verify that there is a spiral sink at (0,0) for $\mu < 0$ and a source at (0,0) surrounded by a limit cycle for $\mu > 0$. The limit cycle evolves continuously from the centre at (0,0) for $\mu = 0$ as μ increases, Fig. 3.d. The bifurcation is named after E. Hopf, who first classified it.

Note that, in all the cases considered, the nonlinear terms have had an effect opposite to that of the instability caused by the lower order terms. The bifurcation in this case is called supercritical (also normal). However, if the lowest–order nonlinear terms also have a destabilizing influence on the solution (alternative signs in the expressions listed above), the bifucation is subcritical or inverse. We then obtain the bifurcation diagrams presented in Fig. 4.

Codimension One Bifurcations of Periodic Orbits

The usual approach consists in computing Poincarè return maps and then in applying the results of the previous subsection for these discrete dynamical systems.

There are three ways in which a fixed point of Poincarè return maps may fail to be hyperbolic: at least one eigenvalue of the linear part of the map at the fixed point is $+1$, -1, or a pair of complex eigenvalues $\lambda, \overline{\lambda}$, with $|\lambda| = 1$.

The bifurcation theory for fixed points with eigenvalue 1 does not change very much from what has been explained for equilibria with eigenvalues 0. The one parameter family has a two–dimensional center manifold on which the dynamics is locally equivalent to either the saddle–node, transcritical or pitchfork bifurcation.

Bifurcations with eigenvalue -1 do not have an analogue for equilibria, and are associated with flip bifurcations, also referred to as period doubling or subharmonic bifurcation. Let us see what happens when an eigenvalue approaches the critical value -1 and finally attains it. Let γ be a limit cycle of period T, and let O be a fixed point of the corresponding first return map. Before the bifurcation, any displacement from O say x_0 decreases with every period, since its value x is multiplied by the negative factor of absolute value smaller than one. The limit cycle is therefore linearly stable. When the eigenvalues becomes equal to -1, the situations change. The modulus of any initial displacement x_0 is conserved while its sign changes by each intersection. We therefore see a new periodic orbit, whose period is twice that of the original orbit. Note that conditions for the stability of this period two orbits will not be considered here; interested readers should consult Guckenheimer and Holmes (1983) for details.

We now turn to the bifurcations of a periodic orbit at which there are complex eigenvalues $\lambda, \overline{\lambda}$ with $|\lambda| = 1$. Analogy with the theory of the Hopf bifurcation suggested

the name Hopf bifurcation, despite several features which distinguish the two bifurcations. The fixed point of the first return map is replaced by a set of points on a circle. The flows near the bifurcation have quasiperiodic orbits, and more subtle analysis is required to capture these, see Guckenheimer and Holmes (1983) for details.

Globalisation

Note that the essential models of bifurcation outlined above are only valid locally, *i.e.*, in some neighborhood $F \subset U$ of the bifurcating fixed point and in some neighborhood $P \subset R^m$ of the bifurcational value of the control parameter μ. If a number of distinct bifurcations occur, then one must consider problem of fitting the various local models together into an overall scheme. This problem of globalization is largely open and appears generally difficult. For more information readers are referred to Arnold (1989) or Guckenheimer and Holmes (1983).

3.3.3 Routes to Chaos

One of the main interests of current theoretical research in nonlinear dynamics is in characterizing the nature of the transition from regular periodic dynamics to irregular, chaotic dynamics. The structure of the collection of attracting sets and in particular the ways in which they might change with changing the parameter μ is difficult and largely open problem. In the case of one–parameter systems we may quote Arnold (1986) pp. 24,

> "The transition from a stable equilibrium state to a strange a'tractor can take place both by means of a jump, or after a mild loss of stability, Fig. 5. In the latter case the stable cycle which was created itself loses its stability. The loss of stability of a cycle in a generic one–parameter family of systems can take place in a number of ways: 1) collision with an unstable cycle, Fig.6, 2) doubling, Fig.7, and 3) "the birth or death of a torus," Fig. 8.

The proof of the existence of such a routes does not follow from a rigorously demonstrated theory, but rather from a combination of guesses and numerical experimentation.

SECTION 4
NUMERICAL EXPERIMENTATION

In this report numerical simulation for periodic and chaotic response are conducted in order to analyze a behavior of a fluttering panel of a maneuvering airplane. Equations 2.27 were simulated on the digital computer by using a fourth order Runge–Kutta algorithm. For all of results reported below, $\mu/M = 0.023, \nu = 0.3$, and the plate response is calculated at $z/a = 0.75$.

4.1 Response Without Maneuvering

Extensive numerical experiments were performed by varying all the parameters, for maneuvering as well as non–maneuvering conditions. Although our main interest is to study the influence of maneuvering on the panel response, here we will present some unusual non–maneuvering responses.

According to Dowell (1988) the distinctive types of motion which may occur in a phase plane $(u, \dot{u})$ (with u being the panel vertical displacement at a given point, *e.g.*, $x/c = 0.75$) are the following, see Fig. 9: (1) For a small in–plane force, R_x, a flow velocity might not be sufficiently large to disturb the zero equilibrium position, Fig. 9.a, (2) The buckled plate corresponds to two points in the phase plane. Depending on the initial conditions either one of these equilibrium positions is possible, Fig. 9.b, (3) Small R_x and moderate velocity parameter λ will give simple harmonic response, which correspond to elliptic limit cycle in a phase space, Fig. 9.c, (4) The more complicated periodic limit cycle motion is comprised of a smaller orbit about each buckled state and a larger orbit that evolves from the simple periodic motion, Fig. 9.d, (5) Finally, a chaotic response is possible.

It is interesting to note that we observed an even more complicated periodic limit cycle. For the value of the in–plane load $R_x = -4.0\pi^2$, and with the velocity parameter between $\lambda = 119.275$ and $\lambda = 120.496$, the limit cycle of the form presented in the Fig. 10 has been found. Deformed version of this limit cycle has been observed in the maneuvering case, see Fig. 20.n.

Another interesting result is related with the influence of the initial conditions. Although, our attempt was not to study the initial–condition problem, basins of attractions, or fractal basin boundaries, a certain section of initial condition space was examined. The sequence of Figs. 11.a - 11.e shows the transient from the chaotic response (Fig. 11.a, with initial condition $a_1 = 0.084$) to a simple limit cycle (Fig. 11.b, $a_1 = 0.251$), and then through a period 3 motion (Figs. 11.c and 11.d, $a_1 = 0.600$, to

1.600 back to chaos[4] (Fig. 11.e, $a_1 = 2.000$), just by changing the initial condition. Similar behavior have been observed by Moon and Li (1985) and Pezeshki and Dowell (1987) for the Duffing equation.

In order to separate the influence of the initial conditions from the maneuvering the initial conditions are taken to be the same, $\dot{a}_1 = 1.0$ (corresponding to a positive velocity of the first degree of freedom).

4.2 Character of Solution in Presence of Maneuvering

In order to understand the dynamic problem, it is helpful to think in physical terms. The buckled plate is a part of the maneuvering plane, and it is being excited by the one side airflow. Depending on the value of the load factor, and other parameters one or two fixed points may be found. The calculations show that three possible types of stable trajectories may occur. There are the two limit–cycle orbits around each of the static equilibria, and one global limit–cycle orbit around both static fixed points. Note finally, that there is also the possibility of chaotic response. Figure 12 shows selected phase–plane plots of the panel response as well as theirs power spectrum estimates. For the base case of $\lambda = 150$, and $R_x = -3.0\pi^2$, various loads factors were studied. Figure 12.a corresponds to a non–maneuvering case. The motion has non–chaotic character with three closed orbits in evidence. A load factor $n = 1.28$, transforms the response into a chaotic state (see Fig. 12.b) while a load factor $n = 3$ suppresses the periodic character of the motion, the response is a fixed point, and all motion ceases (see Fig. 12.c). The most remarkable result occurs at $n = 1.67$, when the maneuvering has suppressed one of the three orbits that appears for small n (see Fig. 12.d).

4.3 Deterministic Behavior

4.3.1 Convergence

It is of interest to compare results using various degrees of freedom (*i.e.*, number of modes). Such a comparison is made for the load factor $n = 2$ in Fig. 13 where the plate amplitude of the limit cycle is given as a function of λ for $\mu/M = 0.023$, $P = 0.0$, $R_x = 0.0$ for 2, 4, 6, and 8 modes. For six modes of freedom the solution appears converged, whereas with only two modes the results are inaccurate. That is why the most of the calculations presented here has been performed using six degrees of freedom. Also shown in Fig. 13 are non–maneuvering results for 2 and 4 modes. Similar behavior of the convergence process is evident.

4.3.2 Effect of Load Factor

In Fig. 14 the panel amplitude of the limit cycle is given as a function of λ for several load factors n. For aeronautical applications n is typically in the range $1 \div 6$. Several

[4] Word of caution is appropriate here: the responses in the Figs. 11.a and 11.e might as well be quasiperiodic

trends are evident. First, the flutter speed increases with n, (*i.e.*, the linear solution is stabilized by the presence of the load factor). Secondlly, the amplitude is increasing with increasing the load factor. As might be expected on physical grounds, calculations show an increase of the mean amplitude with increasing the load factor. For the relatively large n the response is a fixed point; the given flow velocity is not large enough to disturb the static equilibrium shape (see also Fig. 12.c). Note that increasing the load factor is related to the increase of the static pressure P, which has a destabilizing effect. Such interaction is investigated in the preceding subsection.

4.3.3 Effect of Static Pressure Differential

Another parameter of interest is the uniform static pressure differential across the plate. In the absence of maneuvering, the plate would deform to some static equilibrium position under the pressure differential. With maneuvering, the inertial forces due to maneuvering would decrease the deformation of the plate due to static pressure differential. For sufficiently large flow velocity, this equilibrium position becomes unstable. The plate then begins to oscillate about an unstable equilibrium shape, eventually reaching a new stable dynamic equilibrium shape (a limit cycle).

The results of the analysis of the influence of pressure differential to the amplitude of panel response, for a given load factor $n = 3$, are presented in Figs. 15, and 16. In Fig. 15 the amplitudes of the periodic response are plotted as function of dynamic pressure λ, for several (nondimensional) pressure differentials P. It is apparent that the flutter speed decreases with increasing the static pressure differential. Furthermore, the amplitudes are slightly decreasing with the increasing of the static pressure. In Fig. 16 the mean value of the amplitudes of the limit cycle oscillation are plotted as function of dynamic pressure. For the given load factor $n = 3$, increasing of the static pressure differential is related to increasing the mean amplitude of the limit cycle oscillations.

In Fig. 17 the influence of the maneuvering to the maximum and minimum values of the plate deflection is given. The static pressure differential was constant, $P = 60$, during this analysis. The presence of the maneuvering is related to decreasing of the plate deformation caused by static pressure differential. For the critical value of the parameter $\lambda = 361$ in the non-maneuvering case, and $\lambda = 353$ in the maneuvering case, a supercritical bifurcation occurs. The fixed point in the parameter space bifurcate and the new simple harmonic limit cycle motion, with zero amplitude at the bifurcation point, is created. Note that in the range $\lambda = 353 \div 361$ the presence of the maneuvering changes the character of the response in the phase space, from a fixed point ($n = 1$), to a limit cycle ($n = 2$).

4.3.4 Effect of In-Plane Loading

In this subsection combined influence of the maneuvering and in-plane loading has been studied. Results are presented in Fig. 18. The plate amplitude is shown vs dynamic pressure, λ, for several load factors, $n = 1, 2$, and 3, and in-plane load $R_x = -3/2\pi^2$.

For a small flow velocities λ there are two branches to the curve associated with buckled configurations. Depending on the initial conditions either one of these nonlinear equilibrium positions is possible. With maneuvering, the upper buckled position appears only for very small λ. For a given $R_s = -3/2\pi^2$, with increasing the flow velocity the solution is stable fixed point in parameter space. Since this point is stable, it is an attractor. The changing in the nature of the stable solution occurs for the critical parameter value $\lambda_c = 228$ for the non–maneuvering $n = 1$, and $\lambda_c = 230$ and 233 for the maneuvering conditions $n = 2$ and 3 respectively, through a supercritical or normal bifurcation. The new simple harmonic limit cycle motion with a zero amplitude at the bifurcation point is created. It is apparent that increasing of the load factor is related to increasing the critical parameter value λ at the bifurcation point.

4.4 Routes to Chaos

In the following we will discussed how the maneuvering transforms the response from the steady state regime to the chaotic regime. The attempt is to answer the question how is a chaotic regime established. For the base case of $\lambda = 150$, and $R_s = -3.0\pi^2$, load factor was varied from the non–maneuvering response to a value for which the response is a fixed point. The time step was 0.0025 (nondimensional time), the number of time steps were 60,000, and every other time step from the last 10,000 time steps has been plotted. Near the bifurcation points where achieving a steady state solution requires many cycles the longer time interval, 90,000 time steps, has been used to avoid the transient regime. In order to decrease possibility of mixing the numerical instabilities with the chaotic behavior of the system the representative cases were recalculated with a time steps of 0.001, and 0.0005. Figures 20.a to 20.r (discussed in details in the following subsections) shows the phase portraits of distinct attractors together with the power spectrum plots discovered during the numerical experimentation. Time traces of selected responses are shown in Fig. 21.

4.4.1 Intermittency and Transient Chaos

We begin with the non–maneuvering ($n = 1$) response shown in Figs. 20.a, and 21.a. The motion has nonchaotic character with three closed orbits in evidence. For the maneuvering case up to $n = 1.66$, we see what appears to be a chaotic response. The power spectrum shows large fundamental frequency components accompanied by a less broad band noise than that for the true chaotic response, see Figs. 20.b and 20.c. Furthermore, the time traces show the periodic motion with a short bursts of chaotic transient, see Fig. 21.c. All this suggest that this is a region of transient chaos. By the value of the load factor $n = 1.67$, a new stable attractor appears (see Fig. 20.d). This trajectory experiences a cascade of period–doubling bifurcations culminating in chaos. This process is discussed in following subsection.

4.4.2 Period–Doubling Bifurcation

A period doubling bifurcation is easily seen for $n = 1.83$ (see Fig. 20.e) and is well established for $n = 1.90$ (see Fig. 20.f). The usual splitting of the trajectory is seen in the phase portrait. The spectrum also shows the bifurcation with the presence of new spectral lines. The new spectral lines show that the period has now doubled. Increasing n further causes the previous pattern to repeat; a splitting of each of the previous harmonic bands into two bands as shown in Fig. 20.g. One anticipates that by continuing to increase n, the same phenomenon will be repeated. We expect to see a cascade of bifurcation, each accompanied by the period doubling associated with a subharmonic instability, leading to chaos. The numerical calculations support this anticipation, showing the chaotic response for $n = 2.02$.

4.4.3 The Inverse Cascade and More Chaos

We have seen that the approach to chaos via period doubling is a highly structured process. One element of order, to be observed in Figs. 20.i thru 20.k, is the existence of normal period demultiplying bifurcations, culminating in another new limit cycle, see Fig. 20.k.

Further increase in n cause the region, $n = 2.44 - 2.97$, of the chaotic response to occur. An unexpected limit cycle (at $n = 2.66$, Fig. 20.n) appears in an island bounded by chaos on both sides, (Figs. 20.l thru 20.q). Uppon further examination one may conclude that this is basically the new limit cycle discovered in the non–maneuvering case (see Fig. 10), after the maneuvering has suppressed one of the orbits.

Finally, when a load factor reaches $n = 3.00$ the inertial forces suppress the chaotic character of the motion, the response is a fixed point, and all motion ceases, see Fig. 20.r. As n continues to increase, the deflection of the plate increases

4.5 Nonautonomous Equations

In the case when the angular velocity of maneuvering is a given function of time, the differential equations, Eq. 2.27, are nonautonomus and they will be briefly considered in this subsection. We are considering an airplane in a pull-up maneuver during the time interval $t_1 - t_2$. The angular velocity is given by $\omega = \omega_0 \sin(\alpha t)$, with $\alpha = \pi/(t_1 - t_2)$. Under these assumptions, the angular velocity at the beginning and at the end of the maneuver is equal to zero (see Fig. 22). As might be expected on physical grounds, our calculations show a disturbance of the limit cycle by the inertial forces due to maneuvering. After the completion of the maneuver the panel returns to its previous motion. Phase plane response of the panel is given in the Fig.23.

In some regions of the initial condition space one may expect more dramatic changes of the dynamical behavior due to time dependent maneuver, especially close to the boundaries of the basin of attraction. It is clear that this study has to be related to the analysis of the influence of initial conditions. This may be a subject of future research.

SECTION 5
CONCLUDING REMARKS

A general geometrically–exact Lagrangian mechanics formulation for the aeroelastic analysis of a maneuvering aircraft has been specialized to the case of a fluttering plate undergoing a pitching maneuver. The formulation includes geometric non–linearities associated with the occurrence of tensile stresses in the middle surface, as well as the effect of the rigid–body rotation on the other degrees of freedom. The general response of the system were simulated on the digital computer by using a fourth–order Runge–Kutta algorithm with adaptive step size control. Long–time histories, three–dimensional view of orbits, phase planes, and power spectra have been used to characterize the response.

We have chosen system parameters such that there are two equilibrium position for the non–maneuvering case. The numerical simulation for periodic and chaotic response are conducted in order to analyze the influence of the maneuvering to the dynamic behavior of the panel. Several important conclusions derive from the preceding work. A new type of limit cycle has been observed in the non–maneuvering case. It was shown that chaos could occur in a maneuvering case for system parameters in the actual flight range. The presence of a load factor n can transform the response from the fixed point into a simple periodic or even chaotic state. It can also suppress the periodic character of the motion, transforming the response into a fixed point, and all motion ceases. Regions of the chaotic motion with an island of non–sinusoidal periodic motion has been observed. When $n = 1.83$ we observed a cascade of period–multiplying bifurcations, culminating in chaos, followed by a series of period–demultiplying bifurcations as the system returns to a starting limit cycle response. The region of intermittent and transient chaos has been observed as well.

The numerical experiments were performed with a different time simulation length in order to ensure that the steady state response has been reached and the transient has decayed. Furthermore, the calculations were performed with various step size. The results were in good agreement and showed that for a sufficiently small time step, no numerical instability occurred and the results for the time simulation were closely reproducible.

The results indicate that the study of this deterministic system is important from the practical, and theoretical viewpoint. First, the fact that maneuvering can change the character of the panel response is of practical interest to the aeroelasticians as it affects, for instance, fatigue analysis. Secondlly, the techniques employed in this study can be extended to the problem of aeroelasticity of aircraft (with all non–linearities geometric, dynamic, and aerodynamica included). From the theoretical point of view, this physical

system is a rich source of static and dynamic instabilities and of associated limit–cycle motions and it could be used for instance as a test case for assessing techniques for the study of nonlinear dynamics and chaos.

Subjects for the consideration in future research include the use of other stability concepts such as Liapunov exponents, and Poincare maps. Application of a complementary methods of differentiable dynamics, in particular, of center manifold and bifurcation theory, to analyze the problem from a qualitative viewpoint would be helpful. Knowledge of the generic structures of attracting sets in N–space, might make the interpretation of numerical solutions of evolution equations considerably clearer.

REFERENCES

Anosov, D. V., and Arnold, V. I., (1988), *Dynamical Systems I*, Springer–Verlag.

Arnold, V. I., (1986), *Catastrophe Theory*, Springer–Verlag.

Arnold, V. I., (1989), *Dynamical Systems V*, Springer–Verlag.

Ashley, H., (1974), *Engineering Analysis of Flight Vehicles*, Addison-Wesley.

Baillieul, J., and Levi, M., (1987), "Rotational Elastic Dynamics", Physica 25D, North-Holland, Amsterdam.

Berge, P., Pomeau, Y., and Vidal, C., (1984), *Order Within Chaos*, John Wiley&Sons.

Bispilghoff, R. L., and Ashley, H., (1962), *Principles of Aeroelasticity*, Dover.

Bolotin, V. V., (1963), *Nonconservative Problems of the Theory of Elastic Stability*, Pergamon Press.

Dowell, E. H., (1966), "Nonlinear Oscillations of a Fluttering Plate", AIAA Journal, Vol. 4, No. 7, pp. 1267-1276.

Dowell, E. H., Ilgamov, M., (1988), *Studies in Nonlinear Aeroelasticity*, Springer–Verlag.

Dowell, E. H., and Pezeshki, C., (1986), "On the Understanding of Chaos in the Duffing's Equation Including a Comparison with Experiment", Journal of Applied Mechanics, 52, pp. 949-957.

Guckenheimer, J., and Holmes, P., (1983), *Nonlinear Oscillations, Dynamical Systems, and Bifurcations of Vector Fields*, Springer–Verlag.

Hao Bai–Lin, (1984), *Chaos*, World Scientific Publishing Co Pte Ltd.

Holden, A. V., (1986), *Chaos*, Princeton University Press.

Holmes, P. J., (1979), "Nonlinear Oscillations, Dynamical Systems and Bifurcations of Vector Fields", Phil. Trans. Roy. Soc. A, Vol. 292, pp. 419-448.

Holmes, P. J., and Marsden, J., (1981), "A Partial Differential Equation with Infinitely Many Periodic Orbits: Chaotic Oscillations of a Forced Beam", Archives for Rational Mechanics and Analysis", Vol. 76, pp. 135-166.

Moon, F. C., (1987), *Chaotic Vibrations*, John Wiley&Sons.

Moon, F. C., and Li, G. -X., (1985), "Fractal Basin Boundaries and Homoclinic Orbits for Periodic Motion in Two-Well Potential", Physical Review Letters, Vol. 55, No. 14, pp. 1439-1442.

Morino, L., and Baillieul, J., (1988), "A Geometrically-Exact Non-Linear Lagrangian Formulation for the Dynamic Analysis of Flexible Maneuvering Aircraft", Technical Report 88-1, Boston University.

Pezeshki, C., and Dowell, E. H., (1987), "An examination of Initial Condition Maps for the Sinusoidally Excited Buckled Beam Modeled by the Duffing's Equation", Journal of Sound and Vibration, Vol. 117(2), pp. 219-232.

Priestley, M. B., (1981), *Spectral Analysis and Time Series*, Academic Press.

Zavodney, L. D., and Nayfeh, A. H., (1988),"The Response of a Single–Degree–of–Freedom System With Quadratic and Cubic Non-Linearities to a Fundamental Parametric Resonance", Journal of Sound and Vibration, Vol. 120(1), pp. 63-93.

Zavodney, L. D., Nayfeh, A. H., and Sanchez, N. E., (1989),"The Response of a Single–Degree–of–Freedom System With Quadratic and Cubic Non-Linearities to a Principal Parametric Resonance", Journal of Sound and Vibration, Vol. 129(3), pp. 417-442.

ACKNOWLEDGEMENTS

Research sponsored by the Air Force Office of Scientific Research (AFSC), under Contract No. F49620-86-C-0040. The United States Government is authorized to reproduce and distribute reprints for governmental purposes notwithstanding any copyright notation herein. The authors wish to thank Dr. Anthony K. Amos of the Air Force Office of Scientific Research, Mr. Carey S. Buttrill of NASA Langley Research Center, and Professor Gvido Sandri of Boston University for the valuable discussions on this work.

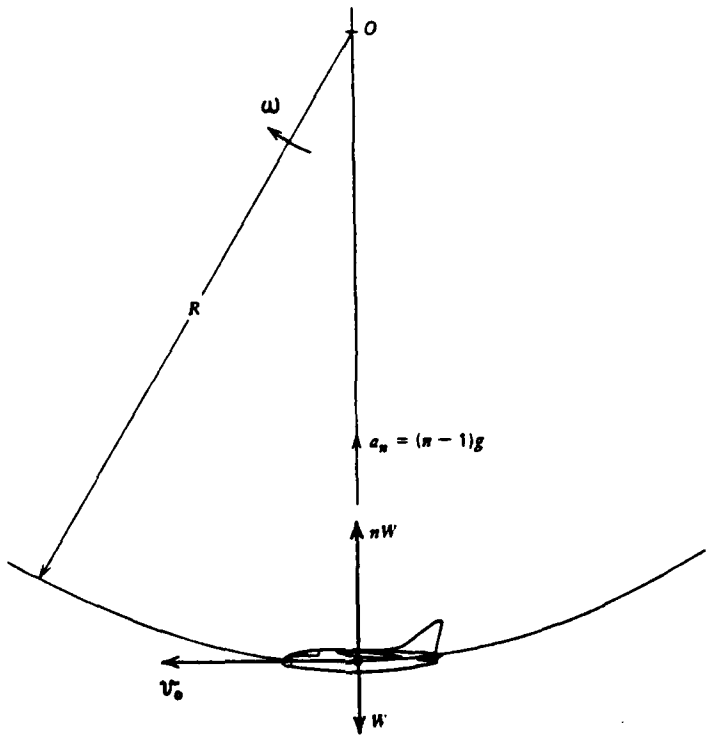

Figure 1(a) Airplane in a pull–up

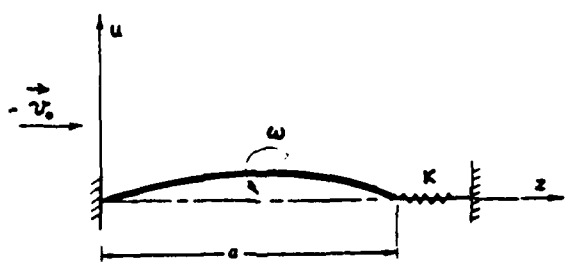

Figure 1(b) Buckled plate of a maneuvering airplane

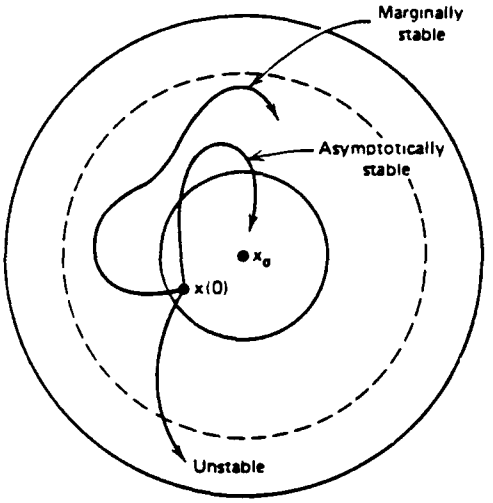

Figure 2(a) Stability

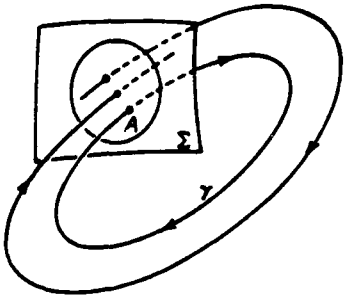

Figure 2(b) First-return map

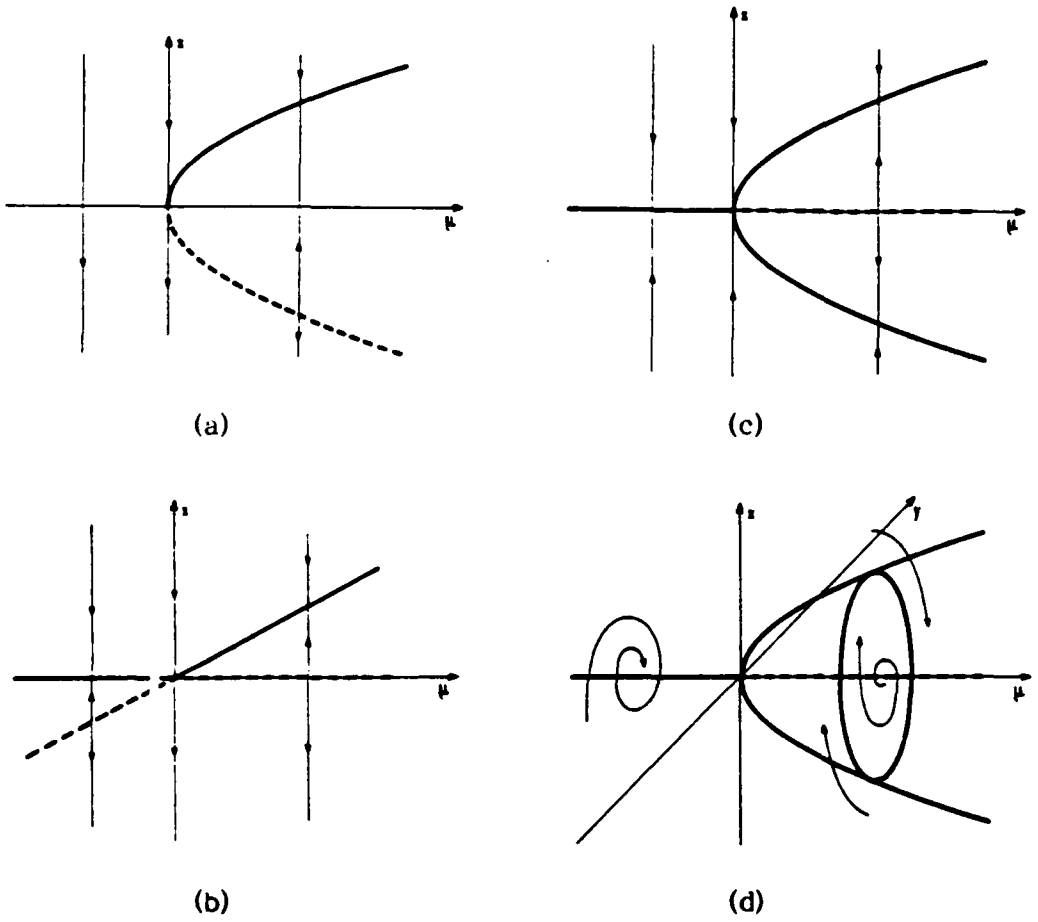

Figure 3. Diagrams of supercritical bifurcations
a) Saddle-node
b) Transcritical
c) Pitchfork
d) Hopf

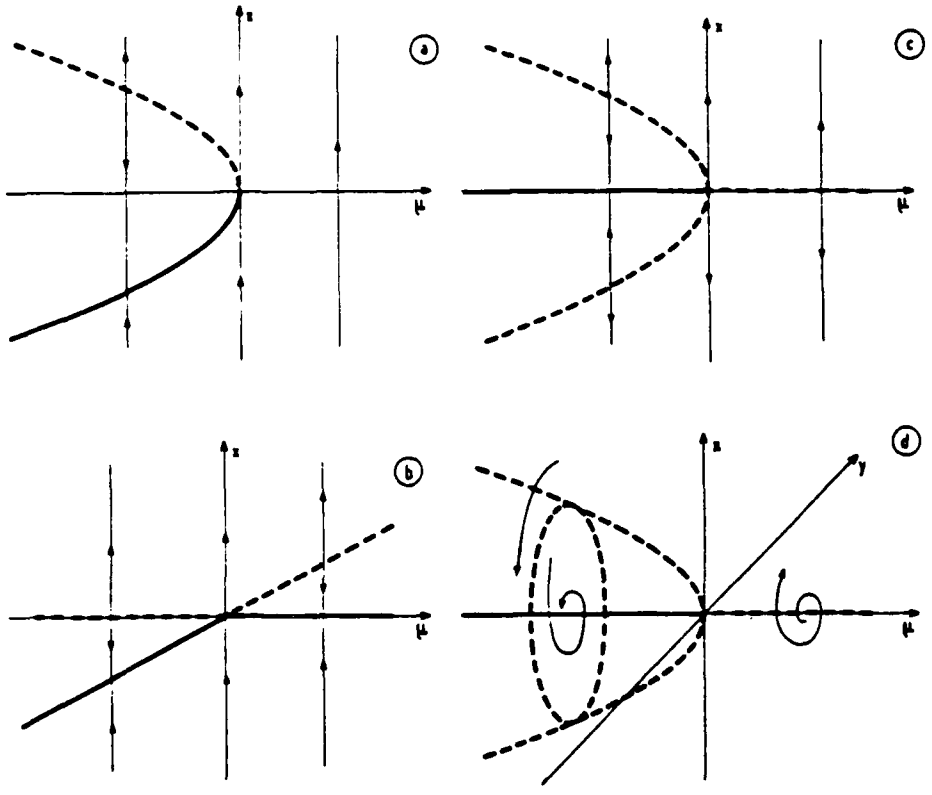

Figure 4. Diagrams of subcritical bifurcations
a) Saddle-node
b) Transcritical
c) Pitchfork
d) Hopf

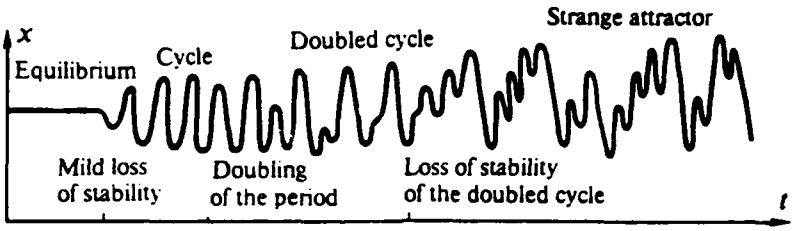

Figure 5. Transition from a stable equilibrium to a strange attractor

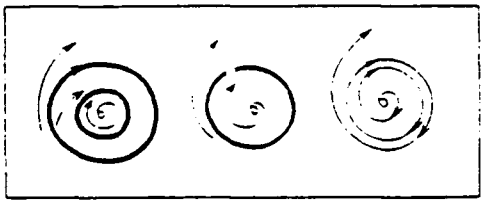

Figure 6. Collision

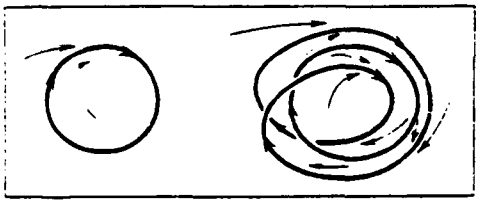

Figure 7. Doubling

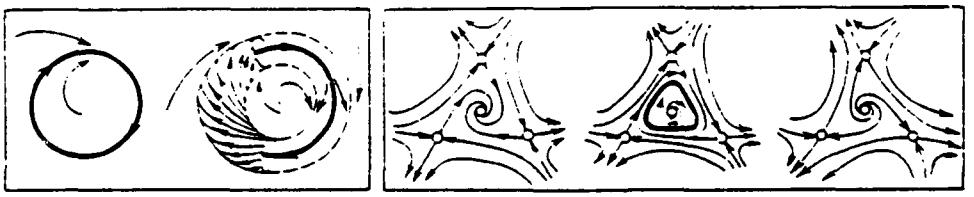

Figure 8. Birth or death of a torus

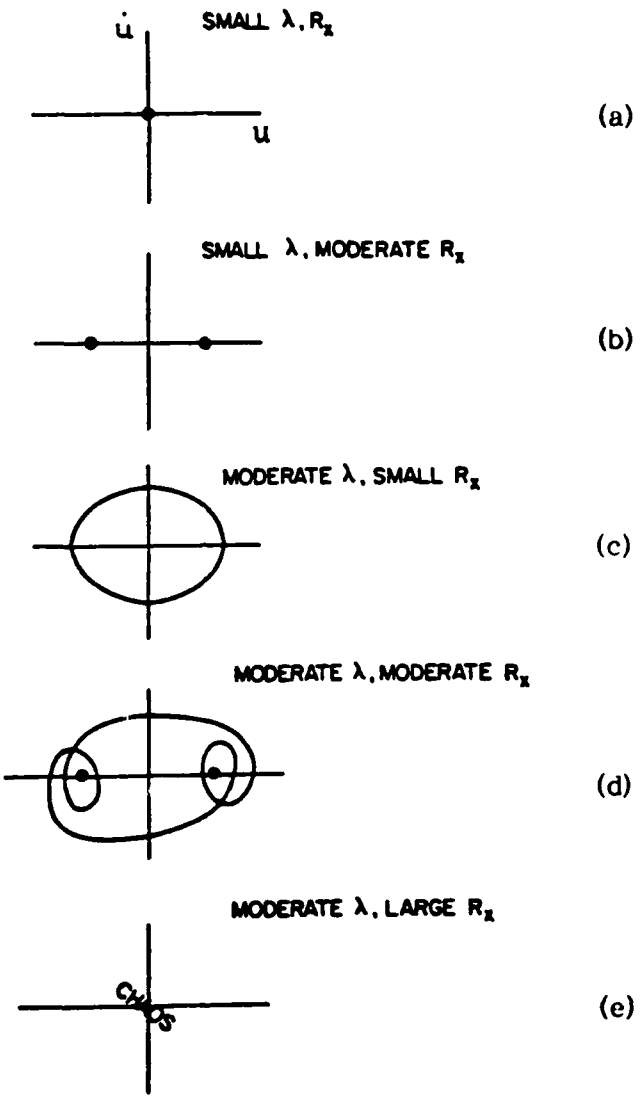

Figure 9 Sketch of representative phase plane orbits

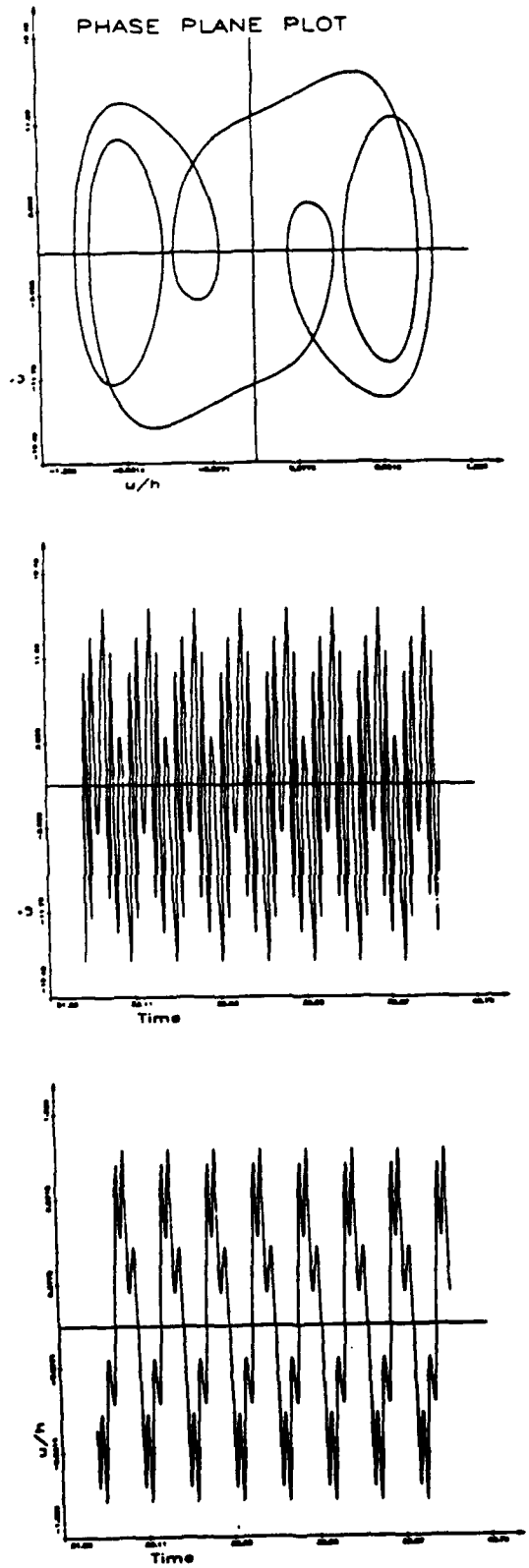

Figure 10 New more complicated limit cycle response for $\lambda = 119.5$, and $R_a = -4.0\pi^2$

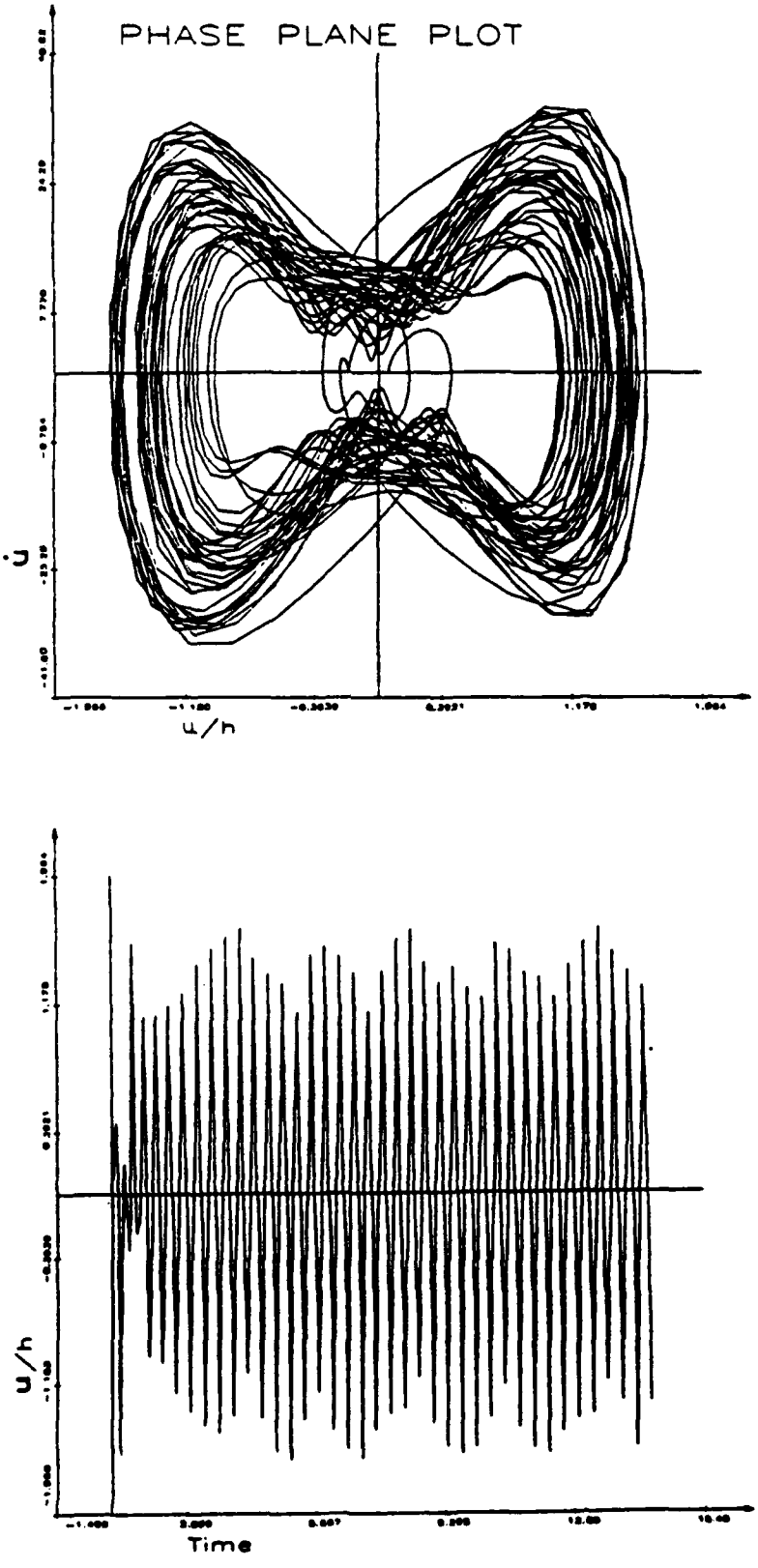

Figure 11(a) Phase plane response $a_1 = 0.084$ (chaos)

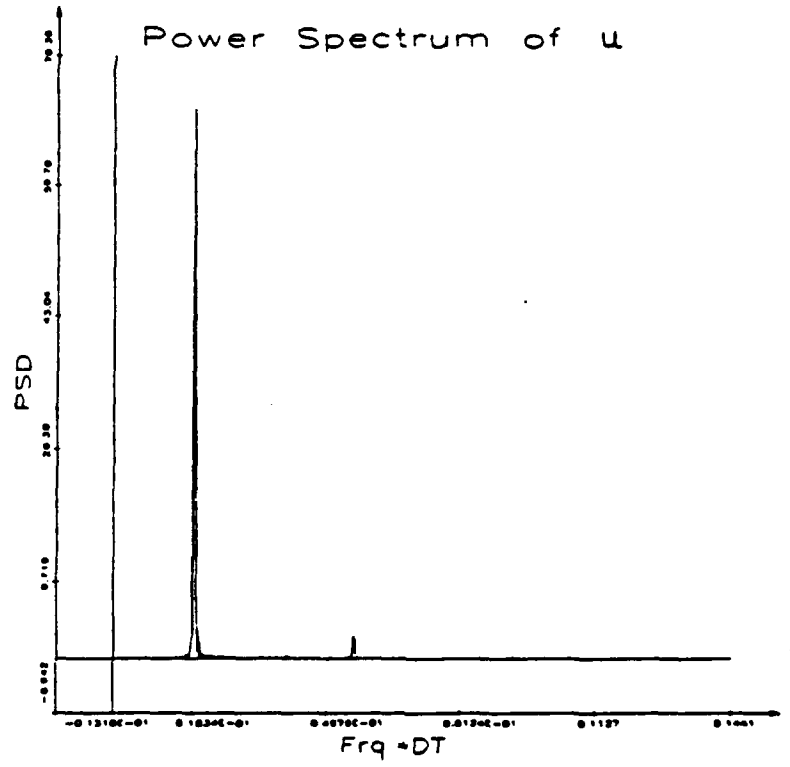

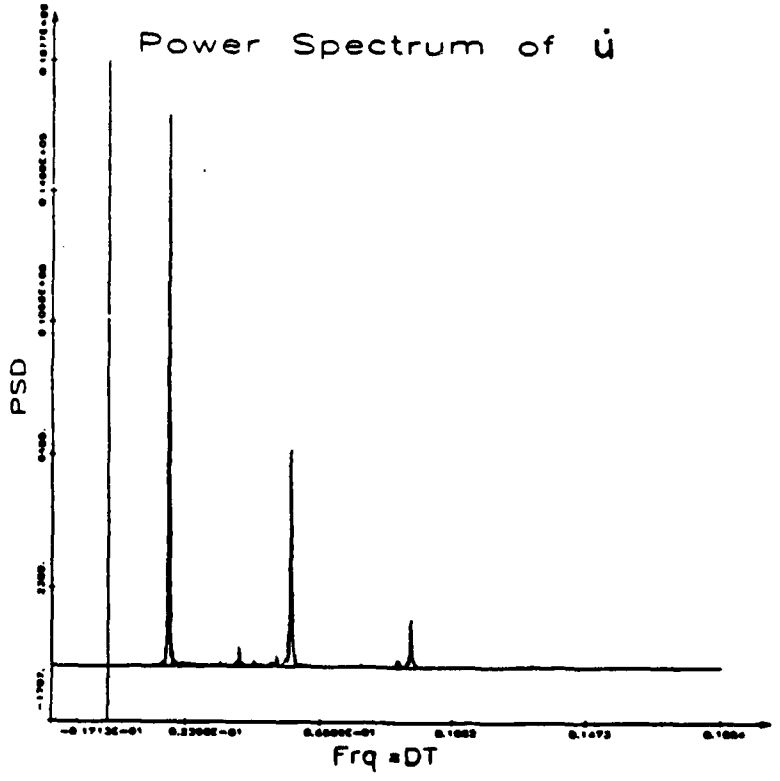

Figure 11(a) Continued

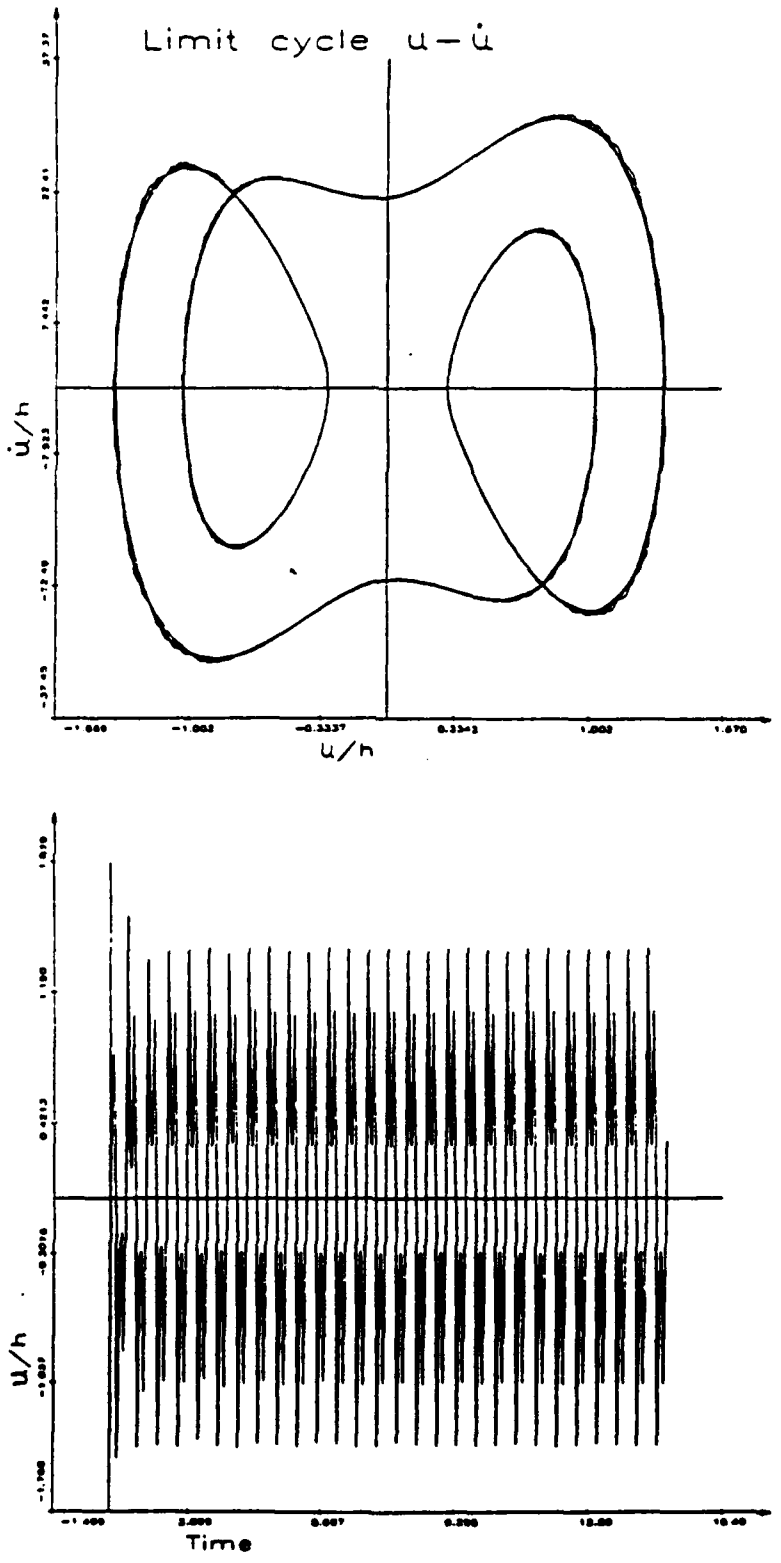

Figure 11(b) Phase plane response $a_1 = 0.251$ (period 1 motion)

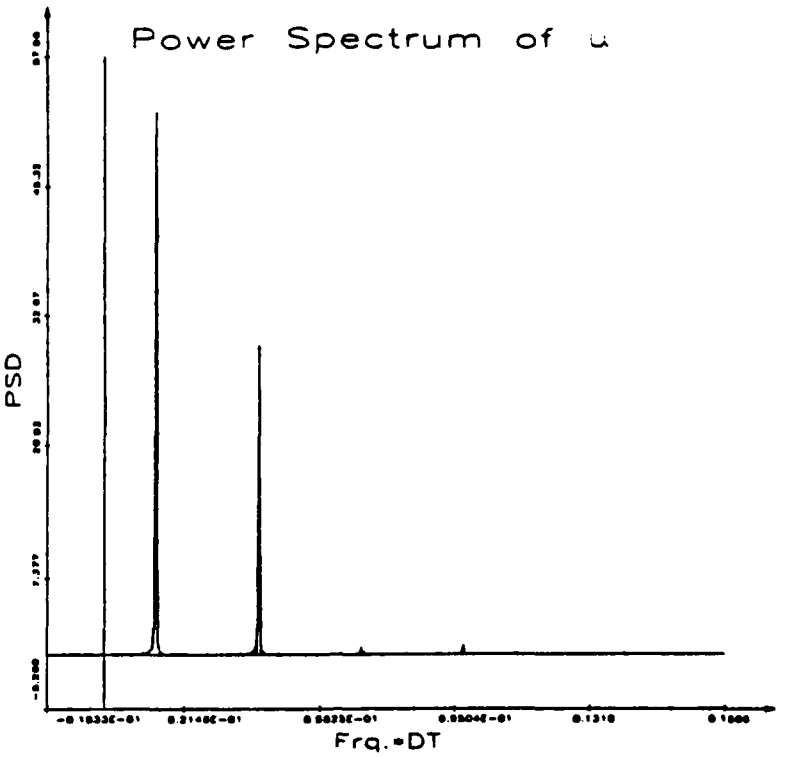

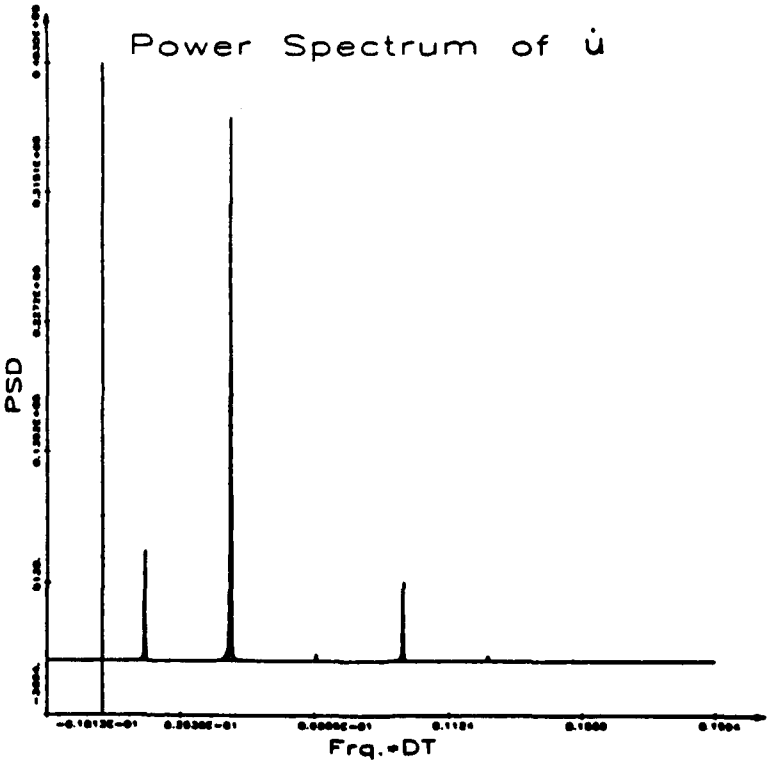

Figure 11(b) Continued

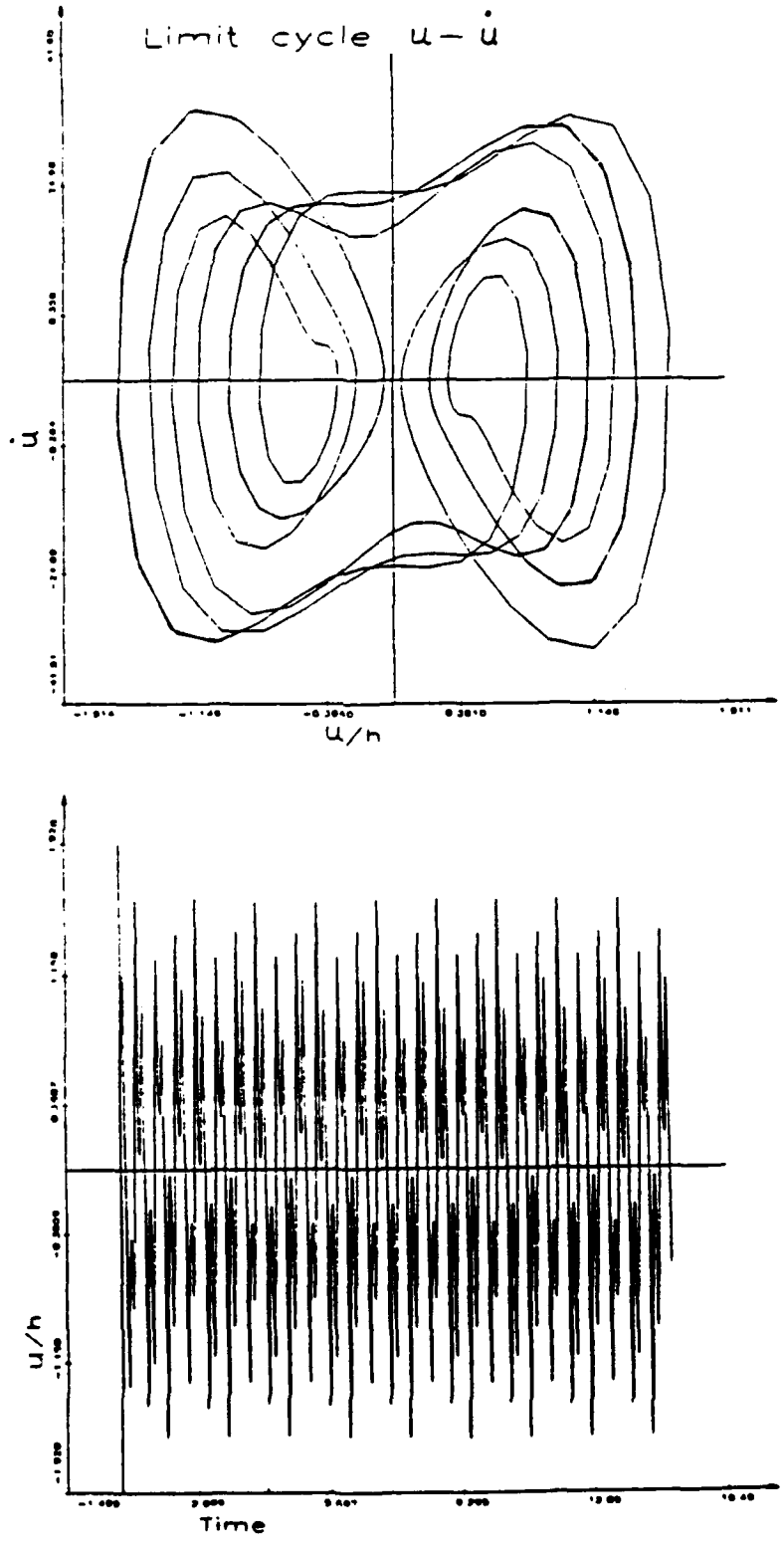

Figure 11(c) Phase plane response $a_1 = 0.600$ (period 3 motion)

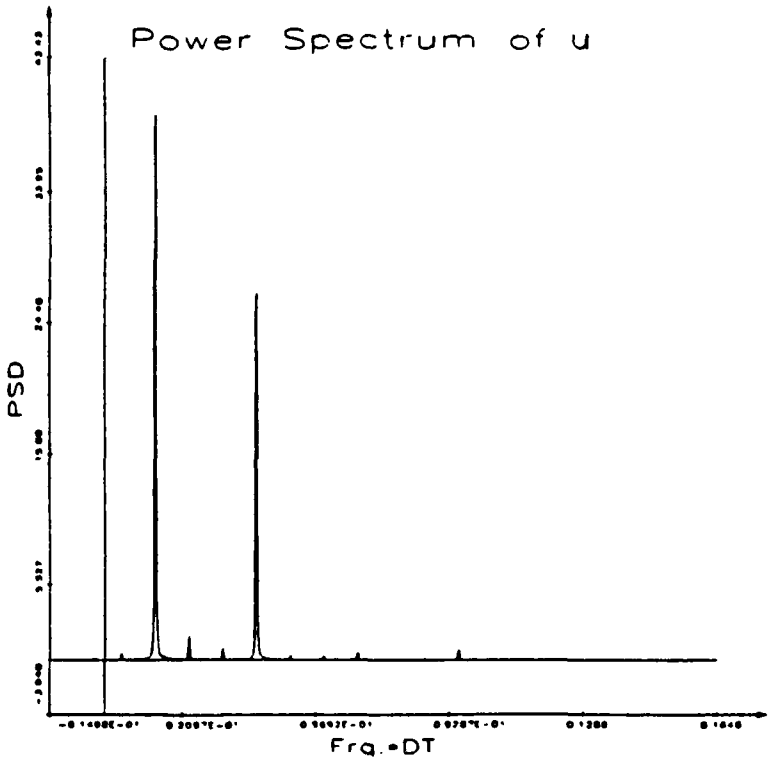

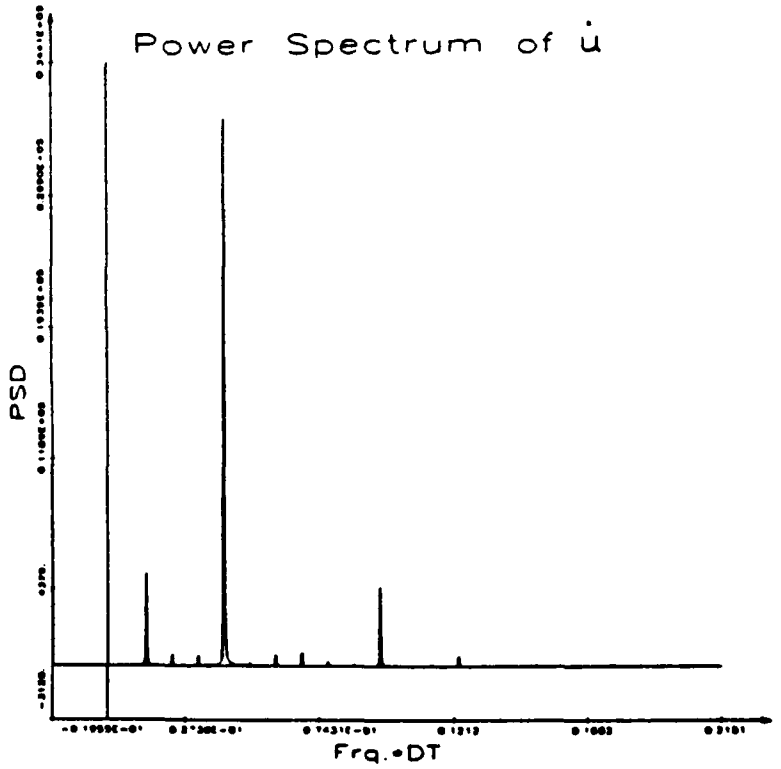

Figure 11(c) Continued

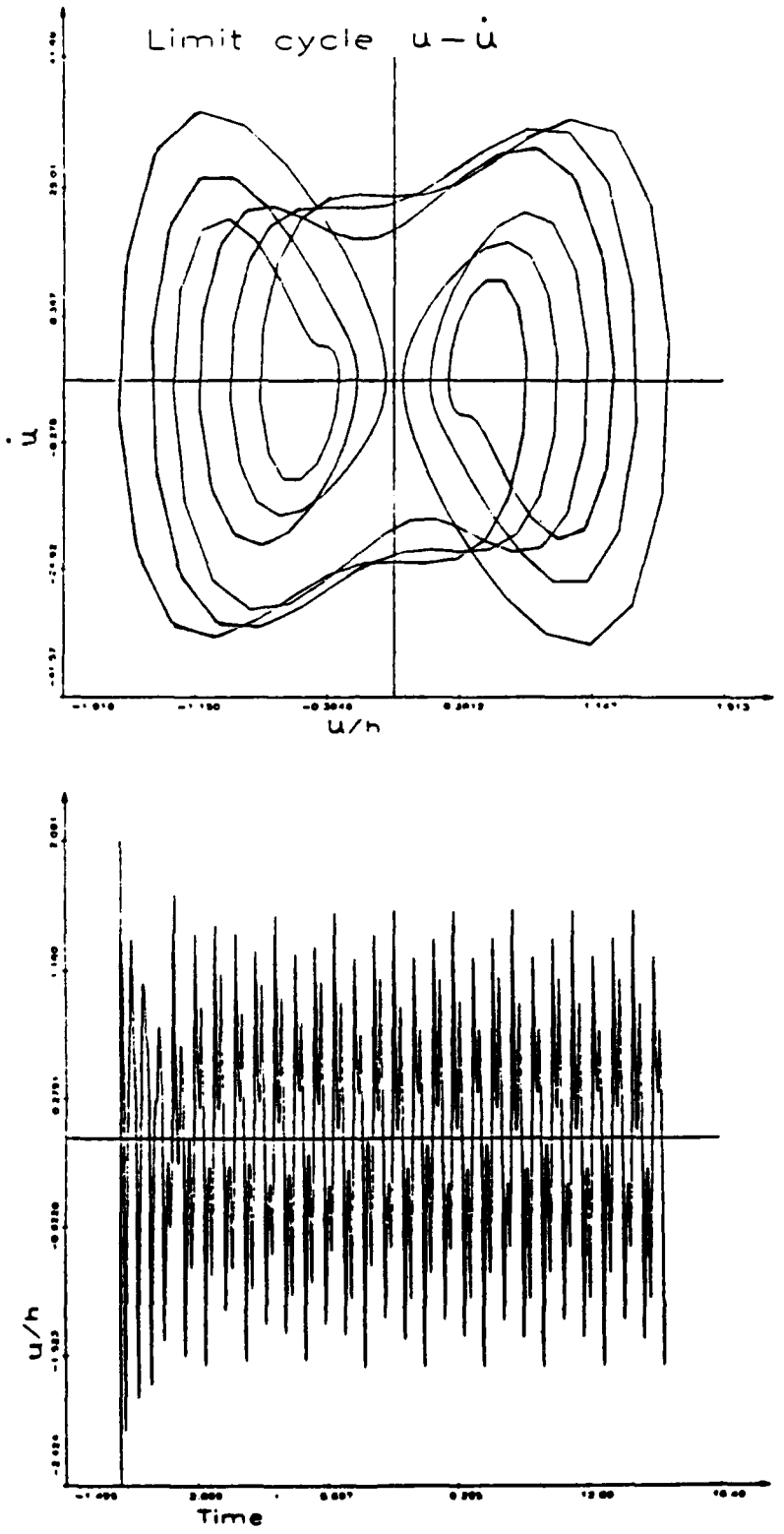

Figure 11(d) Phase plane response $a_1 = 1.600$ (period 3 motion)

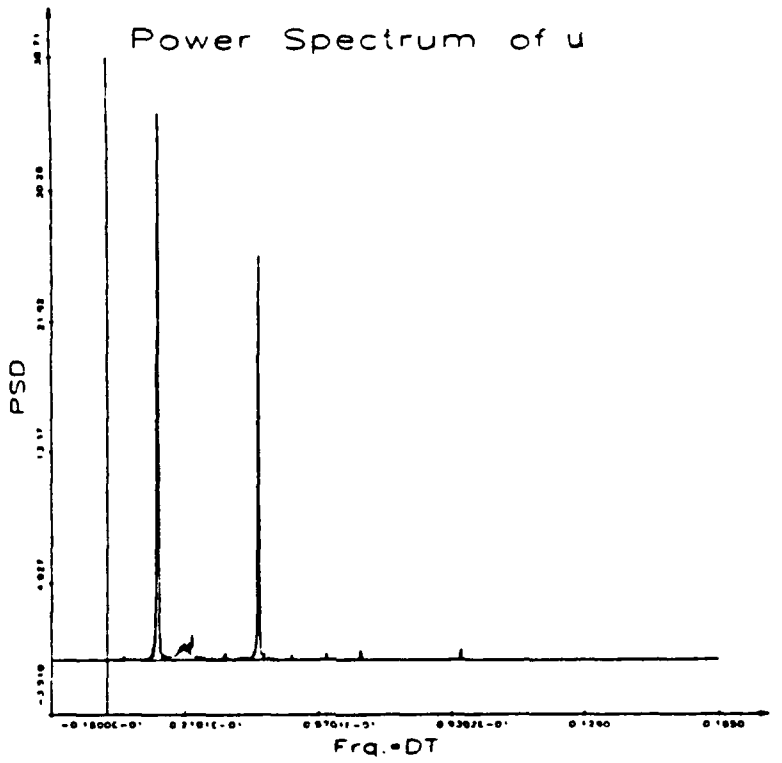

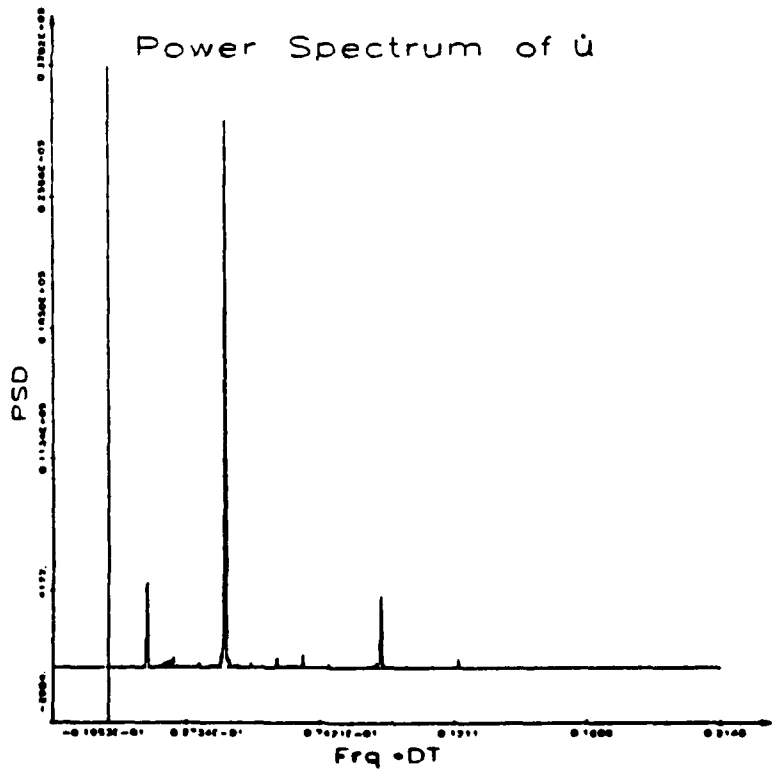

Figure 11(d) Continued

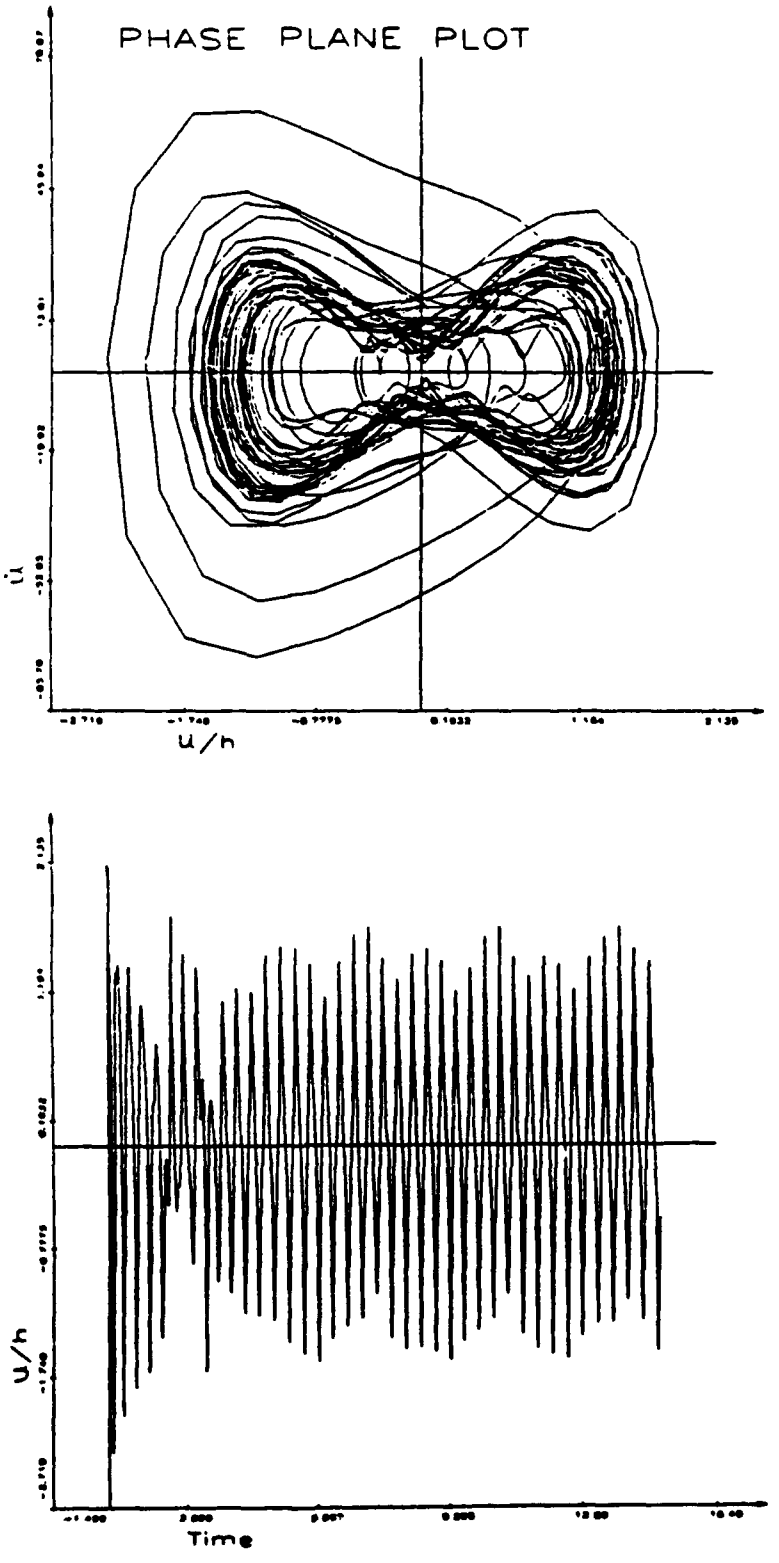

Figure 11(e) Phase plane response $a_1 = 2.000$ (chaos)

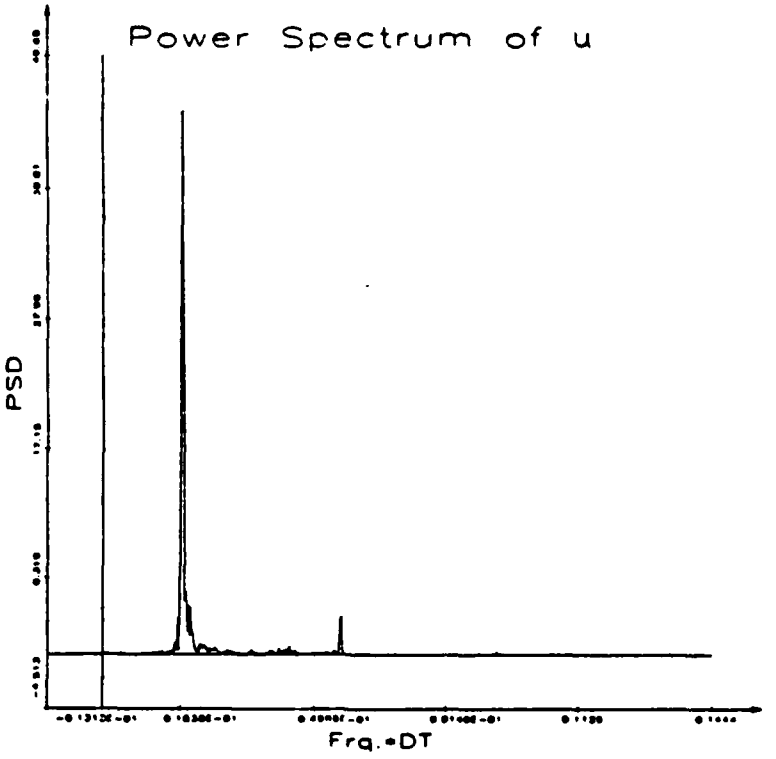

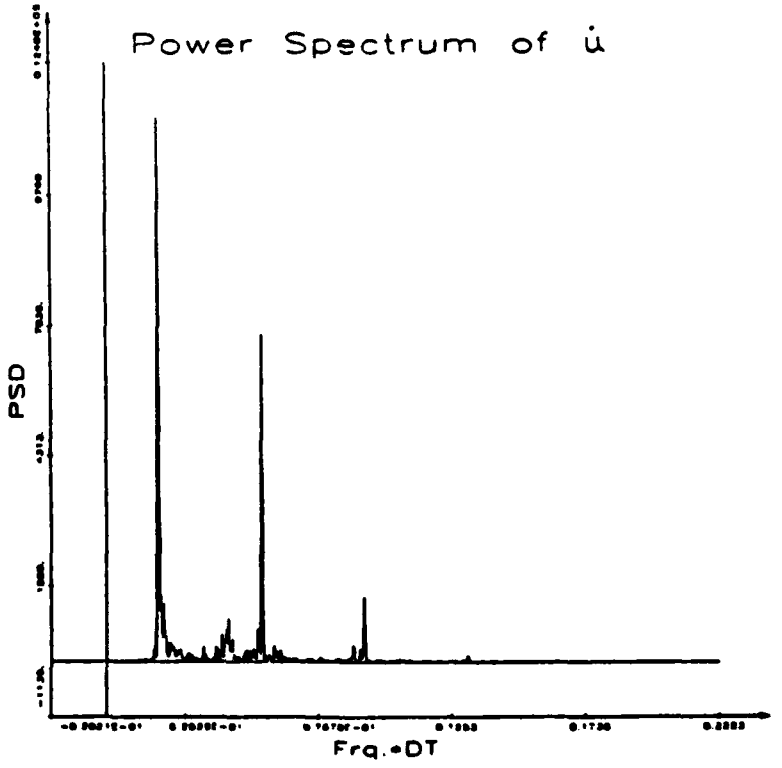

Figure 11(e) Continued

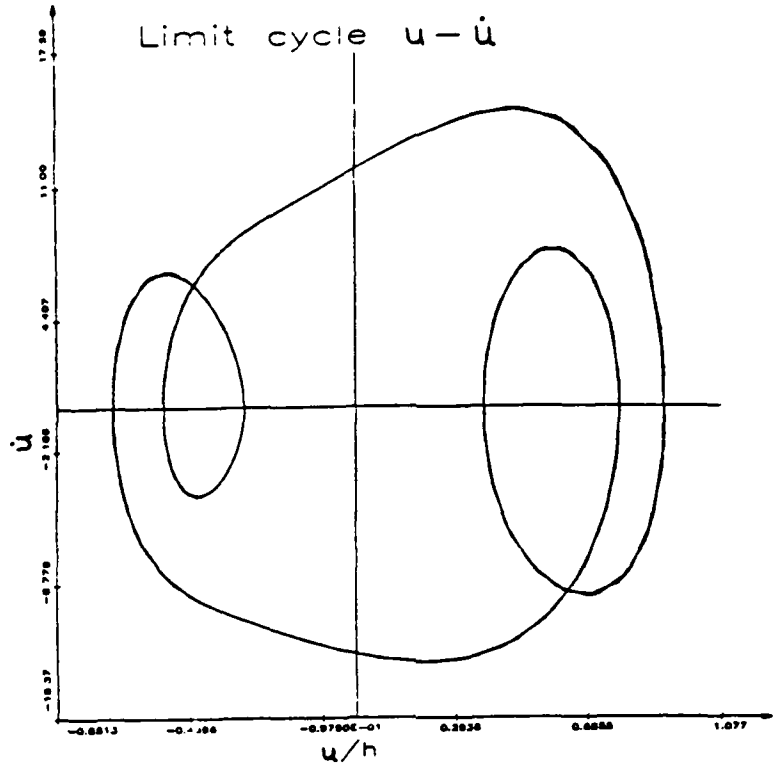

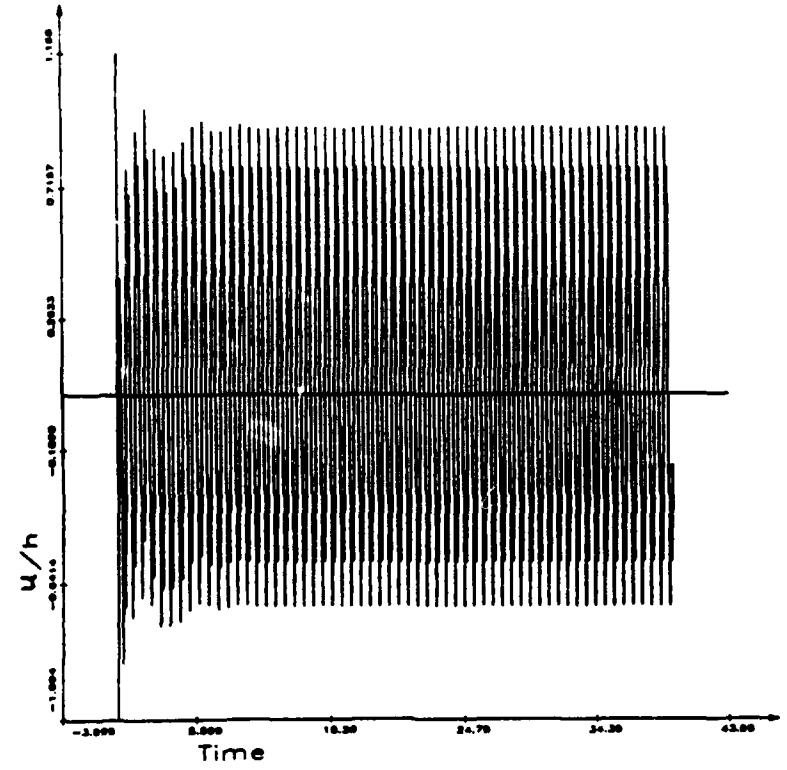

Figure 12(a) Limit cycle response for $\lambda = 150$, $R_a = -3.0\pi^2$, and $n = 1.00$

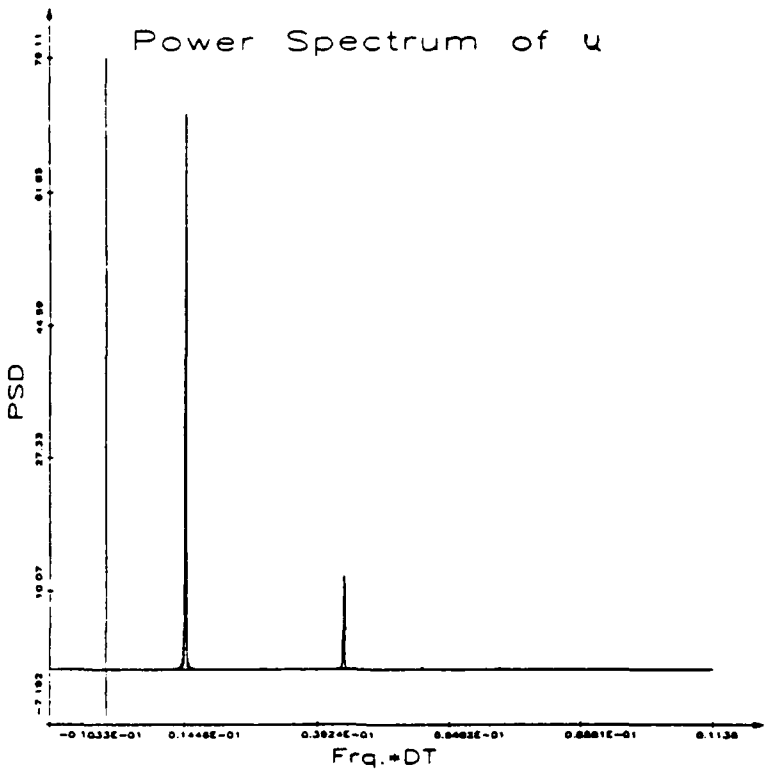

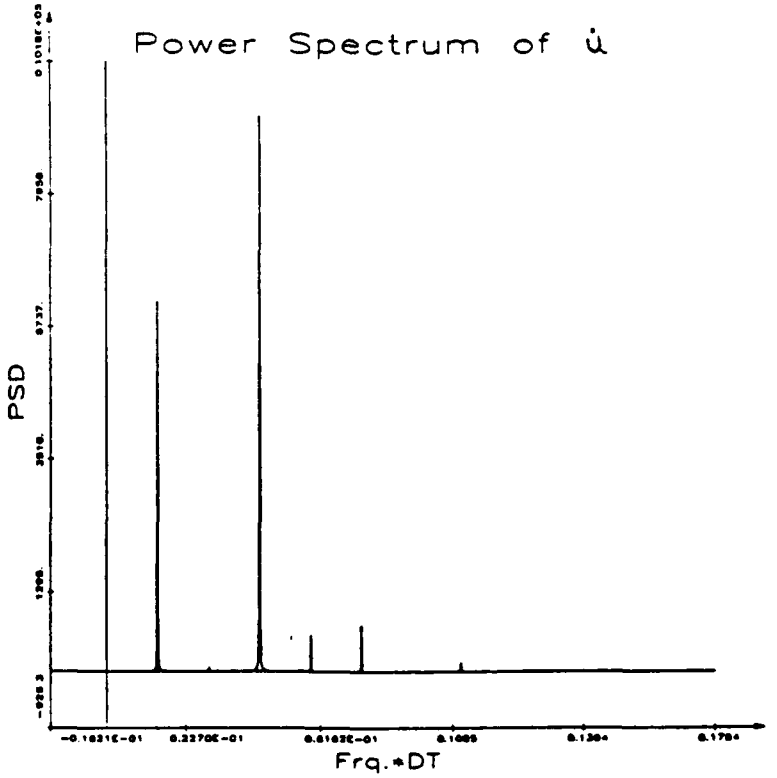

Figure 12(a) Continued

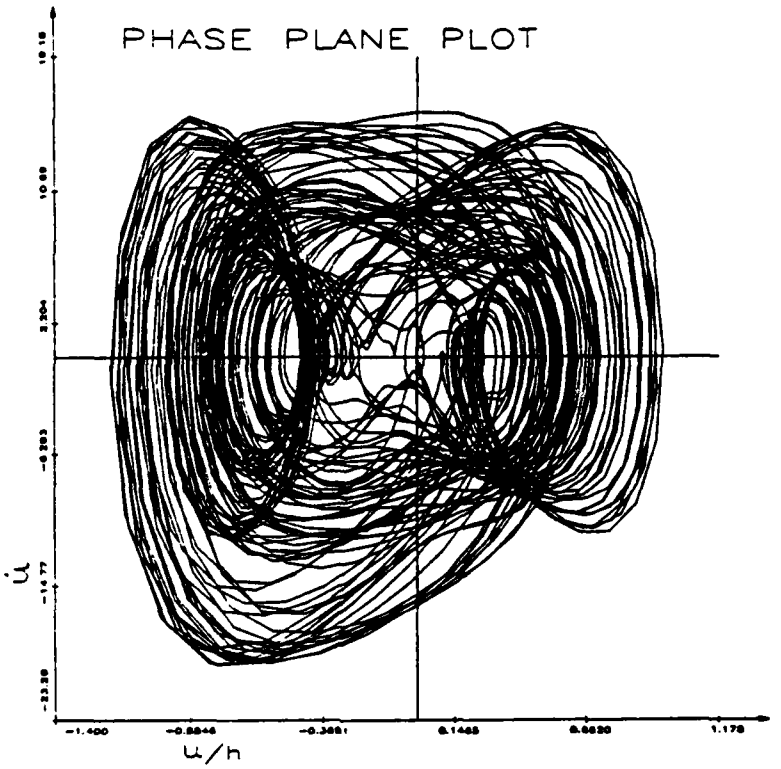

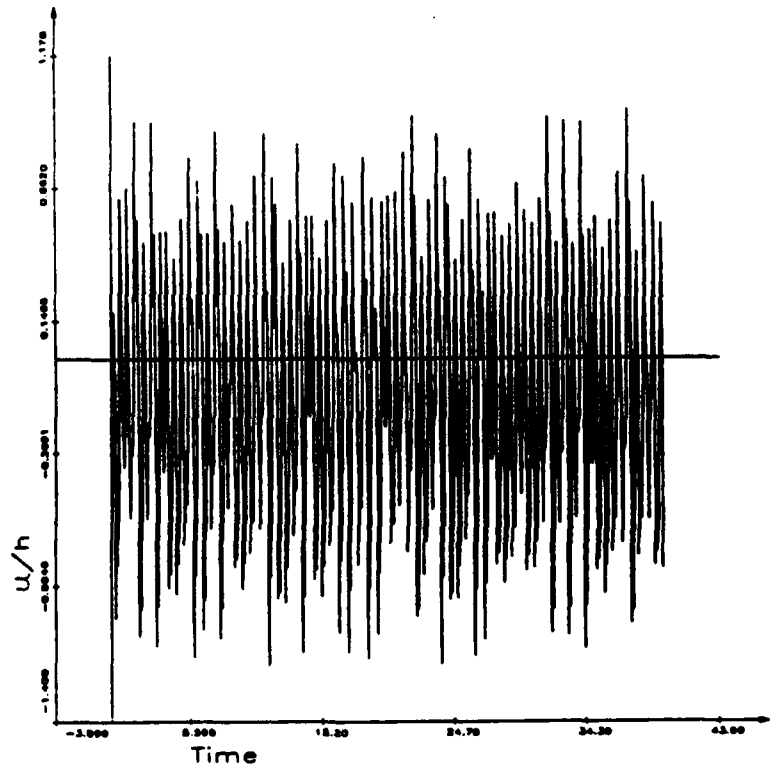

Figure 12(b) Chaotic response for $\lambda = 150$, $R_a = -3.0\pi^2$, and $n = 1.28$

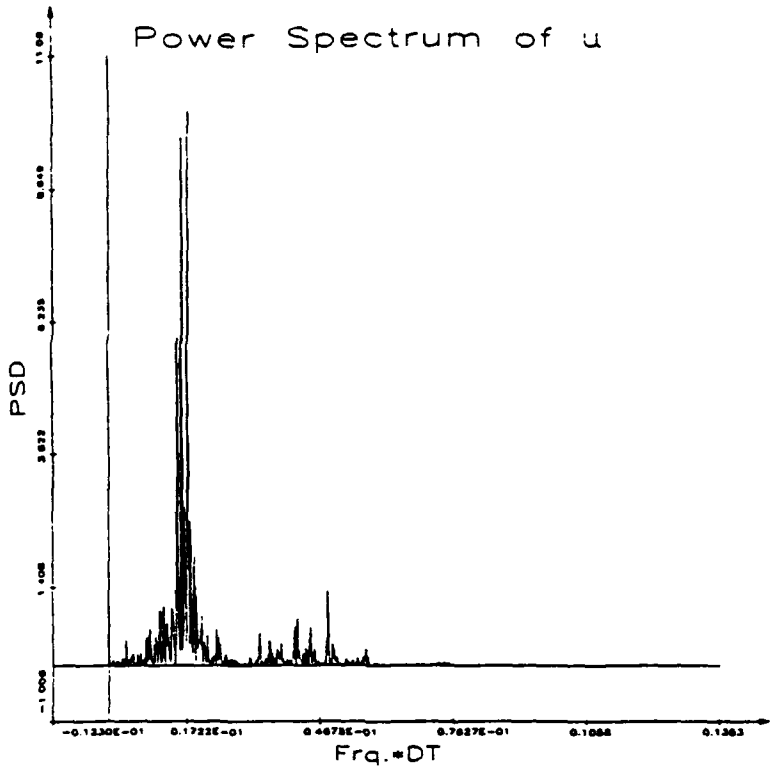

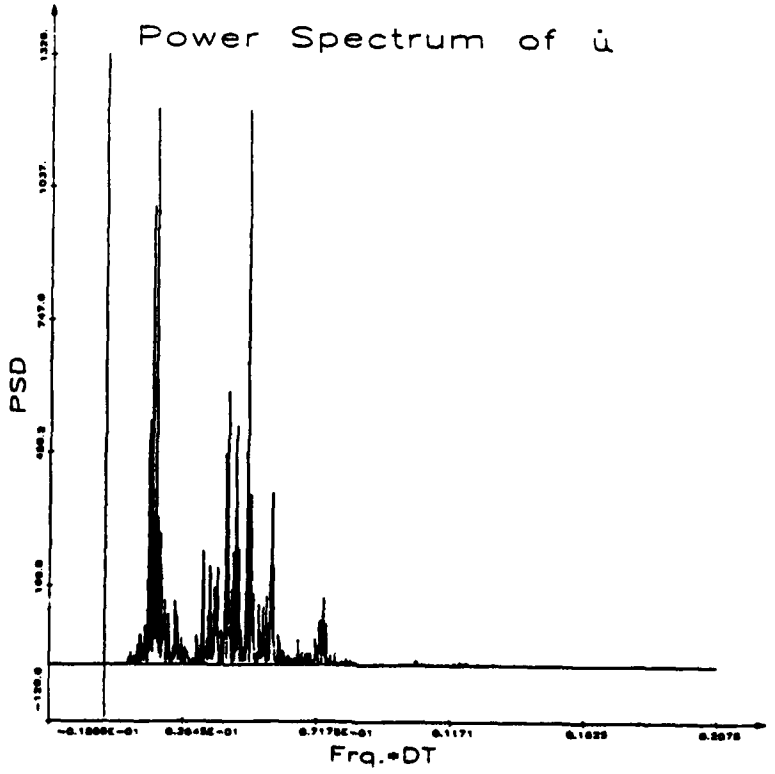

Figure 12(b) Continued

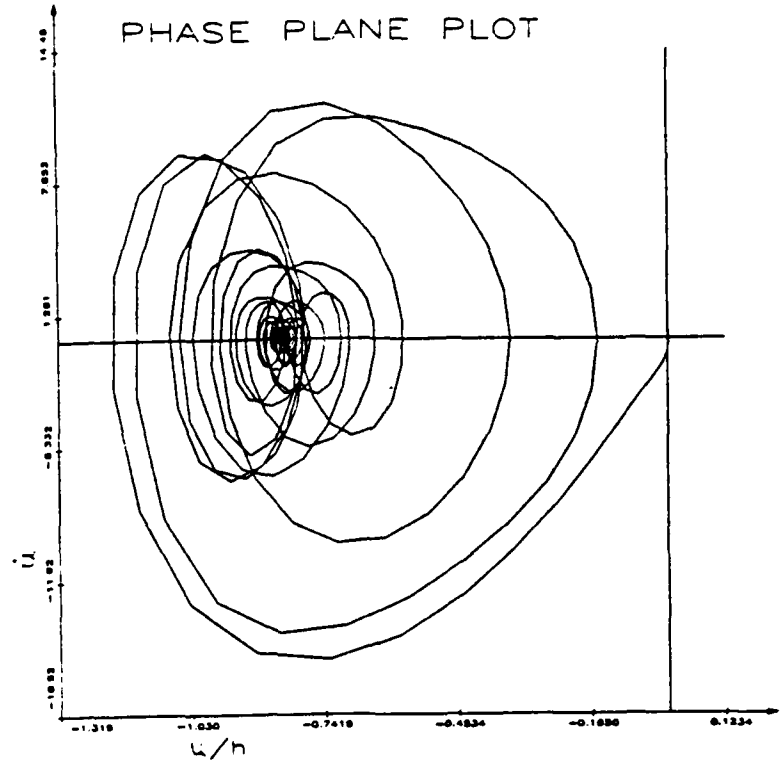

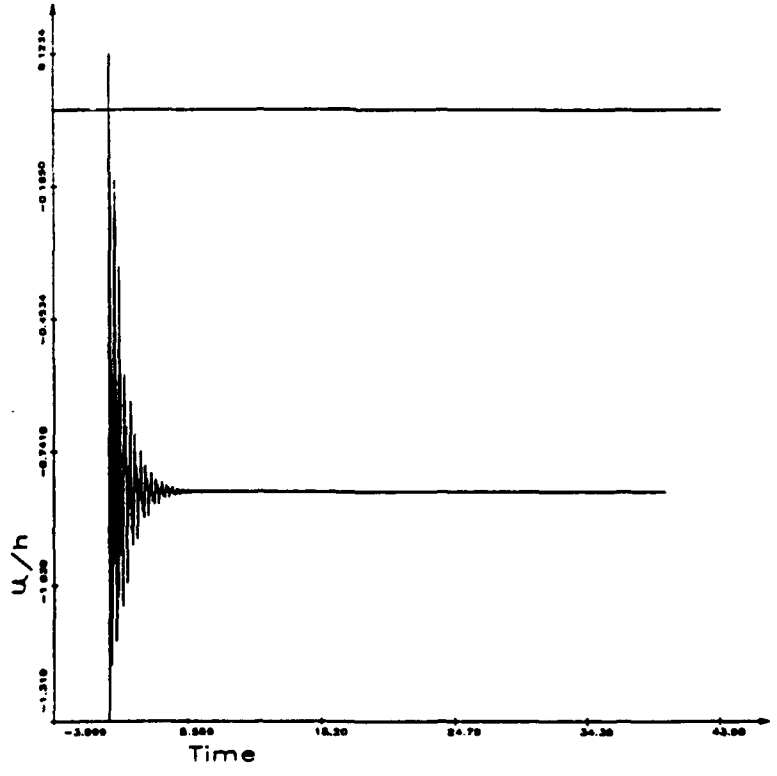

Figure 12(c) Fixed point response for $\lambda = 150$, $R_a = -3.0\pi^2$, and $n = 3.00$

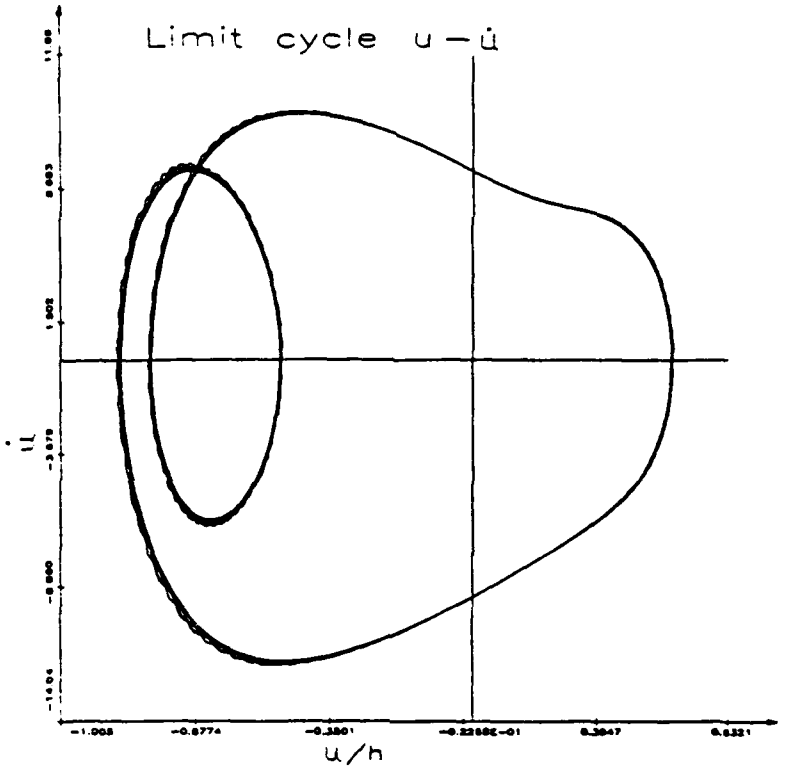

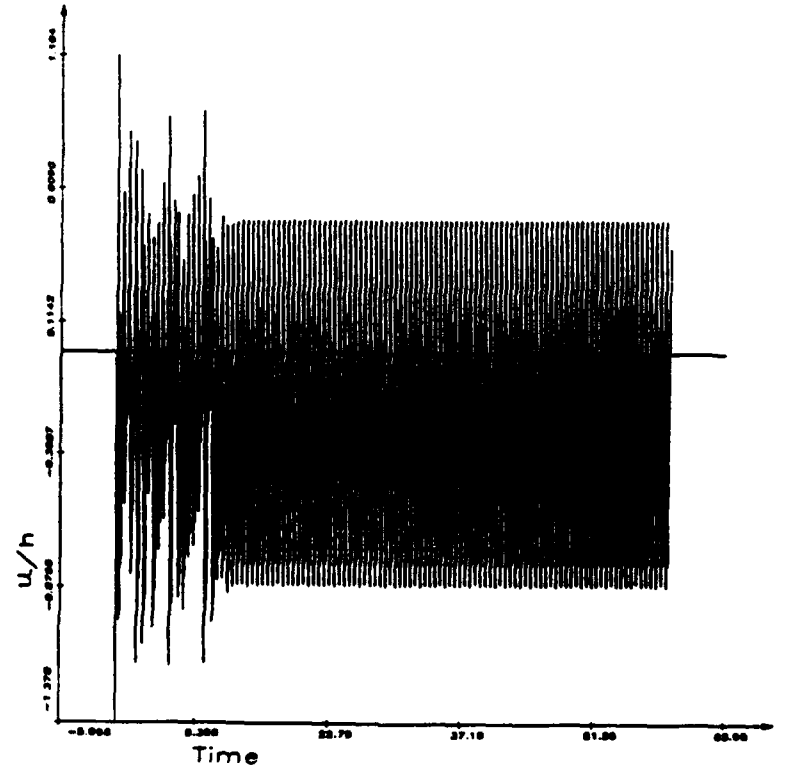

Figure 12(d) Limit cycle response for $\lambda = 150$, $R_a = -3.0\pi^2$, and $n = 1.67$

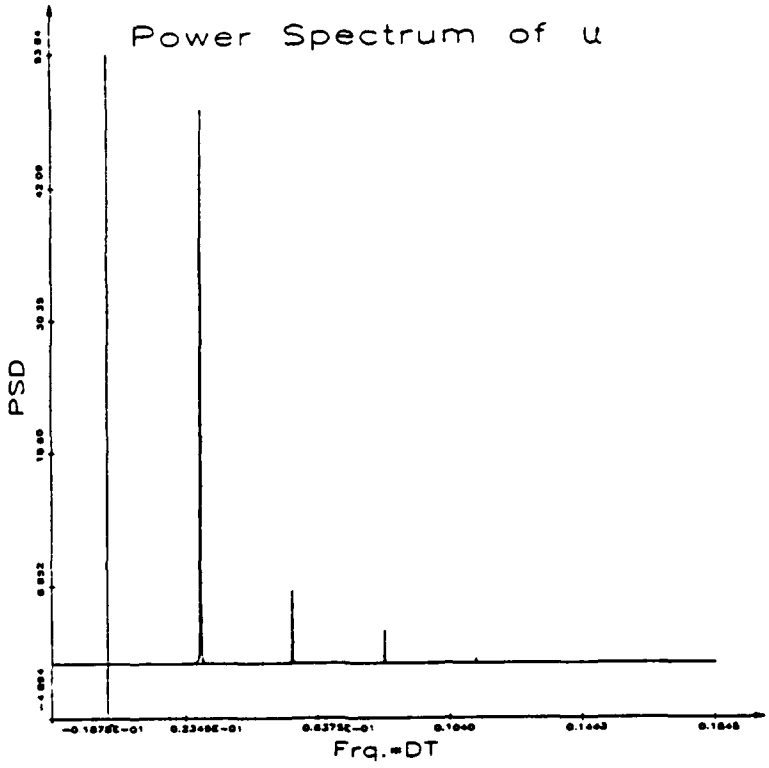

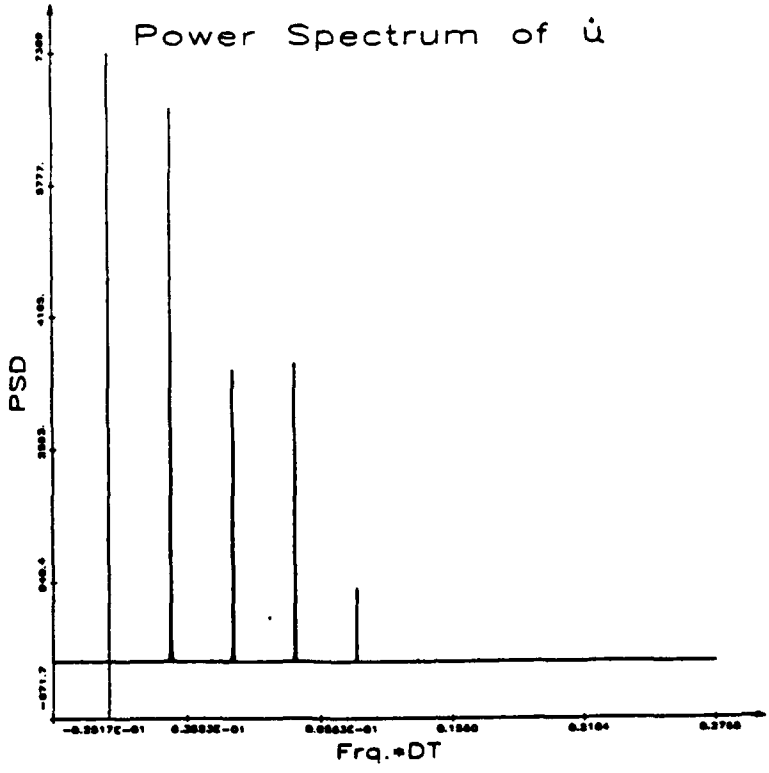

Figure 12(d) Continued

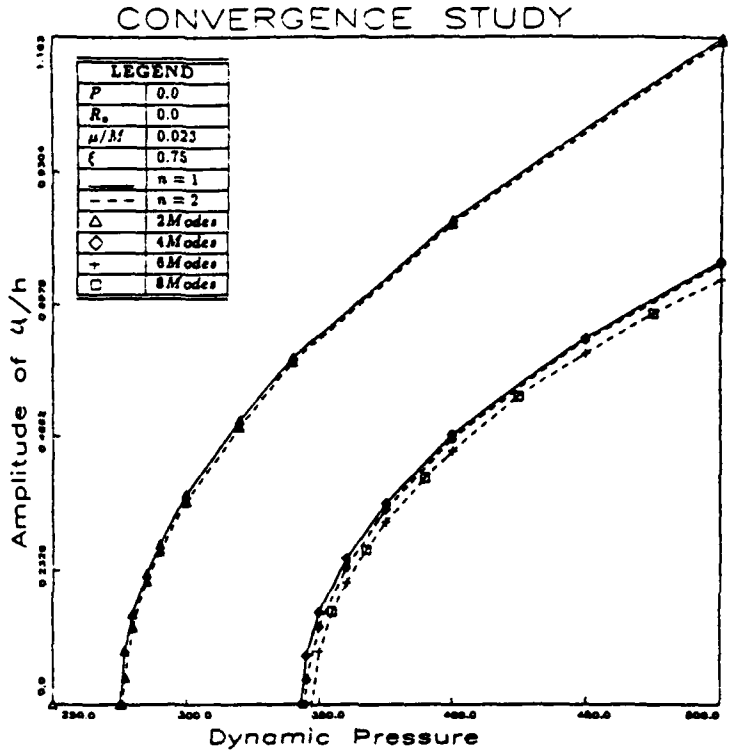

Figure 13 Amplitude convergence study

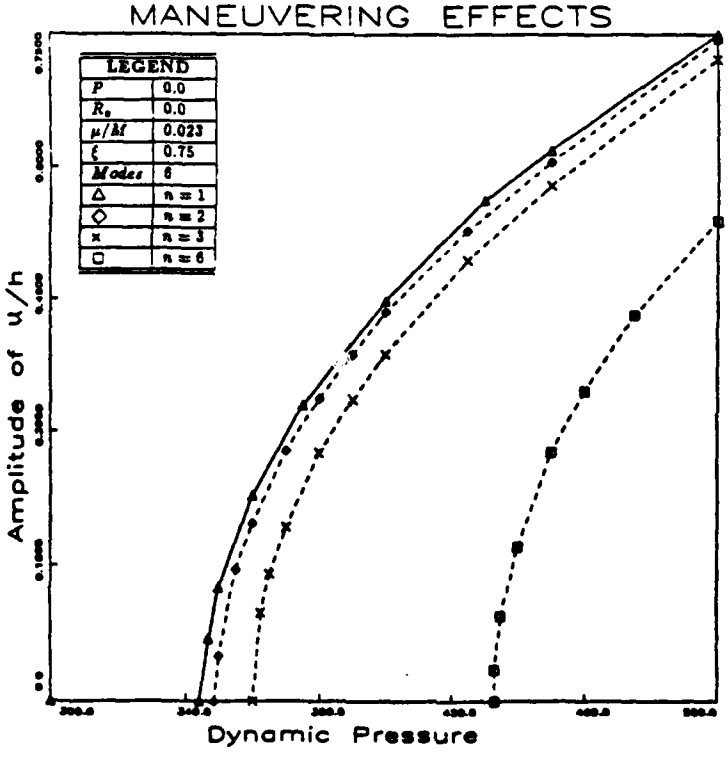

Figure 14 Effect of load factor

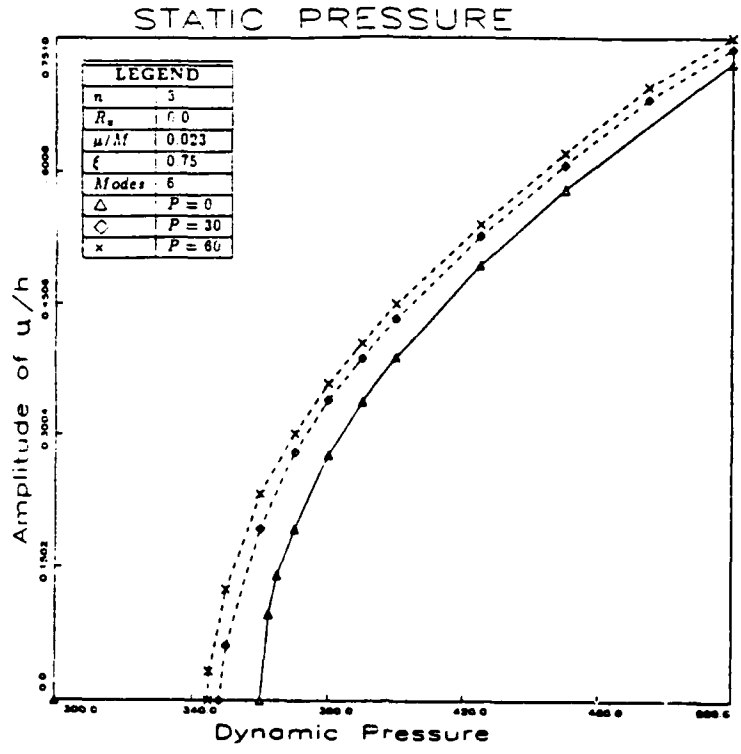

Figure 15 Influence of static pressure differential

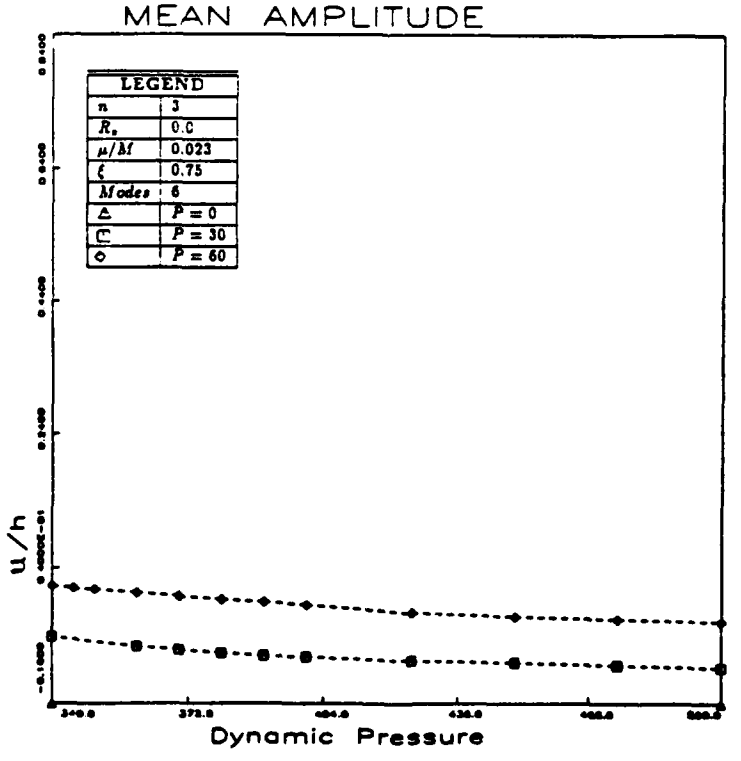

Figure 16 Influence of static pressure to mean amplitude of limit cycle

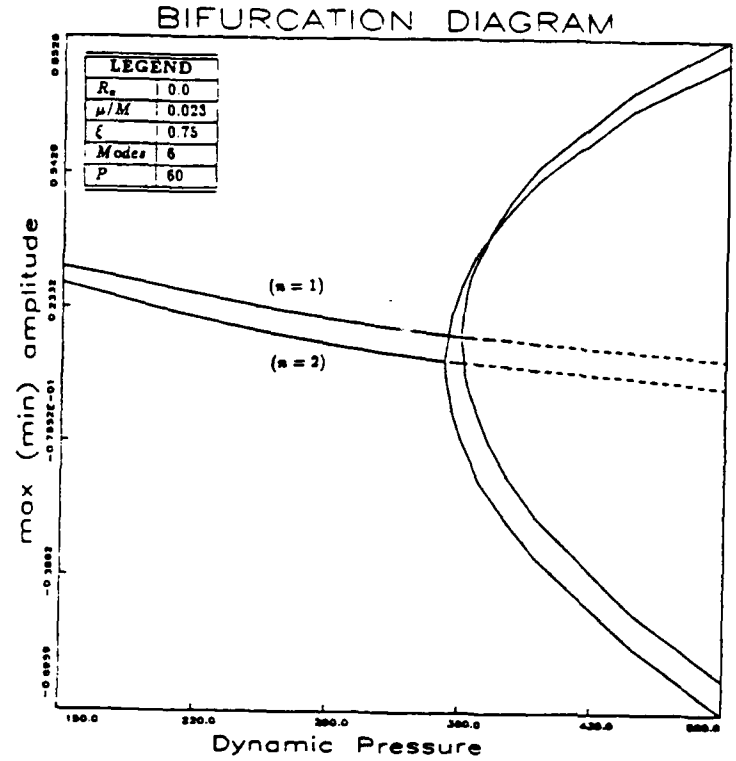

Figure 17 Combined influence of maneuvering and static pressure differential

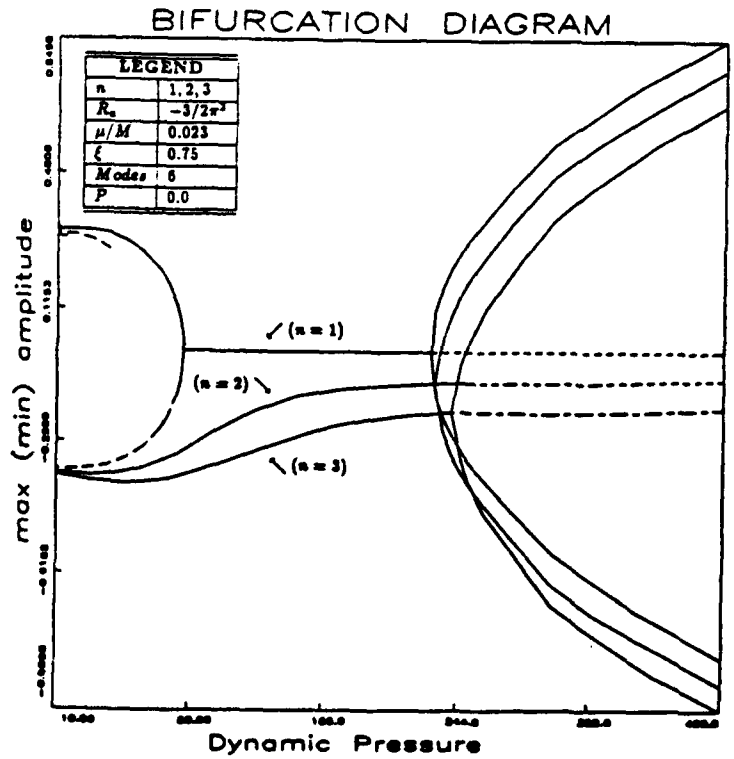

Figure 18 Combined influence of maneuvering and in-plane loading

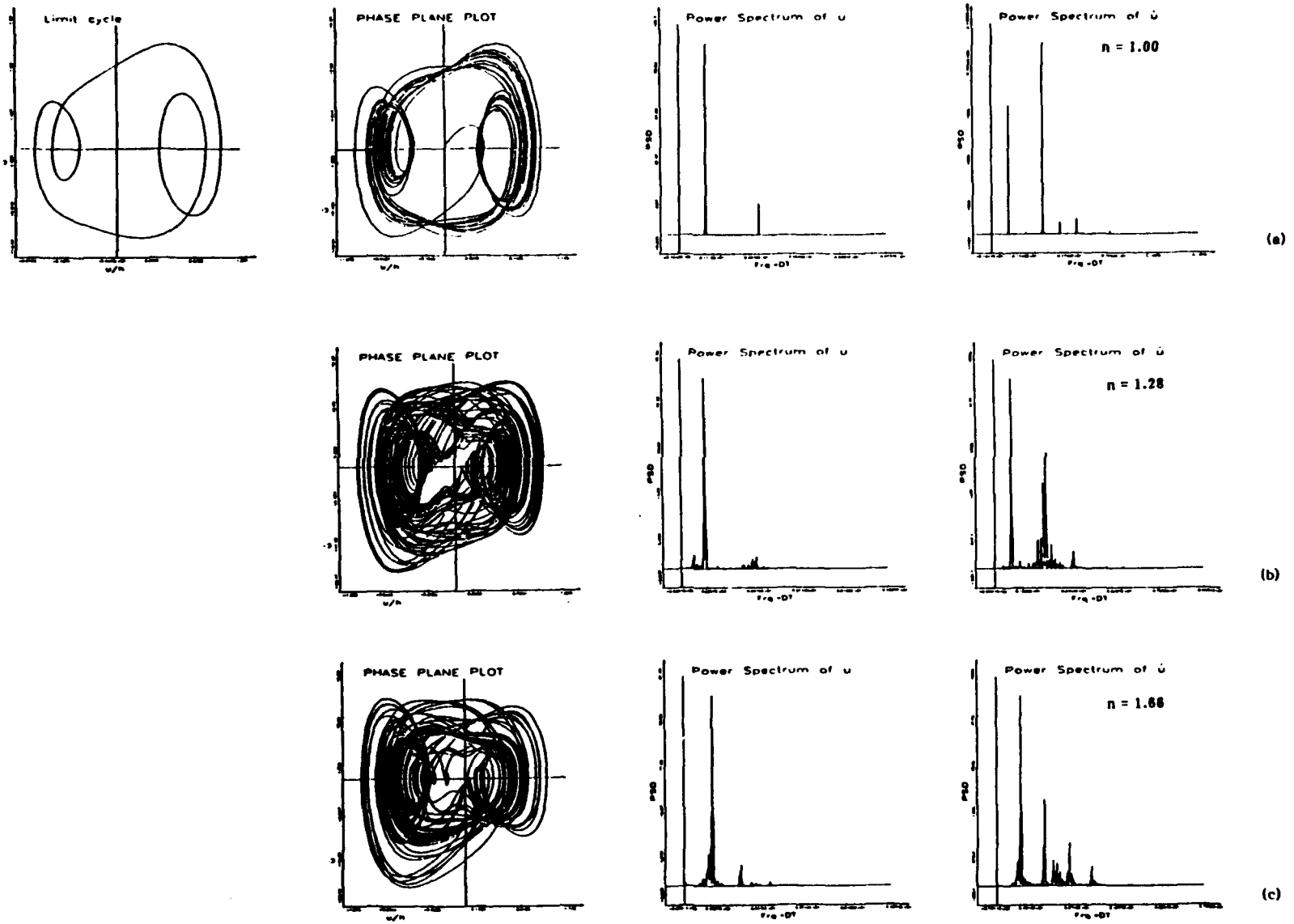

Figure 20 Phase-plane portraits and accompanying frequency spectra of system response. The maneuvering varies from $n = 1.0$, to $n = 3.0$

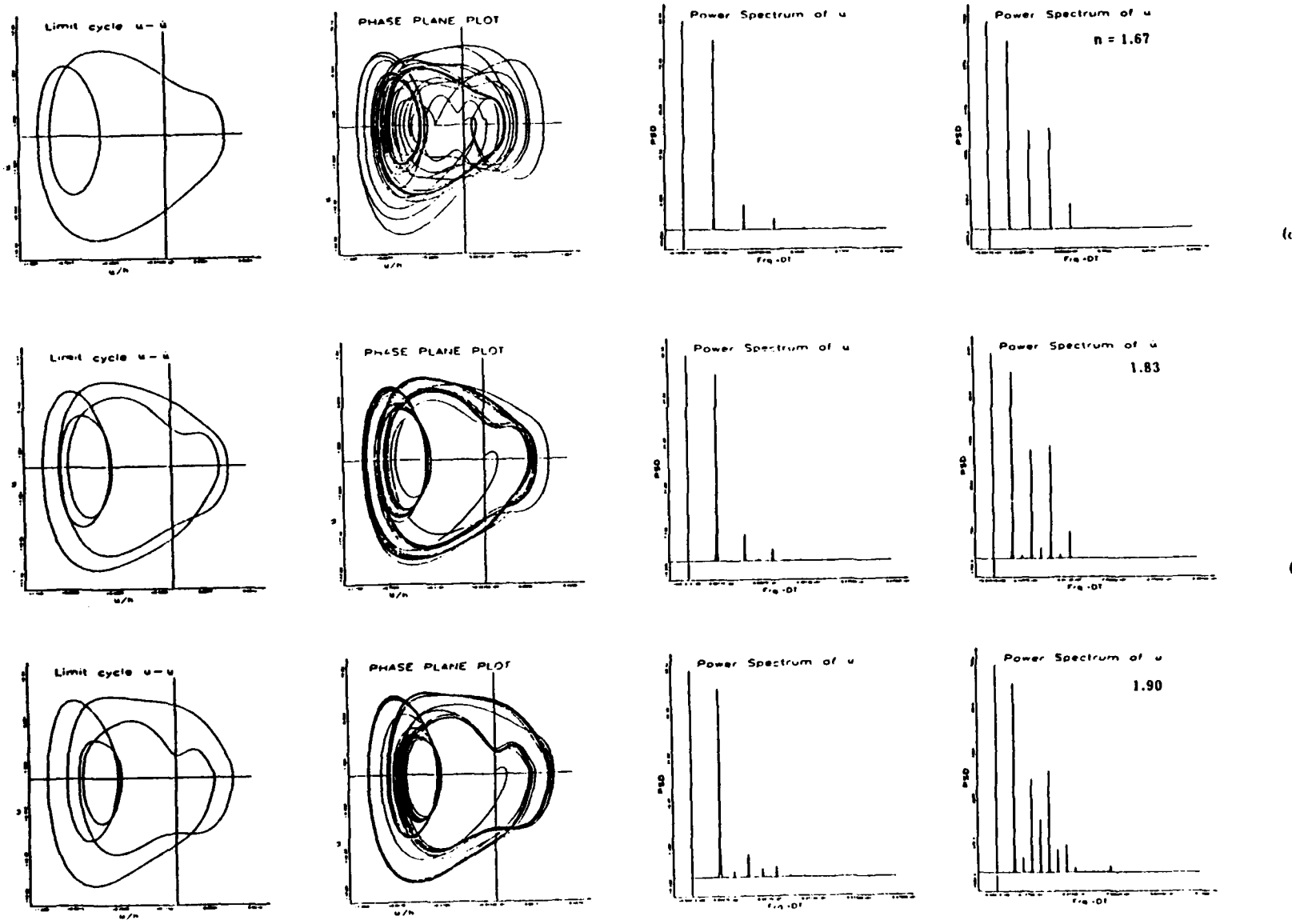

Figure 20 Continued

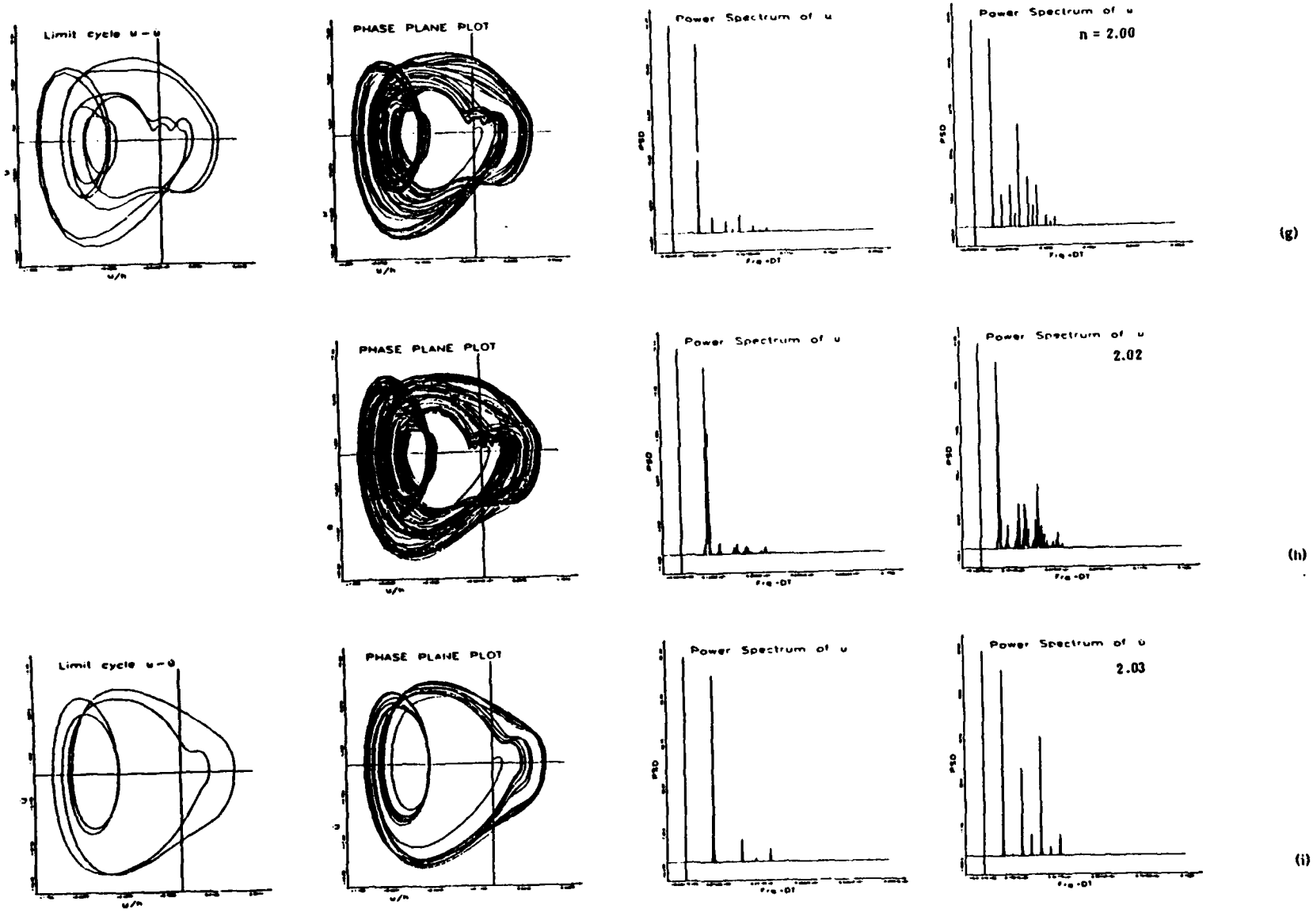

Figure 20 Continued

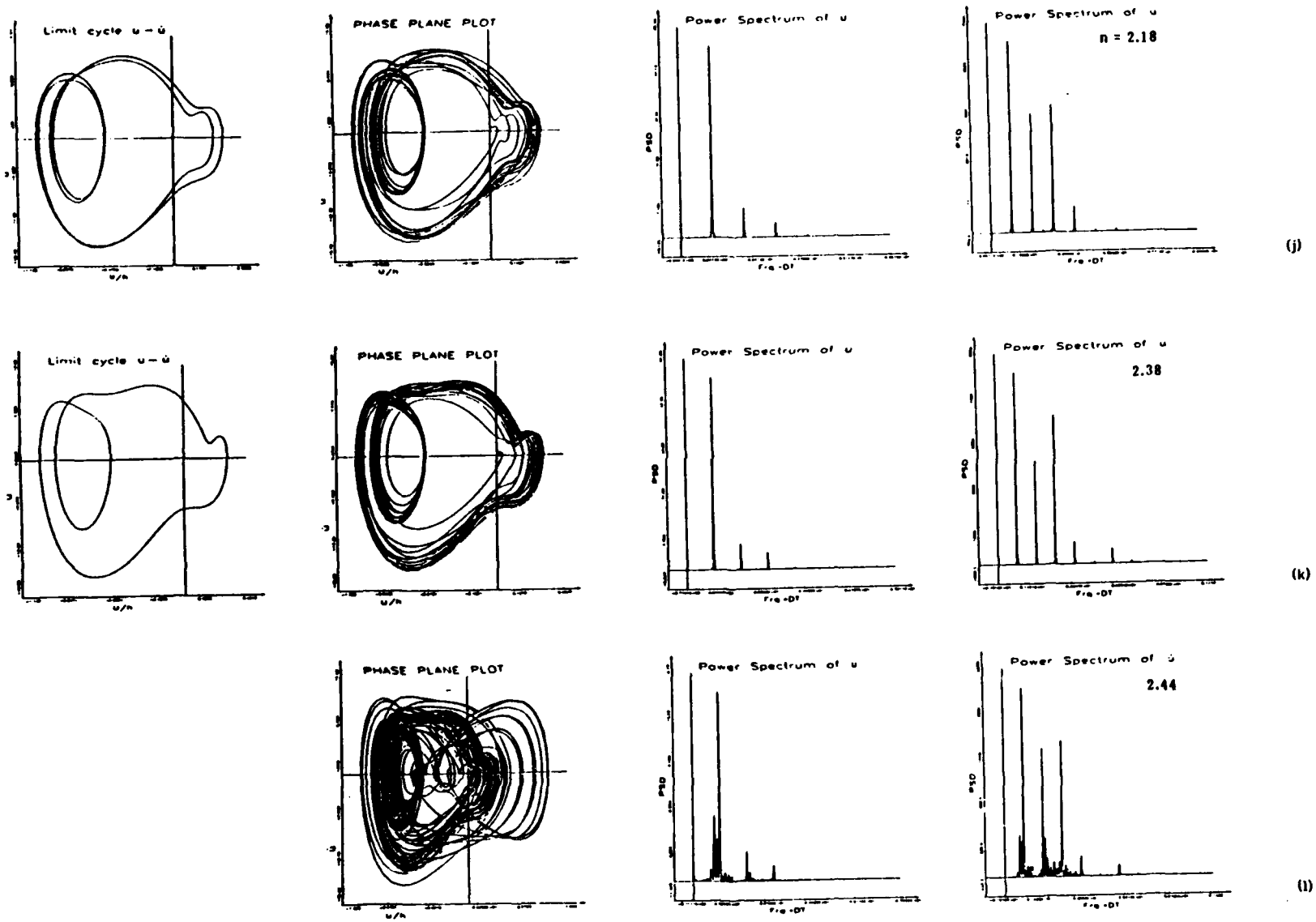

Figure 20 Continued

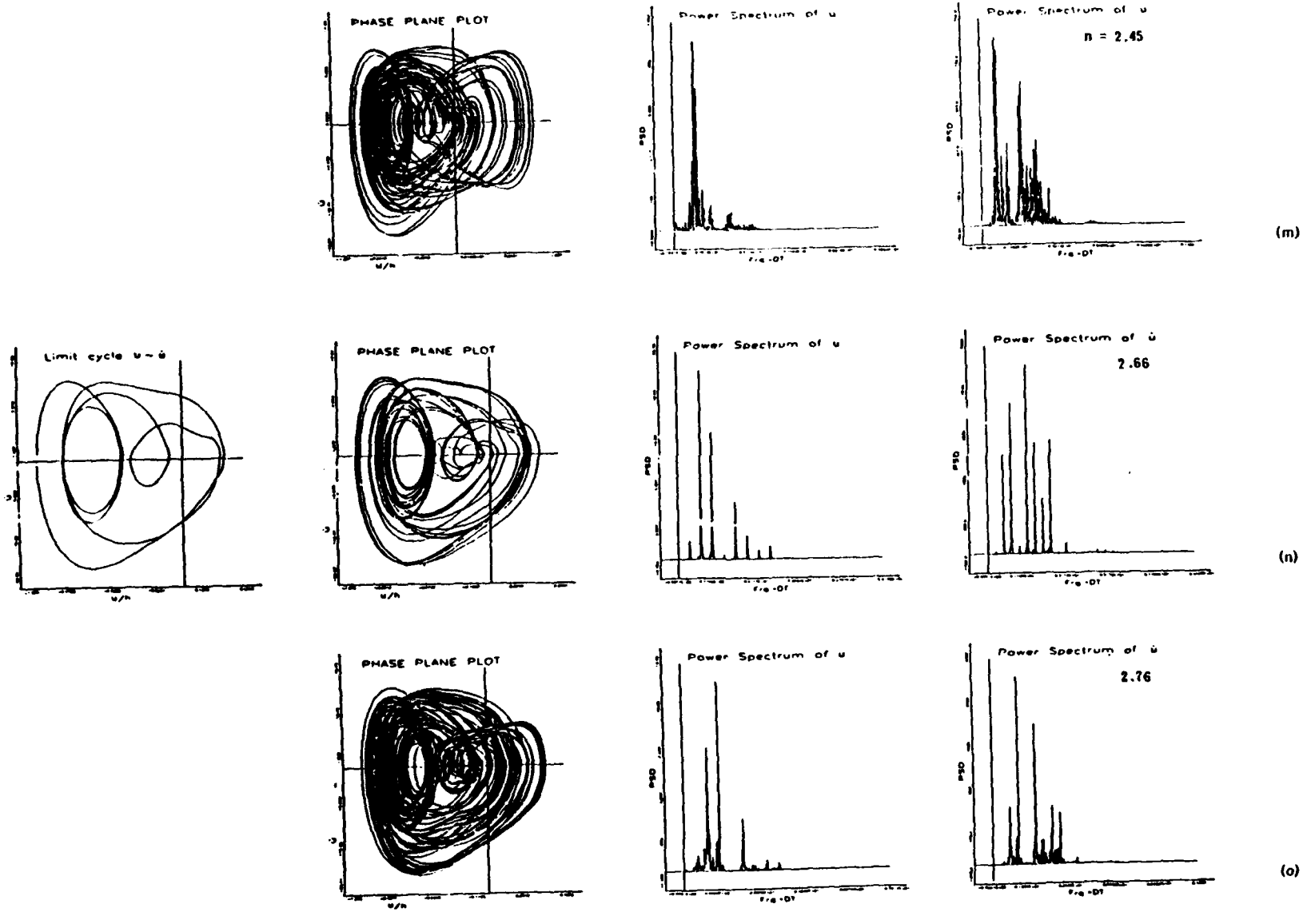

Figure 20 Continued

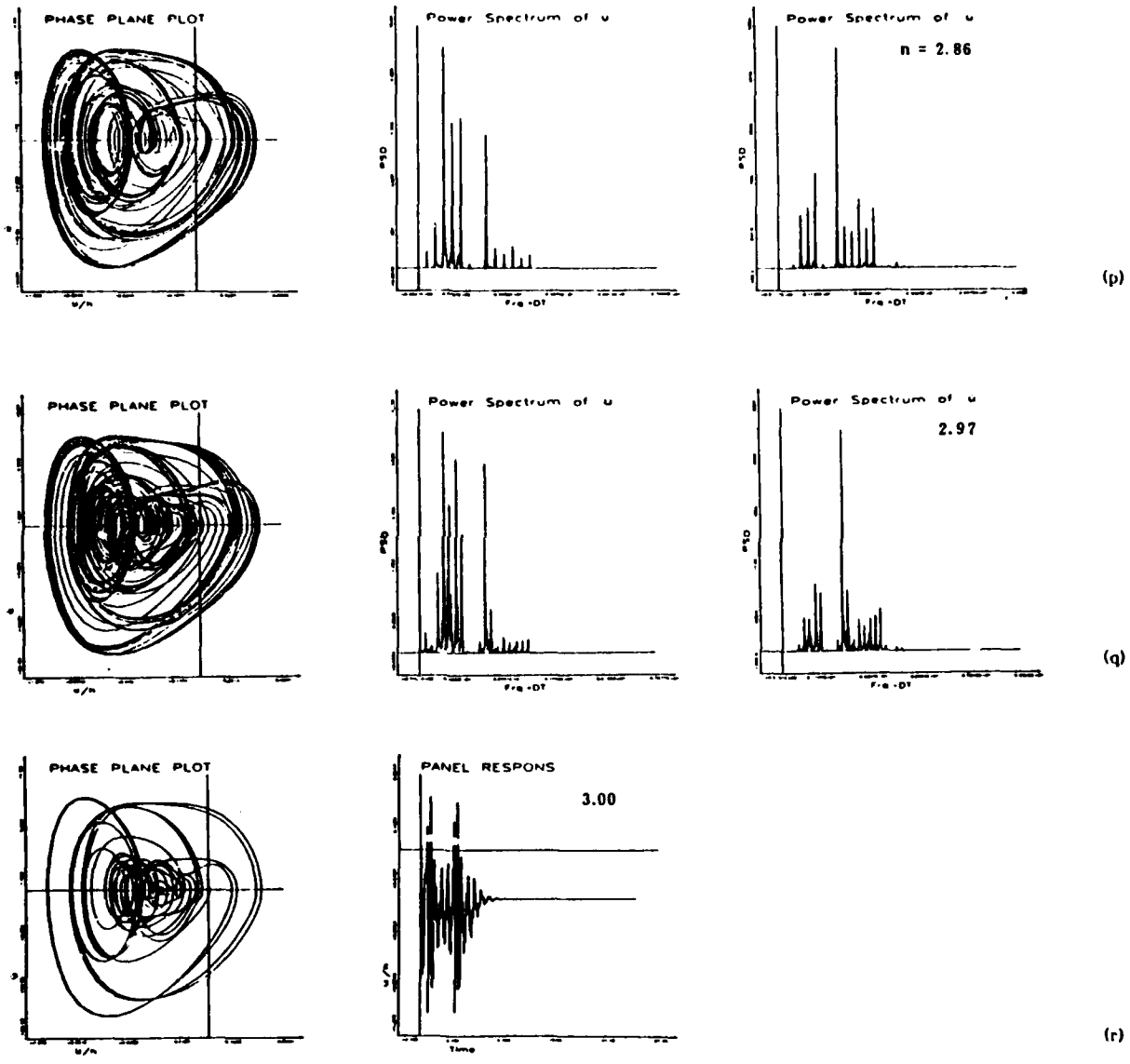

Figure 20 Continued

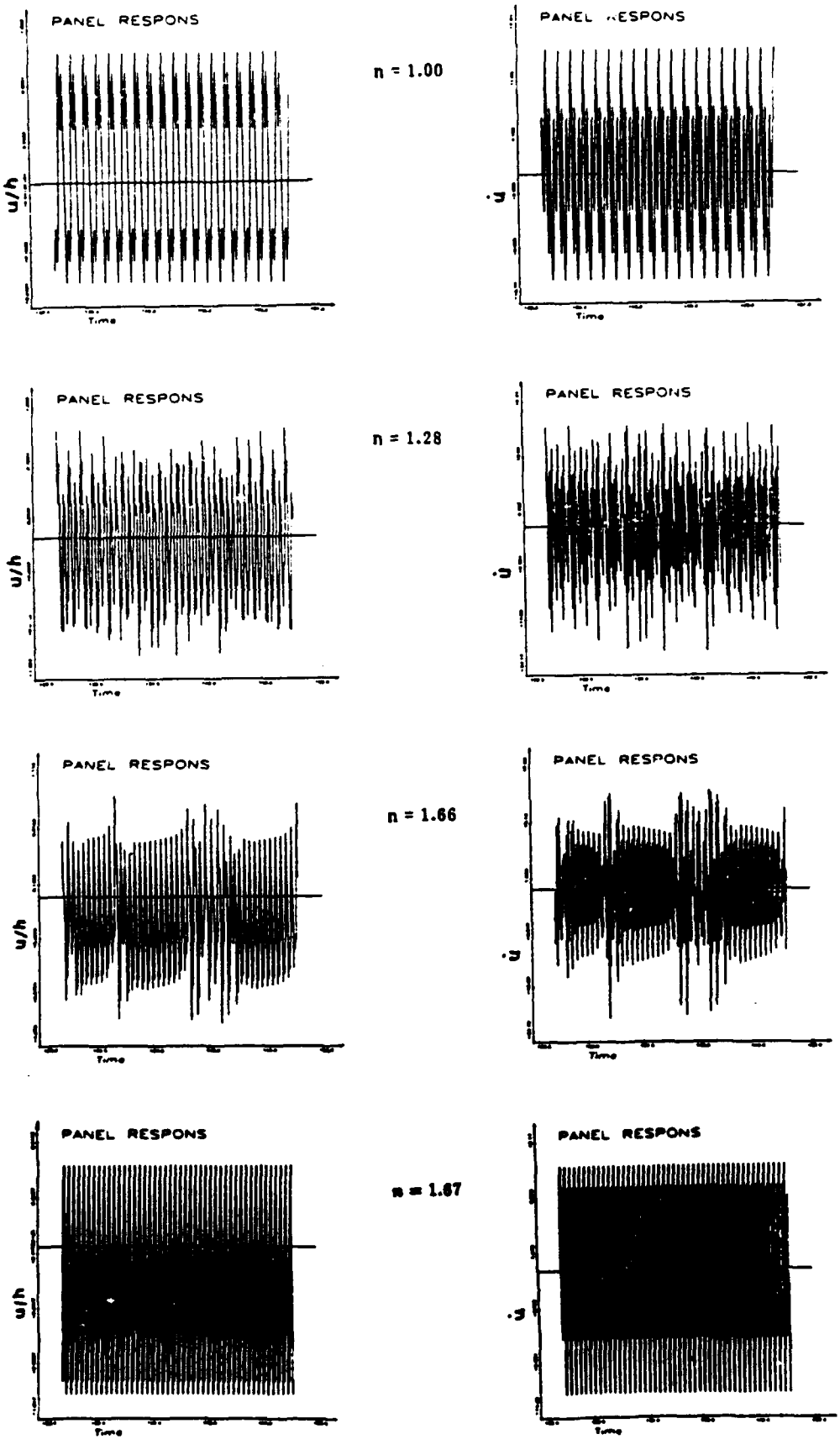

Figure 21 Long-time history for selected cases shown in Figure 20

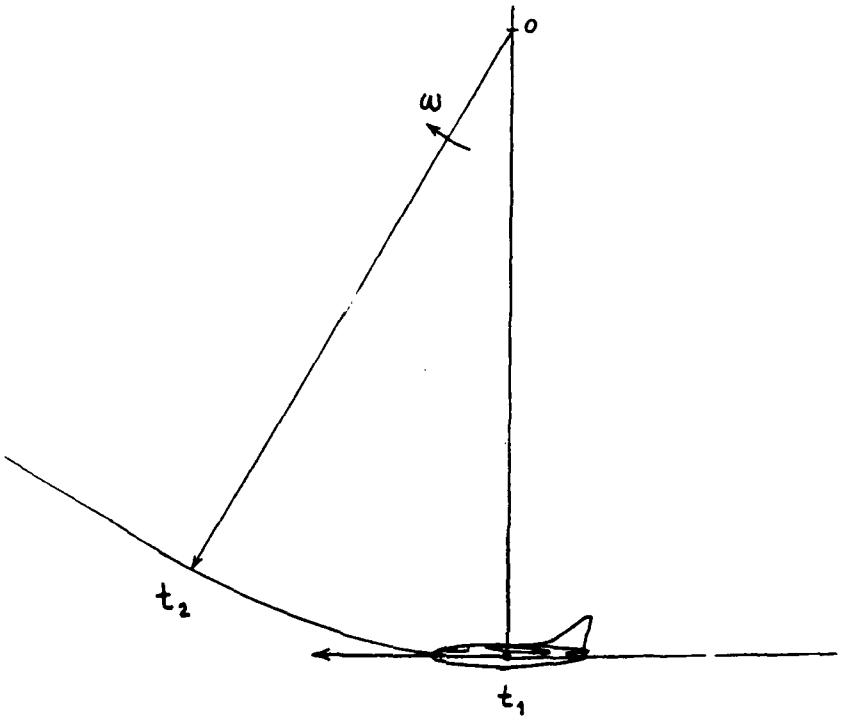

$$\omega = \omega_0 sin(\alpha t)$$

$$\alpha = 2\pi \frac{n}{t_2 - t_1}$$

n–number of periods in $t_2 - t_1$

Figure 22 Airplane in time dependent pull–up maneuver

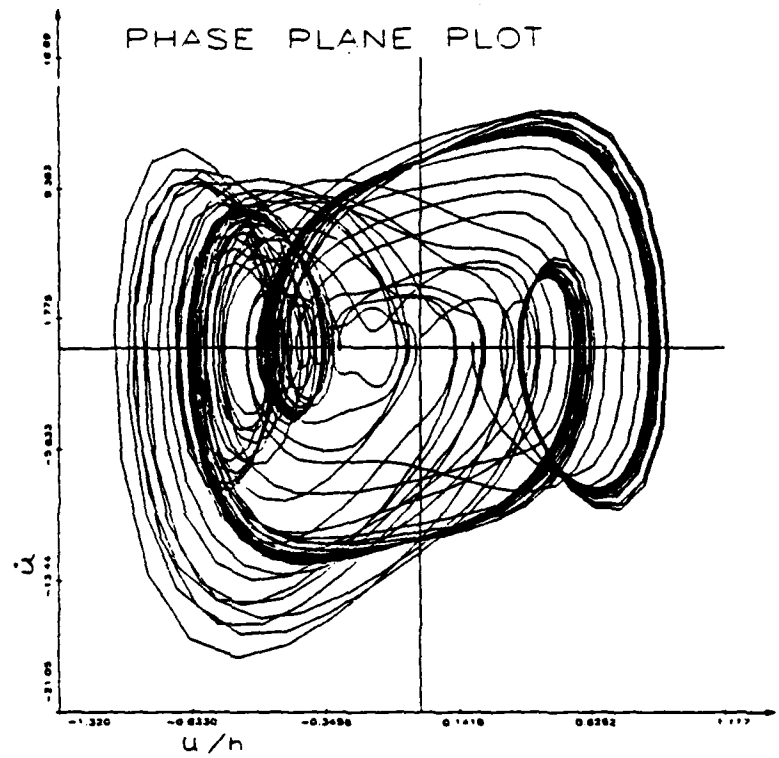

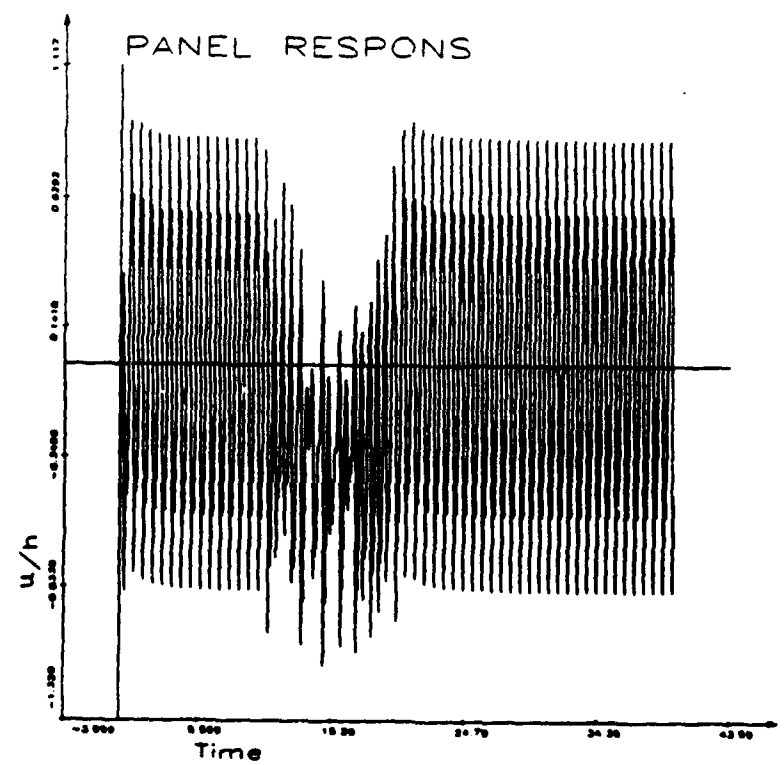

Figure 23 Panel response to time dependent angular velocity